MUTUAL COUPLING STUDIES IN STACKED WAVEGUIDE SLOT ARRAYS

by

Neil Williams, B. Eng.(Hons)

A Thesis submitted for the degree of
Doctor of Philosophy of the
University of London
and for the Diploma of Imperial College

Department of Electrical Engineering
Imperial College of Science & Technology
London SW7.

ACKNOWLEDGEMENTS

The author wishes to thank everyone who has contributed to the production of this thesis. He is indebted to his supervisor, Mr J. Roberts, for his guidance and encouragement throughout the course of this work. He also gives thanks to his colleagues in the Department for many helpful discussions, particularly Dr R.J. Chignell, with whose work this study is closely related. He acknowledges the financial support given by the Science Research Council and, during the final year, the Admiralty Surface Weapons Establishment. To his wife, Jenny, he expresses his gratitude for her ever-renewed understanding and patience, particularly during the final stages of preparation. Finally he thanks Miss T. Richardson for typing the manuscript so efficiently.

Neil Williams

ABSTRACT

Mutual coupling is generally considered not to be a serious problem in slotted waveguide arrays. Its effects have either been neglected or included in an experimental determination of the slot characteristics which, for two dimensional arrays, can be both time-consuming and costly. The array considered in this thesis uses interlaced sum and difference slotted waveguide arrays to produce a monopulse cluster of beams. Low loss complex shaped slots which are resonant in the side wall of reduced height waveguide provide horizontal polarisation and allow phase scanning in the plane transverse to the linear arrays to replace mechanical nodding of the beams. Cross polarised beams are suppressed by baffles running transverse to the arrays. The complexity and proposed size of such an array precluded the usual treatment of mutual coupling in slotted waveguide arrays and a different solution was sought.

First, a brief survey of mutual coupling models is presented and an admittance type approach, which has certain advantages in the problem considered, is chosen. Then the impedance properties of the slots used in the array are discussed. A technique for measuring the mutual coupling between pairs of waveguide fed slots, suitable for such an approach, is established with narrow rectangular slots. It is then used for Z shaped slots radiating into half space and the results are compared with simple theory. I shaped slots, which provide a range of conductances suitable for the actual array, are then considered in the presence of the baffles which form the cross polarisation filter. With assumptions based on experimental data, a design

procedure for the whole array is developed and discussed. As is usual practice, phase scanning is not included in the design and the array performance is optimised at a chosen scan angle.

CONTENTS

LIST OF FIGURES

LIST OF TABLES

1. INTRODUCTION

1.1. BACKGROUND

Slotted waveguides have been used extensively in the realisation of linear array antennas at microwave frequencies. The principal attraction lies in their structural simplicity and ease of manufacture: in the commonest configurations the narrow rectangular slots are milled in the broad or narrow wall of rectangular waveguide with the locations and orientations chosen to provide the correct excitation and the lengths adjusted for half-wave resonance. The advantages of arrays in comparison to reflector systems, including a greater control of the aperture illumination, no spillover or back radiation, have made slotted waveguides dominant for marine navigation and similar radar applications. Pencil beam antennas have been constructed by stacking slotted waveguides to form a two-dimensional aperture. The arrays are excited, either at the end or centre, from a common transverse waveguide feed via directional couplers. Such configurations have been employed in limited beam scanning applications. The beam can be frequency scanned (sufficient range is secured by incorporating serpentine feeds to increase the dispersion) or phase scanned in the plane transverse to the linear arrays (with phase shifters at the input to each waveguide). The design of slotted waveguide arrays is well established and is reviewed in the following section.

A specific application to be considered here is a monopulse antenna in which two stacks of slotted waveguide arrays are interlaced to provide a single aperture producing independent sum and difference beams with phase scanning in the plane transverse to the arrays (as described above). The overall system design is dealt with elsewhere [1] but a description is given in section 1.3. In this thesis interest is confined to mutual coupling in the array. It will be seen in following discussions that mutual coupling is not generally considered to be a serious problem in slotted waveguide arrays. However, the monopulse antenna has features which introduce mutual coupling effects which have not been considered previously. The problems associated with such effects instigated the present study and are summarised in section 1.4.

1.2. THE DESIGN OF SLOTTED WAVEGUIDE ARRAYS

The principal parameter in any antenna design is the far field radiation pattern. In Appendix 1 it is shown that the far field radiation of an array of identical slots, in the absence of mutual coupling, may be expressed as the product of the far field radiation pattern of one slot in isolation and the array factor which is dependent only on the relative positions and excitations of the slots. In general, the slots are electrically small and have a very broad radiation pattern. Then (except in wide angle scanning applications, for which slotted waveguide systems are not suited) the radiation characteristics are dominated by the array factor. Since one has virtually independent control

over the array factor, arrays are very amenable to pattern synthesis techniques. Many formulations are available (for example, the Dolph Chebyshev distribution) in which the element excitations may be specified directly in terms of the principal parameters of the far field radiation pattern. As the subject is very extensive and highly developed, it is not considered in detail in this thesis. Here, the principal concern is in establishing a specified aperture distribution, particularly when mutual coupling cannot be neglected. Design procedures for slotted waveguides will now be reviewed.

1.2.1. The Design of travelling wave, series feed linear arrays

A series feed implies the use of a transmission line with energy tapped off to radiating elements at regular intervals along its length. In a slotted waveguide array the slots act as both power dividers and radiators, with the amount of power radiated a function of its dimensions and position in the waveguide wall. The slot produces a discontinuity in the waveguide and in general may be represented by a π- or T-network in the equivalent dominant mode transmission line. Usually, however, the slots are resonant and cut in such a position that they can be represented as a shunt conductance across the transmission line. It should be noted that this condition must be established in the array situation where the effects of mutual coupling are included. The admittance about resonance of various slots milled in the side wall of a rectangular waveguide is

established in Chapter 3.

The design procedures for these arrays is well-known and documented [2]. For simplicity, the waveguide is assumed to be lossless and the array described by the equivalent circuit in Figure 1.1. The slot spacing, d, determines the phase differences between adjacent slots and thus the main lobe direction. (It also has an important effect on the input voltage standing wave ratio (VSWR) since it governs the relative phases of the waves reflected from each slot). To prevent the formation of grating lobes d must be less than the free space wavelength, λ_o. In arrays in which the beam is squinted away from the broadside direction, the spacing is further restricted by the inequality:

$$d < \frac{\lambda_o}{1+\cos\theta_p} \qquad 1.1$$

θ_p is defined in Figure 1.2. where a wave travelling from left to right is coupling to radiators (with real coupling coefficients) spaced d apart.

To realise such a spacing in a slotted waveguide it is necessary to excite successive elements in anti-phase (by suitable orientation of the slots). Then, with reference to Figure 1.2., the following relation is obtained:

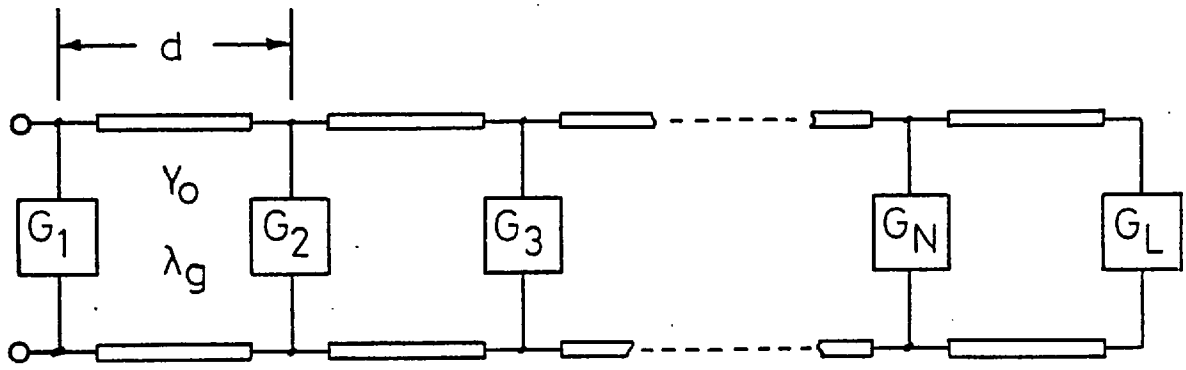

Fig. 1.1: Approximate equivalent circuit of a linear array.

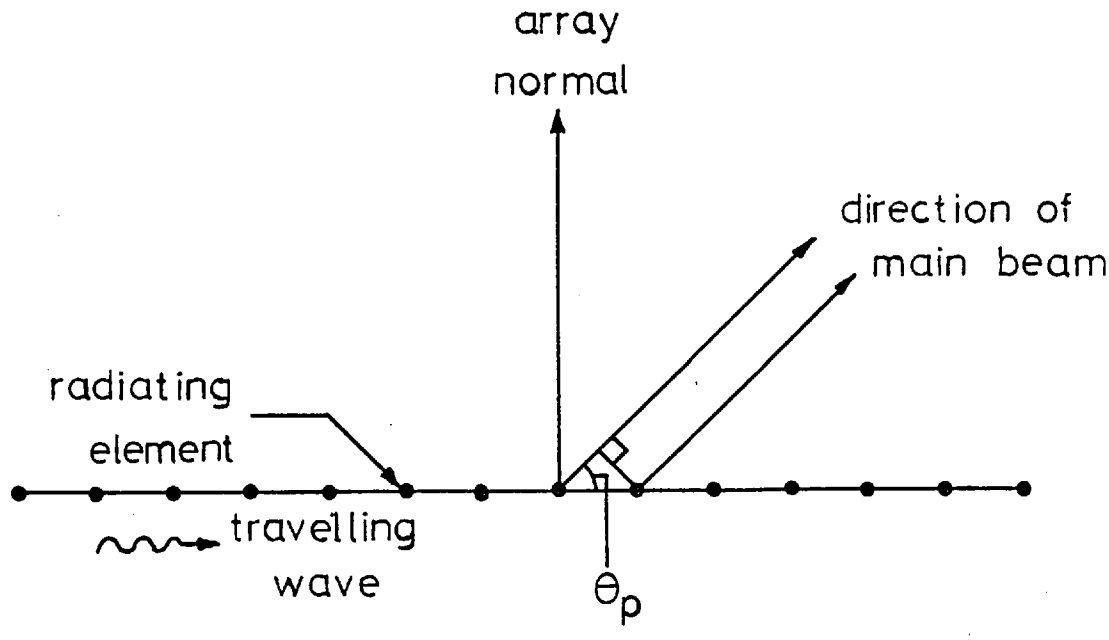

Fig. 1.2: Beam Squint in a travelling wave linear array.

$$\frac{2\pi d \cos \theta_p}{\lambda_o} = \frac{2\pi d}{\lambda_g} - \pi \qquad 1.2a$$

or,
$$\cos \theta_p = \frac{\lambda_o}{\lambda_g} - \frac{\lambda_o}{2d} \qquad 1.2b$$

where λ_g is the wavelength of the dominant waveguide mode.

It may be noted from Figure 1.2. that a travelling wave in the opposite direction will set up a beam in the image position. Forthis reason, travelling wave arrays are terminated in a matched load. In a standing wave (or resonant) array an open circuit is established at the last slot position and an appreciable reflection set up, but, with a slot spacing of $\lambda g/2$, the phase of the two waves coincide and a single beam at broadside results. This arrangement is efficient but extremely narrowband and travelling wave antennas are generally preferred; the slot spacing may be different from $\lambda g/2$ and chosen to minimise the input VSWR as demonstrated in the next section, although the beam is then squinted away from broadside.

In a travelling wave array, the values of normalised slot conductances ($G_1, G_2, \ldots, G_N$) are determined from the required aperture distribution and the fraction of the input power, P_{in}, dissipated in the terminating load, G_L. The simplest analysis assumes the conductances to be small such that the reflection from each slot may be ignored and that the waveguide beyond any slot appears to be matched. Then, the power radiated by the n^{th} slot, P^n_{rad}, is:

$$P^n_{rad} = P^n_{inc} \cdot \frac{G_n}{1 + G_n} \qquad 1.3$$

where P^n_{inc} is the power incident on the n^{th} slot, and the slots are assumed to be lossless.

Re-arranging,

$$G_n = \frac{P^n_{rad}}{P^n_{inc} - P^n_{rad}} \qquad 1.4$$

The input power is given by:

$$P_{in} = P_L + \sum_{n=1}^{N} P^n_{rad} \qquad 1.5$$

where P_L is the power dissipated in the terminating load.

The power incident on the n^{th} slot is:

$$P^n_{inc} = P_{in} - \sum_{r=1}^{n-1} P^r_{rad} = P_L + \sum_{r=n}^{N} P^r_{rad} \qquad 1.6$$

Substituting Eqn. 1.6 into 1.4 yields:

$$G_n = \frac{P^n_{rad}}{P_L + \sum_{r=n+1}^{N} P^r_{rad}} \qquad 1.7$$

This defines the normalised slot conductance, G_n, required to radiate the power, P^n_{rad}. This is a function of the aperture distribution and the power dissipated in the load which must be adjusted to provide a practical range of values of G_n for the complete array. In the next section a more general analysis is presented, which allows for complex

slot admittances and includes the reflections in the main line, so that the effects of various parameters (including mutual coupling) on the aperture distribution and input VSWR can be assessed.

1.2.2. Feed line equations

In the previous section it was assumed that the slots could be represented by shunt conductances. Mutual coupling and other sources of error change the slot admittance and thereby the reflected wave in the waveguide. Consider, therefore, a general equivalent circuit in which the slot conductances have been replaced by complex admittances, Y_n, normalised to the TE_{01} mode transmission line. Two sections of such a circuit are shown in Figure 1.3; the first is located in an arbitrary position whilst the second includes the waveguide termination. The following difference equations for the equivalent voltages at the slot positions may be derived [3]:

$$V_{N-1} = V_N[\cos\psi + j(Y_N+Y_L)\sin\psi] \qquad 1.8a$$

$$V_{N-2} = 2V_{N-1}[\cos\psi + \tfrac{1}{2}j\,Y_{N-1}\sin\psi]-V_N \qquad 1.8b$$

$$V_{n-1} = 2V_n[\cos\psi + \tfrac{1}{2}j\,Y_n\sin\psi]-V_{n+1} \qquad 1.8c$$

where $\psi = K_o d$

and K_o is the propagation constant of the TE_{10} mode. The above equations can be used to assess the effect of the reflections and mutual coupling when Y_n and Y_L are known.

A general analysis of the equivalent circuit is difficult, but a qualitative insight into the dependence of the input VSWR on the slot admittances can be obtained by considering the effect of varying the slot spacing. This may be done most conveniently by abandoning the voltage (and current) representation used above and using a scattering approach. Using standard notation [4], we define normalised wave amplitudes a and b by the equations:

$$a = \frac{1}{2}(V + Z_o I) \qquad 1.9a$$

$$b = \frac{1}{2}(V - Z_o I) \qquad 1.9b$$

where V and I are the voltage and current respectively at a plane along the equivalent transmission line of characteristic impedance, Z_o.

a and b represent the relative amplitudes of the forward and backward waves at the specified reference plane.

Consider the two port network shown in Figure 1.4. The network may be defined using a cascade matrix [4], R:

$$\begin{pmatrix} b_1 \\ a_1 \end{pmatrix} = \begin{bmatrix} r_{11} & r_{12} \\ r_{21} & r_{22} \end{bmatrix} \begin{pmatrix} a_2 \\ b_2 \end{pmatrix} = R \begin{pmatrix} a_2 \\ b_2 \end{pmatrix} \qquad 1.10$$

If the output port is matched, the reflection coefficient at the input is given by:

$$\Gamma = \frac{r_{12}}{r_{22}} \qquad 1.11$$

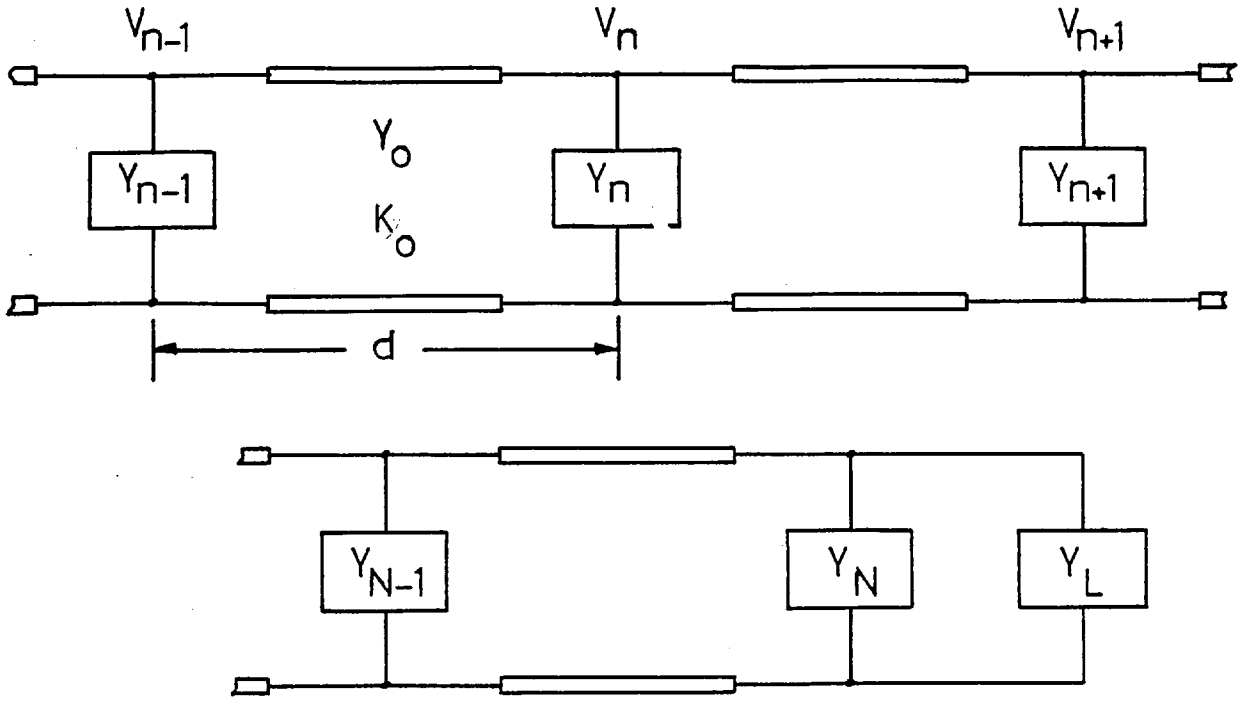

Fig. 1.3: General equivalent circuit of a linear array.

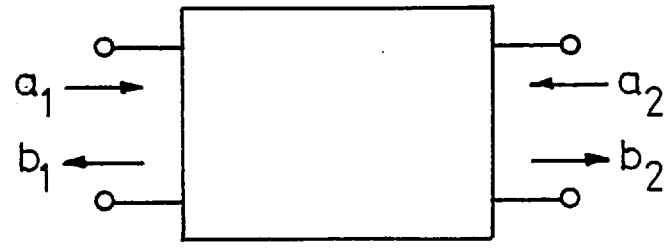

Fig. 1.4: General two-port network.

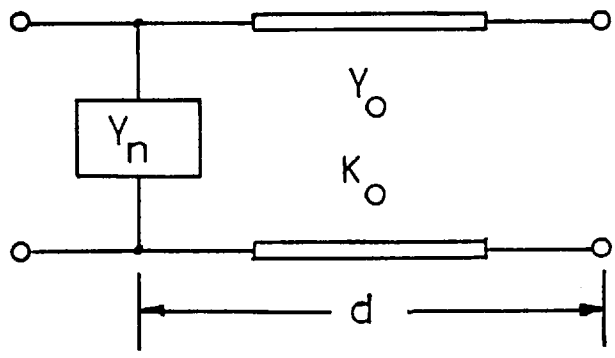

Fig. 1.5: Single section of a slotted waveguide array.

Cascading N such networks may be described with respect to the input and output wave amplitudes as:

$$\begin{pmatrix} b_1 \\ a_1 \end{pmatrix} = \prod_{n=1}^{N} R^{(n)} \begin{pmatrix} a_N \\ b_N \end{pmatrix} = R^{(P)} \begin{pmatrix} a_N \\ b_N \end{pmatrix} \qquad 1.12$$

A linear array of N slots may be represented by the cascading of N similar networks of which a typical example is shown in Figure 1.5. This section is obtained by cascading a length of the equivalent TE_{01} mode transmission line and the slot shunt admittance, Y_n. The cascade matrix for these components may be found in Reference 4. The resultant matrix for the complete section is:

$$R^{(n)} = \frac{1}{2} \begin{bmatrix} (2-Y_n)e^{-\gamma d} & -Y_n e^{-\gamma d} \\ Y_n e^{\gamma d} & (2+Y_n)e^{\gamma d} \end{bmatrix} \qquad 1.13$$

and for the whole array:

$$R^{(P)} = \prod_{n=1}^{N} \frac{1}{2} \begin{bmatrix} (2-Y_n)e^{-\gamma d} & -Y_n e^{-\gamma d} \\ Y_n e^{\gamma d} & (2+Y_n)e^{\gamma d} \end{bmatrix} \qquad 1.14$$

Ignoring terms involving products of two or more admittances (which is equivalent to neglecting multiple reflections in the feed line and is valid for small admittance values), the elements of $R^{(P)}$ can be obtained by induction. Using Equation 1.11 the reflection coefficient is:

$$\Gamma = \frac{-\sum_{n=1}^{N} \frac{1}{2} Y_n e^{-2n\gamma d}}{1 + \sum_{n=1}^{N} \frac{1}{2} Y_n} \qquad 1.15$$

It is of interest to consider the case of identical resonant slots, $Y_n = G$, cut in a lossless waveguide for which $\gamma = j\ 2\pi/\lambda_g$. Then,

$$\Gamma = \frac{-\frac{1}{2} G(\sum_{n=1}^{N} e^{-j4\pi nd/\lambda_g})}{1 + \frac{1}{2} NG} \qquad 1.16$$

The series in the numerator of Eqn. 1.16 is geometric and may be summed to give:

$$\Gamma = \frac{-\frac{1}{2}G}{1+\frac{1}{2}NG} \frac{\sin(2\pi Nd/\lambda_g)}{\sin(2\pi d/\lambda_g)} \qquad 1.17$$

The corresponding input VSWR is shown in Figure 1.6 as a function of d/λ_g for N = 10 and G = .1. It can be seen that values of d/λ_g can be chosen for which the input VSWR is close to unity. The result is relatively independent of the number and values of slot admittances and for an array with such element spacings, the input VSWR will not be greatly affected by mutual coupling effects.

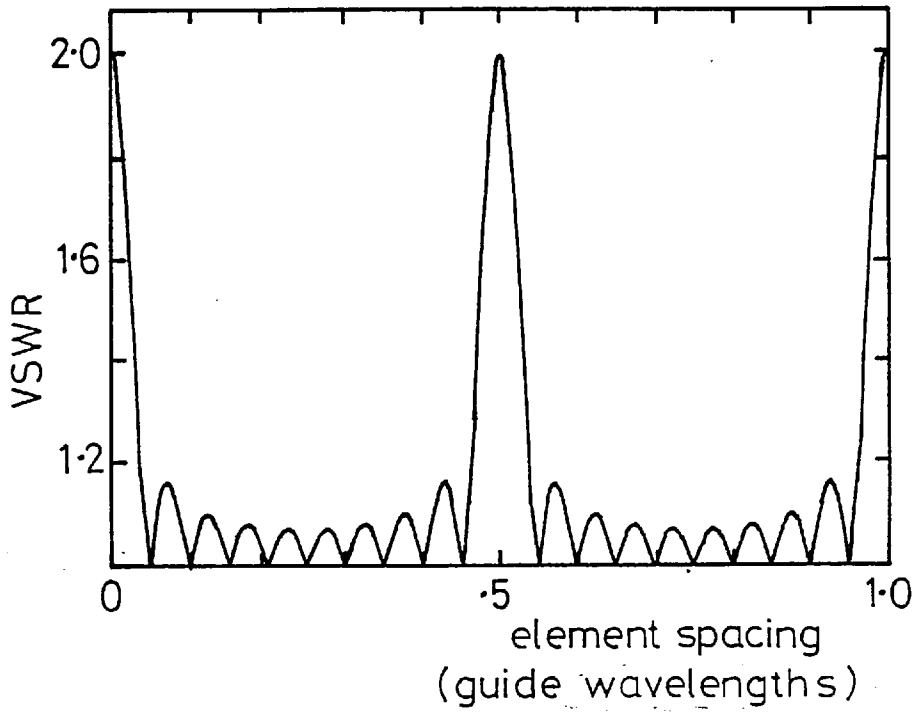

Fig. 1.6: Input VSWR of a travelling wave series fed linear array as a function of the normalised slot spacing. N=10, G= 0.1.

1.3. THE APPLICATION OF SLOTTED WAVEGUIDE ARRAYS IN MONOPULSE RADAR SYSTEMS

In conventional monopulse radar systems, the sum and difference beams are generated by a cluster of primary feed horns illuminating a reflector. With this simple configuration it is not possible to optimise the tracking accuracy, antenna gain and sidelobe suppression since this requires independent control of the sum and difference aperture distributions [5]. Recently, phased arrays have been considered both to optimise the radiation characteristics and to satisfy the demand for higher data rates. Lopez [6] has recognised the compact nature of series fed arrays and employed a centre fed ladder network feed to achieve independent control of the two excitations. The use of directional couplers in the feed line restricted the application of such a network to small arrays. In a recent publication [7], a square monopulse array has been described in which each quadrant is made up of a stack of resonant slotted waveguide arrays, each with a travelling wave feed and electronic scanning in one plane. As expected, the frequency bandwidth was quite restricted.

The design considered in this thesis is that first developed by Killick, Salt and Porter [8]. Two sub-arrays, one forming a sum beam and the other a difference beam, each consisting of stacked travelling wave slotted arrays, are interlaced to produce a monopulse beam cluster. The waveguides are stacked in the E plane with the slots milled in the side wall. To ensure that the two arrays appear as a single aperture in the far field, reduced height waveguide is used to provide a separation of $\lambda_o/3$ (where λ_o

is the free space wavelength). As the slots cannot continue into the broad wall of the waveguide, compact 'H' shaped slots are used as shown in Figure 1.7. The cross-bars end load the centre section to secure resonance and the inclination establishes the correct excitation. One serious drawback of this type of slot is the increase in cross-polarised radiation associated with the fields in the cross-bars. This is suppressed by the addition of baffles on the face of the array, perpendicular to the principal polarisation direction, which form parallel plate regions cut-off to the unwanted polarisation. It was also discovered that the slots were less efficient than narrow rectangular slots. This phenomenon has been studied by Chignell [1], who developed alternative slot shapes which had less intrinsic loss. These are considered in later chapters with regard to their mutual coupling characteristics.

The pitch of waveguides in each sub-array is obviously $2\lambda_o/3$, allowing the beams to be phase scanned over a $\pm 25^o$ sector before the onset of grating lobes. The scanning is achieved with phase shifters at the input to each linear array. A schematic diagram of the proposed system is shown in Figure 1.8. It can be seen that the sum and difference beams are generated from a ladder network feeding the horizontal sum arrays. It is shown by Lopez [6] that when lossless reciprocal directional couplers are used, the two input ports are decoupled provided that the distributions excited by them are orthogonal.

The feasibility of the system was assessed by the construction of two slotted waveguide arrays, one designed to produce a sum beam and the other a difference beam.

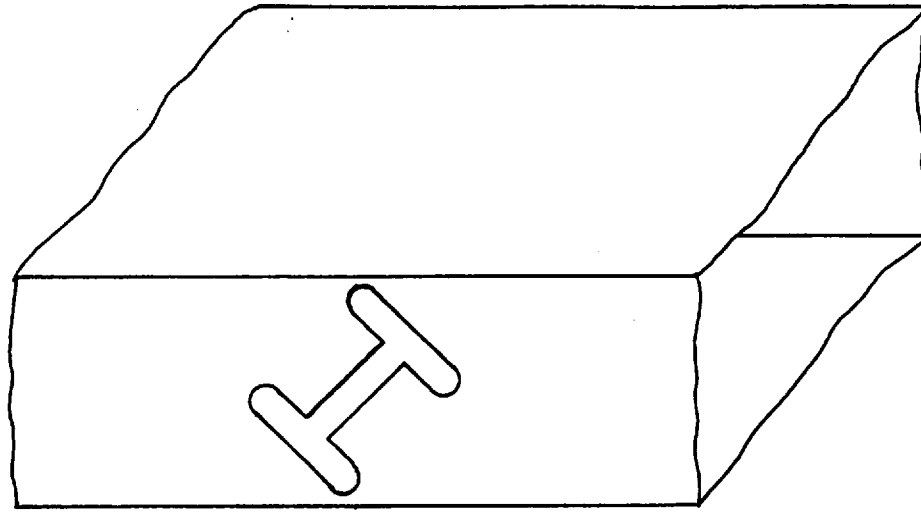

Fig. 1.7: H-shaped slot.

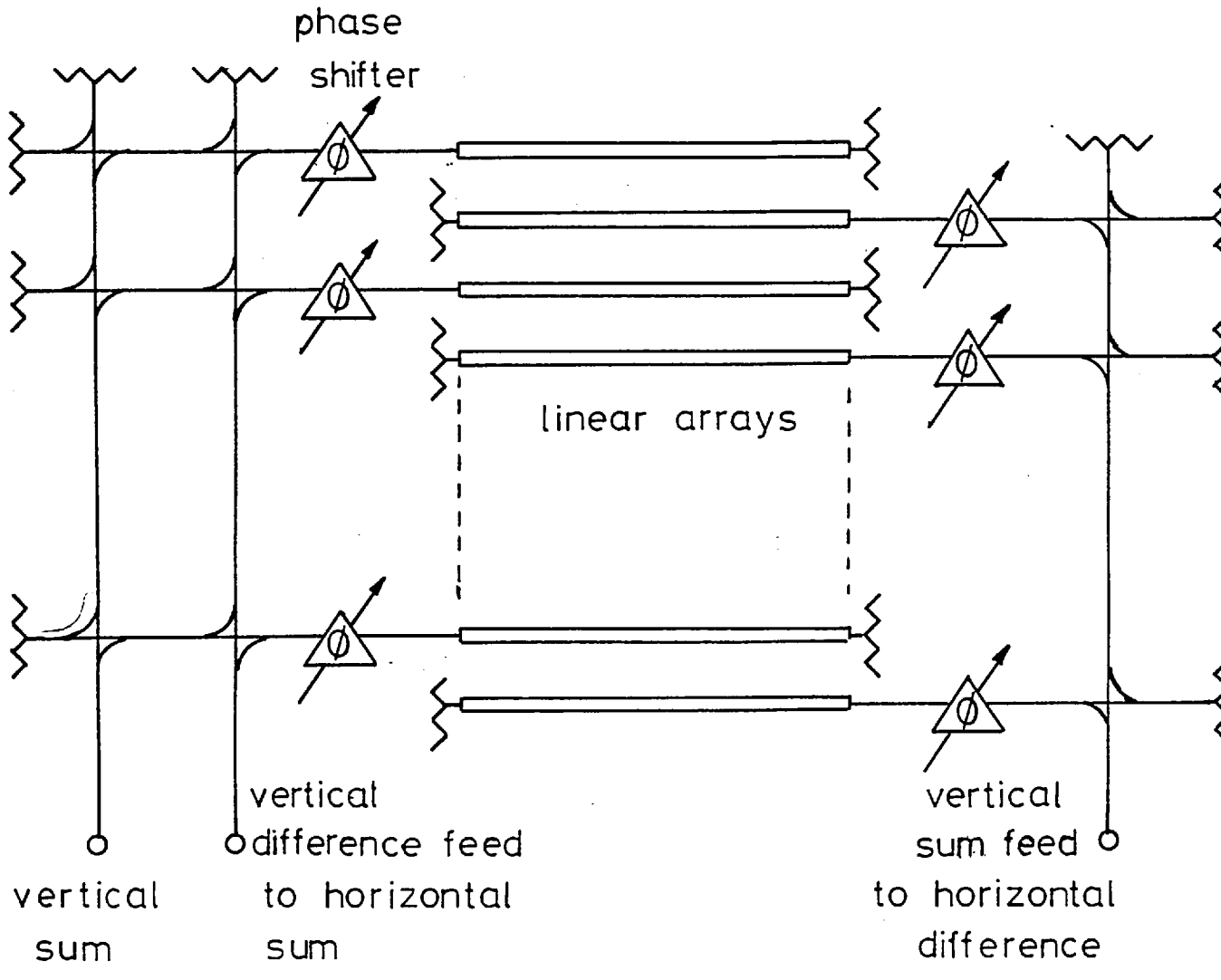

Fig. 1.8: Schematic diagram of the proposed monopulse array antenna.

The effects of mutual coupling between the two arrays were analysed using multiple beam antenna techniques. It was shown that the cross-coupling between the input ports of the two arrays is, in theory, zero due to the orthogonality of the two distributions. The cross-coupling measured in practice was of the order of -30dB. There was, however, significant coupling between individual slots which produced asymmetry in the far field radiation patterns. This is examined in greater depth in the following chapter.

1.4. MUTUAL COUPLING IN SLOTTED WAVEGUIDE MONOPULSE ANTENNAS

Design procedures for slotted waveguide arrays have been described in section 1.2. which provide values for the normalised slot conductances from the desired aperture distribution. The slot dimensions are then established using experimental data obtained from waveguide admittance measurements. For this data to be of use, the measurements must be carried out with the slots in a realistic array environment; that is, mutual coupling must be accounted for. This is not generally considered to be a particular problem because :

1. In large arrays, the aperture distribution is varying slowly with the slot position and the majority of the slots (excluding those near the edges of the array) "see" a similar environment, with neighbouring slots approximately equally excited. Thus only a small number of sub-arrays

need be constructed to characterise the slot admittance in the presence of mutual coupling. Alternatively, the data may be obtained by assuming the array to be infinite and using a waveguide simulator to approximate the region exterior to the slot. This avoids the problem of having to excite all the elements in a sub-array.

2. The input VSWR is insensitive to small variations in the slot admittances if the slot spacing is chosen correctly.

3. Slotted waveguide arrays are not used in wide angle scanning applications. This implies that the measurement procedures described above need only be carried out for a limited number of scan angles to characterise the change in the slot admittance due to mutual coupling.

4. Many pencil beam arrays employ longitudinal slots milled in the broad waveguide wall, with the waveguides stacked in the H-plane. The mutual coupling is inherently low in such configurations.

The majority of the above observations do not apply, however, to the monopulse antenna considered here. The following features demanded special attention with regard to the mutual coupling:

1. The complex shape of the slots.
2. The reduced waveguide spacing.
3. The non-uniform aperture distribution.

4. The presence of cross-polarisation suppressors.

In the next chapter, existing techniques for treating mutual coupling are examined, to establish a convenient model for analysing the above problems.

2. MUTUAL COUPLING IN TWO-DIMENSIONAL ARRAYS

In the last two decades considerable effort has been directed towards the development of phased arrays with the capability of producing multiple independent beams which can be scanned over wide angles. Mutual coupling is a major consideration in such systems and new theoretical techniques have been used to account for its effects. In this chapter, these techniques are examined, together with the more traditional methods, to establish the most appropriate mutual coupling model for the present problem.

2.1. NETWORK APPROACHES

The first theoretical calculations of mutual coupling were made in terms of the mutual impedance. The problem was reduced to network terms by specifying terminals on each radiating element, n, of the array and relating the currents, I_n, and voltages, V_n, at these points with a matrix equation. With N elements, numbered from 1 to N, one possible relationship is:

$$\begin{pmatrix} V_1 \\ \vdots \\ V_n \\ \vdots \\ V_N \end{pmatrix} = \begin{bmatrix} z_{11} & \cdots & z_{12} & \cdots & z_{1N} \\ \vdots & & \vdots & & \vdots \\ z_{n1} & \cdots & z_{n2} & \cdots & z_{nN} \\ \vdots & & \vdots & & \vdots \\ z_{N1} & \cdots & z_{N2} & \cdots & z_{NN} \end{bmatrix} \begin{pmatrix} I_1 \\ \vdots \\ I_n \\ \vdots \\ I_N \end{pmatrix} \qquad 2.1.$$

or

$$\{V\} = [z]\,\{I\} \qquad 2.2.$$

The quantity V_n/I_n is referred to as the "active impedance" of the n^{th} array element and is its input impedance measured in the fully excited array, as distinct from the "isolated impedance". The matrix, z, is referred to as the impedance matrix and has been found particularly convenient in the design of thin wire resonant dipole arrays for the following reasons:

1. The arrays considered were relatively small and the impedance matrix was easy to manipulate.
2. With terminals at the centre of the dipoles, open circuiting the terminals enforced the current on the dipole to be substantially zero, allowing the dipole to be completely removed (thus making it a minimum scattering antenna [9]). This reduces the measurement of the elements of the impedance matrix to pairs of dipoles only.
3. Theoretical calculations of the mutual impedances, z_{mn}, by Carter [10] (using an induced EMF method) agreed well with experiment and could thus be used with confidence.

A similar approach using mutual admittances was successfully applied to slot arrays, much of the theoretical data for dipole arrays being directly applicable by virtue of Babinet's Principle. The corresponding matrix relationship is:

$$\begin{pmatrix} I_1 \\ \vdots \\ I_n \\ \vdots \\ I_N \end{pmatrix} = \begin{bmatrix} Y_{11} \cdots Y_{1n} \cdots Y_{1N} \\ \vdots \\ Y_{n1} \cdots Y_{nn} \cdots Y_{nN} \\ \vdots \\ Y_{N1} \cdots Y_{Nn} \cdots Y_{NN} \end{bmatrix} \begin{pmatrix} V_1 \\ \vdots \\ V_n \\ \vdots \\ V_N \end{pmatrix} \qquad 2.3.$$

The voltage in a narrow half-wave slot may be reduced to zero by shorting out the terminals across the centre of the slot. This is the Babinet equivalent of open circuiting a half-wave dipole, as described above, and allowsthe off-diagonal elements of the admittance matrix to be measured using pairs of slots only. Such measurements have been carried out for rectangular slots in rectangular waveguide although their implementation into slotted waveguide array design has been extremely limited. Designers have generally preferred to measure the active impedance directly using sub-arrays of slots and adjust the slot dimensions to secure half-wave resonance in the presence of mutual coupling on a "cut and try" basis.[11] The reasons for adopting this approach, apart from its directness, may be summarised as general disadvantages of the admittance matrix formulation:

1. The method is based upon what Wheeler [12] refers to as "forced excitation" which implies the use of voltage generators placed directly across the slots and hence the driving voltages are independent of the terminal currents. In practise this is rarely achieved, and, because of the feeding network, the slot voltages are dependent on the terminal currents. The solution of the matrix equation for the active admittance and slot excitations (which determine the radiation characteristics) is then quite difficult

and is further complicated in slotted waveguide arrays where the slots are fed in series.

2. A calculation of the active impedance of any slot or its excitation requires a summing of the contributions from the remaining slots which is prone to build-up errors. The approach is essentially analytic and gives no direct insight into the array behaviour under different feeding conditions (including electronic scanning) which is required in a synthesis technique.

3. The sums are generally slowly convergent which limits the method to small arrays.

For certain types of feed system, some of the above disadvantages may be avoided by using a scattering representation which corresponds to (again using Wheeler's terminology) "free excitation" or constant incident power. That is, the mutual coupling is best represented by the matrix equation:

$$\{b\} = [S]\{a\} \qquad 2.4.$$

where a_n is the amplitude of the wave incident on the n^{th} pair of terminals

b_m is the amplitude of the wave scattered at the m^{th} pair of terminals,

and s_{mn} is the corresponding scattering coefficient.

In many arrays a is independent of the slot impedance and hence b. This is true for arrays with individual waveguide feeds to each radiating element, although not for slotted waveguide arrays. The other advantage lies in the faster convergence of the sums involved in computing the active reflection coefficients ($^{b}n/a_n$). From a physical viewpoint this is because the elements of S, s_{ij}, correspond to scattering from one element, j, to another element, i, with the remaining radiating elements terminated in the characteristic impedances of their feed lines ($a_n = 0$, $n \neq j$). These scatter and absorb some of the energy and produce a more rapid decay in the coupling coefficients with distance. It implies, of course, that the elements of the scattering matrix should be measured with all these elements present, although it is usually possible to use smaller arrays due to the rapid attenuation of the coupling with distance.

In an early paper [13], Blass and Rabinowitz have employed an approximate mutual coupling model using voltage coupling coefficients to calculate the difference in effects of mutual coupling on series and parallel feed networks. Although the results give a clear insight into the mechanisms present (obtaining expressions which represent scattered andreflected waves in the feed lines) the simplifications used in analysis preclude a direct application to an actual slotted waveguide design.

2.2. METHODS BASED ON INFINITE ARRAY MODELS

The infinite array model is now a standard tool in the design of large planar phased arrays. It assumes a doubly periodic infinite structure with identical radiators which are fed with the same amplitude and a zero or progressive phase shift between successive elements. This ensures that all the radiators "see" the same environment and allows interest to be focussed on just one. It has been applied to arrays developed from a basic structure of open ended waveguides, each of which is individually fed. Such structures are compact and allow a wide angle of scan. The mutual coupling between elements can be quite large and the effects on the active reflection coefficient and radiation pattern severe. With an infinite array model it is possible to relate scanning performance directly to such parameters as the element lattice configuration, spacing and matching structures. The present trend is to attempt to treat mutual coupling as a design aid rather than a problem. Such an all embracing design is not possible in the array considered in this thesis, where the spacing of the slots is set by the waveguide dimensions. However, infinite array techniques have been applied to arrays of slots. A value can be obtained for the active admittance of a slot in an infinite array of identical slots which can be used in equivalent circuit representations of the coupling of the slot to a waveguide to derive the corresponding admittance normalised to the dominant mode in the waveguide. The active susceptance is difficult to calculate theoretically but its value can be measured directly by modelling the

exterior region by an equivalent waveguide, the dimensions of which can be obtained from image theory [14]. (It should be noted, however, that a different "simulator" is required for each scan angle).

There remains, however, the problem of how closely the infinite array model corresponds to the actual array environment. This usually entails deciding which elements are sufficiently remote from the array edge such that addition of further elements has no effect on their properties. For specific array structures, it is necessary to establish this by experiment. The remaining edge slots must be considered separately although their effects may be included on a statistical basis; Kurtz [15], for example, has analysed a linear array by assuming errors in the excitation of the edge elements and calculated the worst possible degredation in the sidelobe level.

There are several factors which make the use of an infinite array analysis impractical in the array considered here. They are:

1. Because of the monopulse aperture illumination, very few slots have neighbouring slots which are similarly excited.

2. The proposed array has in the order of eight stacked waveguides, each with approximately 40 slots. With such a configuration, a relatively small proportion may be considered far from the edge.

3. In general, the radiation pattern is not considered sensitive to electronic scanning over the scan range envisaged and a detailed prior knowledge of the scanning

performance is not required. It may be noted, however, that for certain configurations of the cross-polarisation filters a fast wave propagating in a plane parallel to the baffles can exist which can effect the scanning performance. This is discussed in Section 4.1.

2.3. MULTIPLE BEAM ANTENNA ANALYSIS

Multiple beam antenna techniques have been used to calculate the mutual coupling between two slotted waveguides, one producing a sum beam and the other a difference beam. This work described by Killick, Salt and Porter [8], formed the first analysis of the mutual coupling in the specific array described here. Although there appears to be a minor error in their analysis (see Appendix 2) the general results are still valid. It was shown that, because of the orthogonality property of the sum and difference radiation patterns, the cross-coupled power between the input ports of the two arrays is theoretically zero. In practise, with just one linear array of each type, it was not more than -30dB. It was noted, however, that the measured patterns of the isolated arrays were markedly different to those with the second array parasitic, indicating the presence of strong mutual coupling between individual slots. The small net power cross-coupled may be attributed to the anti-symmetric excitation of the difference array. With, for example, the difference array excited and the sum array parasitic, the signal coupled to one half of the sum array will be approximately in antiphase to that coupled into the remaining half. If the spacing of the slots is such that the coupled signals are added in phase, then although

thetotal coupled power in each half may be significant, they will tend to cancel each other at the input, thus satisfying the orthogonality relation. However, it is shown in Appendix 2 that the orthogonality relation cannot be applied to individual elements in the array and, in general, the total power coupled into any element involves contributions from all the other elements. For a full two-dimensional array with each sub-array (i.e. the sum or difference array) consisting of several linear arrays, the mutual coupling between elements of the same sub-array are not included in the expressions given in Reference 7. Thus, in any accurate design procedure, the calculations of mutual coupling to any element must include contributions from all other elements. Also, it has been noted elsewhere [16] that the cross-coupling, which is dependent on an integration of the radiation patterns, can be extremely sensitive to the sidelobe structure, and it was suggested that such calculations were primarily of use in a general prediction of performance, and not in actual designs. Further investigations using this technique were therefore not undertaken.

2.4. DISCUSSION

Various techniques for treating mutual coupling have been considered. Infinite array models have obvious advantages in very large arrays where wide angle volume scanning is required and mutual coupling is a dominant factor. The non-uniformity of the aperture distribution

and the size of the array considered in this thesis, however, made its use here questionable. It was seen that the ideas of multiple beam antennas provide a conceptual simplicity when applied to this type of array. It was not, however, considered to be suitable for use in a practical design. A network approach in terms of admittance was chosen. In the next chapter the admittance of isolated slots is considered, to obtain an equivalent circuit for the complex shaped slots used in the array. In Chapter 4, these equivalent circuits are employed to establish a mutual coupling model.

3. ADMITTANCE PROPERTIES OF WAVEGUIDE-FED SLOTS

Theoretical studies of waveguide-fed slots have mainly concentrated on narrow linear slots cut in the broad wall of rectangular waveguide. Stevenson [17], Silver [18] and Fradin [19] obtained values for the resonant conductance of variously positioned slots, basing their calculations on conservation of energy principles and assuming a sinusoidal electric field distribution in the slot. Lewin [20] and Oliner [21] gave variational expressions for the complex admittance about resonance and the latter author includes the effects of finite waveguide wall thicknesses. Das and Sengal [22] have investigated the properties of waveguide fed slots over larger frequency bandwidths. Bailey [23] and, recently, Yee [24] have discussed modifications to Oliner's results to describe dielectric loading of the slot, radiation into a parallel plate region and the effects of mutual coupling using infinite array approximations. The equivalent circuit of a slot in a metal plate terminating a waveguide has been derived by Harrington [25] using a variational technique.

In this chapter we are concerned with deriving the equivalent circuits of complex shaped slots in the side wall of rectangular waveguide, in particular, those configurations which have been developed for incorporation in the monopulse array antenna discussed in Chapter 1. (The development of these slots is described in detail in Reference 1). Results are also presented for slots cut in the end wall (which are found useful in Chapter 5 where measurements of mutual coupling have been made using end wall slots). The

corresponding parameters for narrow linear slots have been included for comparison. Experimental data is presented to provide confirmation of the general results.

3.1. SUMMARY OF THE ADMITTANCE CHARACTERISTICS OF NARROW RECTANGULAR SLOTS IN RECTANGULAR WAVEGUIDE ABOUT RESONANCE

The admittance of a narrow rectangular slot cut in an infinite ground plane is secured from the impedance of the equivalent dipole using Babinet's Principle [26,27] and, about half wave resonance is typically as shown in Figure 3.1. The conductance at resonance, G_r, is theoretically .00206 mhos With the slot radiating into half space, from symmetry, the admittance is simply halved. Experimental curves for the impedance of a rectangular slot radiating into full space (excited by a twin wire transmission line) have been obtained by Putnam [28] and confirm the general shapes of Figure 3.1.

When the slot is excited by a waveguide or cavity, the field distribution in the slot is generally not equivalent to that obtained for a centre fed dipole of the same dimensions [29]. About resonance, however, the field distribution is relatively independent of the feeding configuration and for both the dipole and slot is well approximated by a sinusoidal function.

A slot in a conducting plate across the end of a waveguide behaves essentially as a direct voltage transformer between the equivalent voltage of the dominant TE_{10} mode wave in the waveguide and the voltage defined across the terminals at the slot centre. The admittance referred to

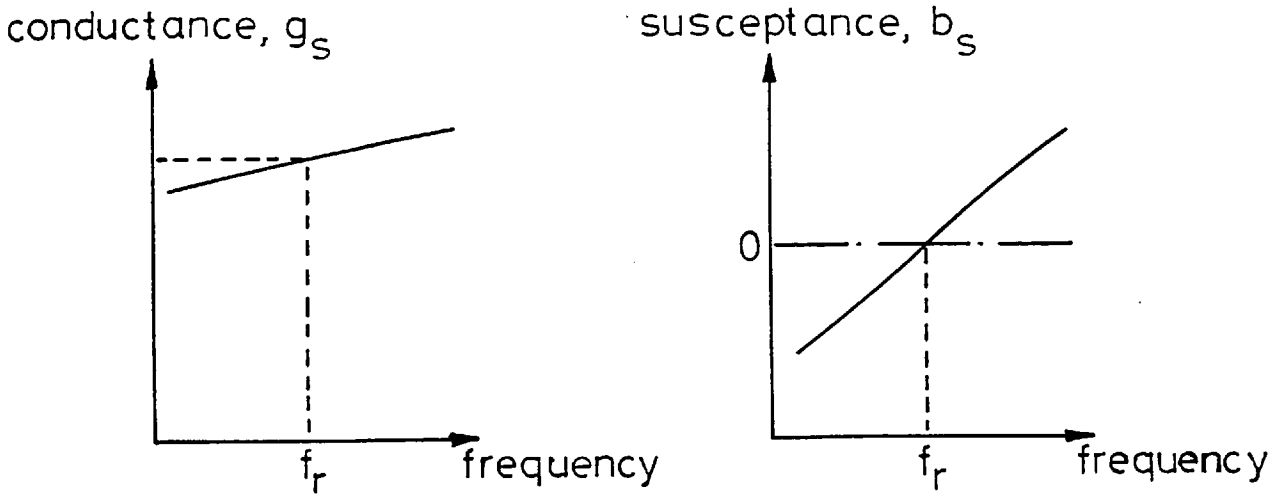

Fig. 3.1: Typical admittance characteristics of a narrow rectangular slot near half-wave resonance.

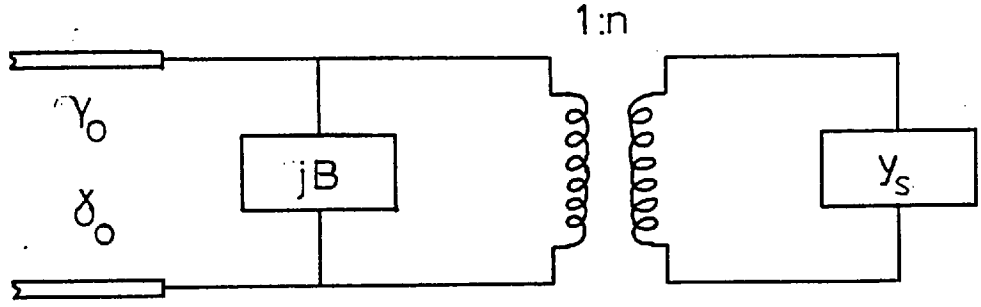

Fig. 3.2: Admittance of a slot milled in the end wall of a wave-guide.

TE_{10} mode, with an infinite ground plane fitted flush with the end of the waveguide, may be represented by the equivalent circuit shown in Figure 3.2., where B is half the susceptance of the equivalent waveguide iris, Y_s is the external admittance of the slot radiating into a half-space as described above and n is a real number representing the ratio of the voltage in the slot compared with that of the TE_{10} mode wave. In this and following discussions upper case characters are used to represent parameters referred to the equivalent TE_{10} mode transmission line, whilst lower case characters represent parameters related to terminals across the centre of the slot. The admittance characteristics are similar in shape to those drawn in Figure 3.1. for the isolated slot, with a shift in resonant frequency due to the susceptance, B.

A slot coupling to half space through the side wall of a waveguide is excited predominantly by the magnetic field of the TE_{10} mode. In this case, the coupling is better described using an "admittance inverter", as shown in the equivalent circuit of Figure 3.3. The impedance at the input port of the admittance inverter, z_{in}, is defined by:

$$z_{in} = \frac{Y_s}{K^2} \qquad 3.1$$

where K^2 is a real number.

It may be noted that the equivalent circuit is similar to that of an H-plane waveguide tee junction, where a quarter-wave transformer is often used to represent the admittance inverter. For a slot in the side wall, the

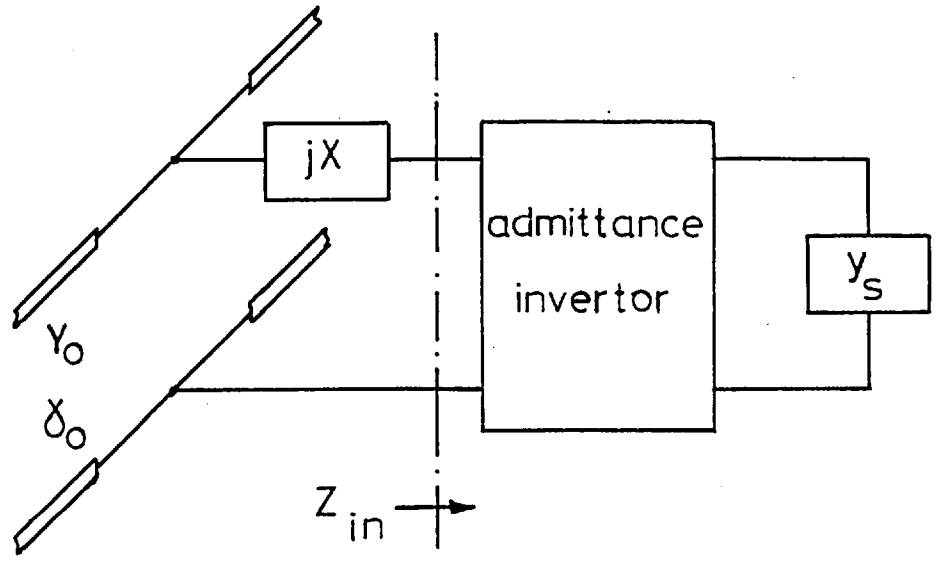

Fig. 3.3: The admittance inverter.

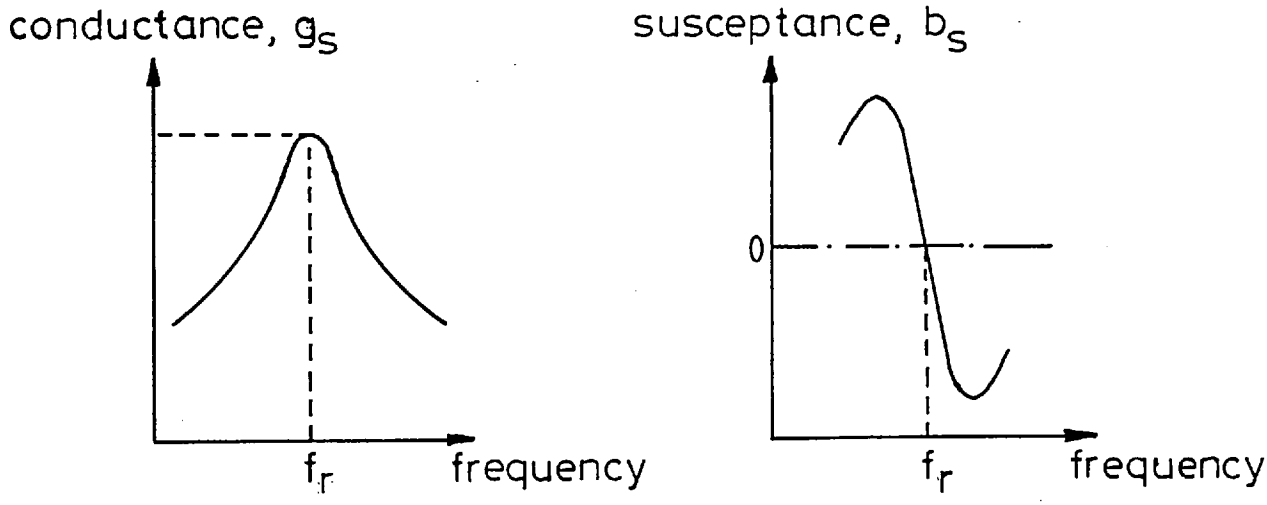

Fig. 3.4: Admittance characteristics of a slot milled in the side wall of a waveguide.

admittance characteristics are typically as shown in Figure 3.4.

In the following sections, the equivalent circuit parameters are derived theoretically.

3.2. PROBLEM FORMULATION

A complete characterisation of waveguide excited slots requires a full knowledge of the fields inside and outside the waveguide. When it is assumed that the electric field in the slot is wholly tangential (i.e. the slot is infinitesimally thin) the problem may be separated into finding independent expressions for the magnetic field in the exterior (radiating) and interior (waveguide) regions and matching them in the slot aperture to obtain an integral equation. A solution is then generally obtained by transforming the integral equation into a variational form.

The exterior problem of determining the fields of a radiating slot cut in a waveguide is very difficult and normally the waveguide surface containing the slot is extended to form an infinite ground plane. When considering two-dimensional arrays on an admittance basis (as discussed in Chapter 2), this is a reasonable approximation. It has been established that, about half-wave resonance, the slot aperture fields are independent of the method of excitation [28] and so the exterior problem is then identical for both end and side wall slots. To remain consistent with the relevant literature, let the exterior magnetic field be defined as [30]:

$$\underline{H} = \iint_A \underline{n} \times \underline{E}^a \cdot \overline{y}\, da \qquad 3.2.$$

where $\underline{E}^a$ is the assumed electric field in the aperture.

$\underline{n}$ is the normal vector directed out of the waveguide.

$\overline{y}$ is the half-space dyadic Green's function

and the surface integral is evaluted over the slot aperture, A, on which da is an elemental area.

Obtaining the interior fields is a classical cylindrical waveguide discontinuity problem. A method applicable to arbitrary obstacles and apertures has been developed by Marcuvitz and Schwinger [30]. For general discontinuities the formulation is obviously quite complicated and here only the specific case of an aperture in the side wall of a rectangular waveguide is analysed. Transmission line solutions are sought from Maxwell's Equations by expressing the transverse fields in a sum of orthogonal vector functions. Let:

$$\begin{aligned} \underline{E}_t(z) &= \sum_i V_i(z)\underline{e}_i \\ \underline{H}_t(z) &= \sum_i I_i(z)\underline{h}_i \end{aligned} \qquad 3.3.$$

where t denotes the transverse component and

i the vector function mode number.

From the orthogonality property of the vector functions, $\underline{e}_i$ and $\underline{h}_i$, the mode voltages, V_i and I_i are defined as:

$$\begin{aligned} V_i(z) &= \iint \underline{E}_t(z) \cdot \underline{e}_i\, da \\ I_i(z) &= \iint \underline{H}_t(z) \cdot \underline{h}_i\, da \end{aligned} \qquad 3.4.$$

where the surface integrals are evaluated over the waveguide cross-section.

Since the fields at the side walls are longitudinal the relationship of the aperture fields to the above transverse fields is not immediately obvious. This relationship can be obtained by replacing the slot by equivalent sources and solving the appropriate Maxwell's Equations. An aperture in which the tangential electric field is $\underline{E}^a$ may be replaced by a magnetic current, $\underline{M}^a = - \underline{n} \times \underline{E}^a$, flowing on a perfectly conducting surface (which fills in the aperture). Now, consider the vector wave equation form of Maxwell's Equations with only magnetic current sources:

$$\nabla^2 \underline{E} - \gamma^2 \underline{E} = - \frac{\nabla \times \underline{M}^a}{j\omega\mu} \qquad 3.5.$$

$$\nabla^2 \underline{H} - \gamma^2 \underline{H} = - j\omega\varepsilon \underline{M}^a$$

where $\gamma^2 = \omega^2 \mu\varepsilon$ and the other symbols have their usual meaning.

With the definition of the transverse gradient operator, ∇_t:

$$\nabla = \nabla_t + \hat{\underline{z}} \frac{\partial}{\partial z} \qquad 3.6.$$

where $\hat{\underline{z}}$ is a unit vector in the z(longitudinal) direction

the longitudinal components of $\underline{E}$ and $\underline{H}$ may be eliminated from Eqns. 3.5 to give

$$\frac{\partial \underline{E}_t}{\partial z} = j\omega\mu\left(\hat{\underline{\varepsilon}} + \frac{1}{\gamma^2}\nabla_t\nabla_t\right).(\underline{H}_t\times\hat{\underline{z}}) + \underline{M}^a\times\hat{\underline{z}}$$

$$\frac{\partial \underline{H}_t}{\partial z} = j\omega\varepsilon\left(\hat{\underline{\varepsilon}} + \frac{1}{\gamma^2}\nabla_t\nabla_t\right).(\hat{\underline{z}}\times\underline{E}_t) + \frac{\nabla_t M_z^a}{j\omega\mu} \qquad 3.7.$$

where $\hat{\underline{\varepsilon}}$ is the transverse unit dyadic.

Taking the scalar products of the first equation and $\underline{h}_i \times \hat{\underline{z}}$, the second equation and $\hat{\underline{z}} \times \underline{e}_i$ and integrating over the waveguide cross-section, Σ, yields the following two equations:

$$-\frac{\partial V_i}{\partial z} = j\omega\mu\ I_i + \frac{1}{\gamma^2}\iint_\Sigma (\nabla_t\nabla_t\cdot\underline{H}_t\times\hat{\underline{z}})\cdot\underline{h}_i\times\hat{\underline{z}}\ d\sigma + \iint_\Sigma \underline{M}^a\cdot\underline{h}_i\ d\sigma \qquad 3.8.$$

$$-\frac{\partial I_i}{\partial z} = j\omega\varepsilon\ V_i + \frac{1}{\gamma^2}\iint_\Sigma (\nabla_t\nabla_t\cdot\hat{\underline{z}}\times\underline{E}_t)\cdot\hat{\underline{z}}\times\underline{e}_i\ d\sigma + \iint_\Sigma \frac{\nabla_t M_z^a}{j\omega\mu}\cdot\hat{\underline{z}}\times\underline{e}_i\ d\sigma$$

The vector mode functions $\underline{e}_i$ and $\underline{h}_i$ satisfy the following equation on the waveguide walls:

$$\nabla_t\cdot(\underline{h}_i\times\hat{\underline{z}}) = (\hat{\underline{z}}\times\underline{e}_i)\cdot\underline{\nu} = 0 \qquad 3.9.$$

Eqn. 3.9. is simply a statement of the boundary conditions at a perfect conductor. Applying this to Eqn. 3.8. results in the following transmission line equations:

$$-\frac{\partial V_i}{\partial z} = -j\, Z_i \gamma_i I_i + v_i$$
$$-\frac{\partial I_i}{\partial z} = j\, Y_i \gamma_i V_i + i_i \qquad 3.10.$$

where γ_i, Z_i and Y_i are the propagation constant, characteristic impedance and admittance, respectively, of the i^{th} mode.

and $$v_i = \iint_\Sigma \underline{M}^a \cdot \underline{h}_i \, d\sigma$$
$$i_i = \iint_\Sigma \frac{\nabla_t M_z^a}{j\omega\mu} \cdot \hat{z} \times \underline{e}_i \, d\sigma$$

The source terms, v_i and i_i may be expressed in a more convenient form by applying the vector integration by parts formula. The result is [30]:

$$v_i = \iint_\Sigma \underline{M}^a \cdot \underline{h}_i \, d\sigma$$
$$i_i = -Y_i \iint_\Sigma \underline{M}^a \cdot \underline{h}_{zi} \, d\sigma \qquad 3.11.$$

where $\underline{h}_{zi}$ is the longitudinal magnetic field mode vector of the i^{th} mode.

A suitable choice of the vector mode functions $\underline{e}_i$ and $\underline{h}_i$ for cylindrical waveguides corresponds to the complete set of transverse electric (TE or H) and transverse magnetic (TM or E) modes. As is usual, we are concerned with the situation where only the lowest dominant mode is able to propagate. For rectangular waveguide this is the TE_{10} mode which we will denote by subscript i = 0. The actual form $\underline{e}_o$ and $\underline{h}_o$ are given in the following section.

It may be shown that for apertures in the side wall, $\underline{M}^a . \underline{h}_o = 0$ and Eqn. 3.10 reduces to:

$$
\begin{aligned}
-\frac{\partial V_o}{\partial z} &= j\, Z_o \gamma_o I_o \\
-\frac{\partial I_o}{\partial z} &= j\, Y_o \gamma_o V_o + i_o
\end{aligned}
\qquad 3.12
$$

The complete solution of Eqn. 3.12 is the sum of the complementary function and particular integral which is, in physical terms, equivalent to the superimposition of the fields generated by the equivalent magnetic current on the source free incident fields in the waveguide. The complementary function is well-known and may be expressed as:

$$
\begin{aligned}
V_o(z) &= Ae^{-j\gamma_o(z-z')} + Be^{j\gamma_o(z-z')} \\
I_o(z) &= Y_o(Ae^{-j\gamma_o(z-z')} - Be^{j\gamma_o(z-z')})
\end{aligned}
\qquad 3.13
$$

where A and B represent the voltage amplitudes of the waves travelling in the positive and negative z-directions, respectively, with the phase referenced to the plane z'.

The source term $i_o(z)$ is obviously distributed along z in the aperture region. To evaluate the particular integral it is convenient to let i_o be made up of elementary current sources $i_o(z')\ \delta(z-z')$:

$$i_o(z) = \int_\tau i_o(z')\ \delta(z-z')\ dz' \qquad 3.14a$$

where $\delta(z-z')$ is the Dirac Function

and τ is the aperture length.

Each elementary current source will set up currents $I_o(z,z')$ and voltages $V_o(z,z')$ defined by the equations:

$$-\frac{dV_o(z,z')}{dz} = j\ \gamma_o Z_o I_o(z,z')$$
$$-\frac{dI_o(z,z')}{dz} = j\ \gamma_o Y_o V_o(z,z') + i_o(z')\ \delta(z-z') \qquad 3.14b$$

which, with the waveguide inputs matched, correspond to the equivalent circuit shown in Figure 3.5. The current source generates dominant wave mode waves travelling outwards from the source and from simple network analysis:

$$V_o(z,z') = -\frac{1}{2} Z_o i_o(z')\ e^{-j\gamma_o|z-z'|}$$
$$I_o(z,z') = -\frac{1}{2} i_o(z')\ u(z,z')\ e^{-j\gamma_o|z-z'|} \qquad 3.15$$

where $u(z,z') = \begin{cases} +1 & , z > z' \\ -1 & , z < z' \end{cases}$

From the definition of the Dirac Function, the response to the total source, i_o, is just the integral of the above solution over the aperture region. The complete solution to Eqn. 3.12 is then:

$$V_o(z) = Ae^{-j\gamma_o z} + Be^{j\gamma_o z} - \frac{1}{2}\int_\tau Z_o i_o(z')\, e^{-j\gamma_o|z-z'|}\, dz'$$

$$I_o(z) = Y_o A(e^{-j\gamma_o z} - Be^{j\gamma_o z}) - \frac{1}{2}\int_\tau i_o(z')\, u(z,z')\, e^{-j\gamma_o|z-z'|}\, dz'$$

3.16

with the phase of the incident sources referred to the plane z = 0 which is here chosen to be the centre of the slot.

The waveguide dimensions are chosen such that the higher order modes are evanescent and, if generated by the slot, are confined to its immediate vicinity. Since there are no incident waves for these modes, the equivalent currents and voltages are given by the particular integral solution of Eqn. 3.10. The voltage source, v_i, which represents a longitudinal discontinuity in voltage, is retained since the TM modes have a transverse component of magnetic field at the side wall. Using a procedure similar to that described for the dominant mode, the sources may be expanded in terms of Dirac Functions and the equivalent circuit for a single elementary source drawn as in Figure 3.6. The corresponding solution for the i^{th} mode voltages and currents is:

$$V_i(z) = -\frac{1}{2}\int_\tau [v_i(z')u(z,z') + Z_i i_i(z')]e^{-j\gamma_i|z-z'|}\, dz'$$

$$I_i(z) = -\frac{1}{2}\int_\tau [i_i(z')u(z,z') + Y_i v_i(z')]e^{-j\gamma_i|z-z'|}\, dz'$$

3.17

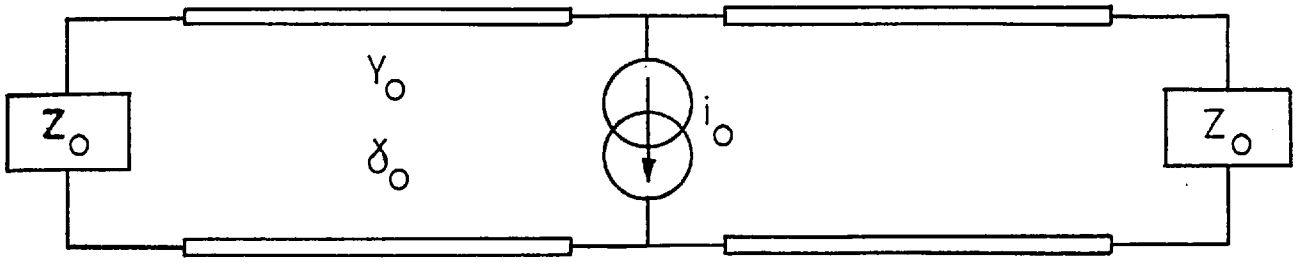

Fig. 3.5: Equivalent circuit of an elementary current source in an infinite waveguide.

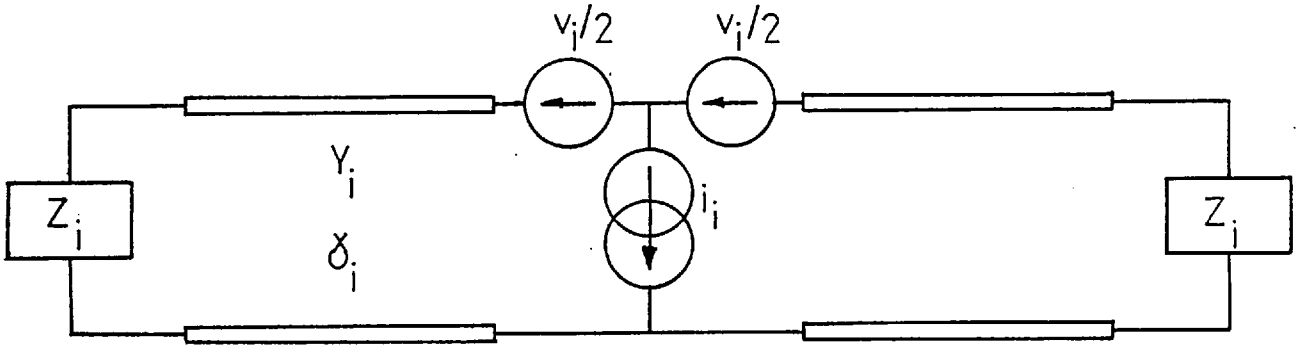

Fig. 3.6: Equivalent circuit of an elementary current and voltage source in an infinite waveguide.

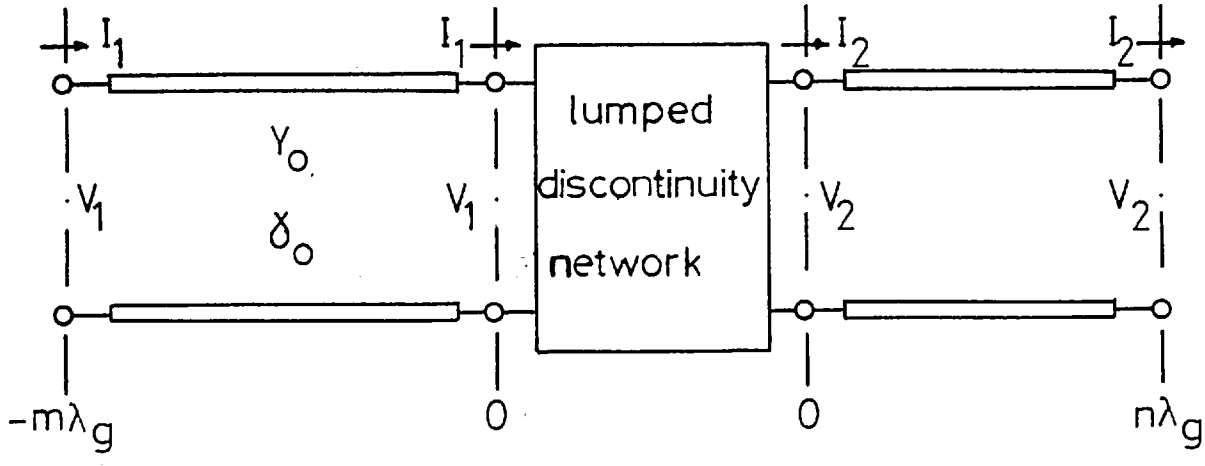

Fig. 3.7: Lumped equivalent circuit representation of a waveguide discontinuity.

In both Eqns. 3.16 and Eqns. 3.17 the exponential terms in z may be taken outside the integrals. Then, outside the aperture region ($|z| > |z'|$) the equations represent propagation in homogeneous transmission lines. If we consider Equations 3.16 and choose reference planes at $z = -\frac{2\pi m}{\gamma_o}$ and $z = +\frac{2\pi n}{\gamma_o}$ and define the voltages and currents at these planes to be V_1, I_1 and V_2, I_2, respectively, it follows that:

$$V_1 - V_2 = \int_\tau j z_o i_o(z') \sin \gamma_o z' \, dz'$$
$$I_1 - I_2 = \int_\tau i_o(z') \cos \gamma_o z' \, dz' \qquad 3.18$$

The corresponding relationships for the higher order modes with reference at $z = -\frac{2\pi n}{\gamma_i}$ and $z = +\frac{2\pi m}{\gamma_i}$ are:

$$V_1 - V_2 = \int_\tau [v_i(z') \cos \gamma_i z' + j z_i i(z') \sin \gamma_i z] dz'$$
$$I_1 - I_2 = \int_\tau [i_i(z') \cos \gamma_i z' + j Y_i v(z') \sin \gamma_i z'] dz' \qquad 3.19$$

Although the voltages and currents have been defined at planes far from the discontinuity region, they can be used to characterise a lumped constant equivalent circuit at $z = 0$ which produces the same discontinuities in the far voltages currents as implied in Figure 3.7. To determine the parameters of this equivalent circuit for the dominant mode, it is useful to re-define the complementary functions of Eqns. 3.16 in terms of the far terminal voltages and currents. From Eqns. 3.16:

$$A = \frac{1}{2}(V_1 + z_o I_1)$$
$$B = \frac{1}{2}(V_2 - z_o I_2) \qquad 3.20$$

Substituting this back into 3.16 results in:

$$V_o(z) = \frac{V_1+V_2}{2}\cos\gamma_o z - j\frac{z_o(I_1+I_2)}{2}\sin\gamma_o z + j\int_\tau z_o i_o(z')\frac{\sin\gamma_o|z-z'|}{2}dz'$$

$$I_o(z) = \frac{I_1+I_2}{2}\cos\gamma_o z - j\frac{Y_o(V_1+V_2)}{2}\sin\gamma_o z - \int_\tau i_o(z')u(z,z')\frac{\cos\gamma_o|z-z'|}{2}dz' \qquad 3.21$$

It is now possible to obtain a complete representation of the magnetic field within the waveguide. From Eqn. 3.3, with separation into H and E modes:

$$\underline{H}_t(z) = \sum_i^H I_i^H(z)\underline{h}_i^H + \sum_i^E I_i^E(z)\underline{h}_i^E \qquad 3.22$$

where the superscripts H and E indicate H and E modes, respectively.

The z-directed magnetic field is defined in terms of H modes as:

$$\underline{H}_z(z) = \frac{1}{j\omega\mu}\sum_i^H V_i^H(z)\nabla t.\underline{\hat{z}} \times \underline{e}_i^H \qquad 3.23$$

From the additional H mode definitions

$$\underline{h}_{zi}^{H} = \frac{\nabla_t \cdot \underline{h}_i^H}{j\gamma_i^H}$$

$$\underline{e}_i^H = \underline{h}_i^H \times \hat{\underline{z}} \qquad 3.24$$

$$Y_i^H = \frac{\gamma_i^H}{\omega\mu}$$

it follows that:

$$\underline{H}_z(z) = \sum_i^H Y_i^H V_i^H(z)\, \underline{h}_{zi}^H \qquad 3.25$$

Thus, the total magnetic field is given by:

$$\underline{H}(z) = \sum_i^H (I_i^H(z)\underline{h}_i^H + Y_i^H V_i^H(z)\underline{h}_{zi}^H) + \sum_i^E I_i^E(z)\underline{h}_i^E \qquad 3.26$$

On substitution of Eqns. 3.11, 3.17 and 3.21, one obtains:

$$H(z) = \tfrac{1}{2}(I_1+I_2)\{\underline{h}_o \cos\gamma_o z - j\underline{h}_{zo}\sin\gamma_o z\}$$
$$- j\tfrac{1}{2}Y_o(V_1+V_2)\{\underline{h}_o \sin\gamma_o z + j\underline{h}_{zo}\cos\gamma_o z\}$$
$$- j\iint_A \underline{n}\times\underline{E}^a.\overline{\beta}\, da \qquad 3.27$$

where $\overline{\beta}$ is defined as the susceptance dyadic and represents the negative of the imaginary part of the vector magnetic field produced at the plane z by unit vector magnetic current at the plane z'.

$$\overline{\beta} = \frac{1}{2}u(z,z')\ Y_o[(\underline{h}_o \sin\gamma_o z' + j\underline{h}_{zo}\cos\gamma_o z')(\underline{h}_o\cos\gamma_o z - j\underline{h}_{zo}\sin\gamma_o z)$$
$$-(\underline{h}_o\cos\gamma_o z' - j\underline{h}_{zo}\sin\gamma_o z')(\underline{h}_o\sin\gamma_o z + j\underline{h}_{zo}\cos\gamma_o z')]$$
$$+ \sum_{i,i\neq o}^{H} \frac{1}{2}Y_i(\pm\underline{h}_i^H + \underline{h}_{zi})(\mp\underline{h}_i^H + \underline{h}_{zi})e^{\pm\gamma_i(z-z')}$$
$$+ \sum_{i,i\neq o}^{E} \frac{1}{2}Y_i\ \underline{h}_i^E\ \underline{h}_i^E\ e^{\pm\gamma_i(z-z')} \qquad 3.28$$

The expression for the impedance of a slot in the side wall of rectangular guide may be found using Eqn. 3.27 and the discontinuity relations, Eqns. 3.18. The voltage equation reduces to $V_1 - V_2 = 0$ for a slot in the side wall, indicating that it may be represented as a wholly shunt equivalent network. The current discontinuity equation, in field terms is:

$$I_1 - I_2 = Y_o \iint_A \underline{n}\times\underline{E}^a \cdot \underline{h}_{zo}\cos\gamma_o z'\ da \qquad 3.29$$

Applying the condition of continuity of magnetic field through the slot and equating the interior and exterior representations of Eqns. 3.27 and 3.2 yields:

$$\frac{I_1+I_2}{2}(\underline{h}_o\cos\gamma_o z - j\underline{h}_{zo}\sin\gamma_o z) - jY_o\frac{(V_1+V_2)}{2}(\underline{h}_o\sin\gamma_o z +$$
$$j\underline{h}_{zo}\cos\gamma_o z) - j\iint_A \underline{n}\times\underline{E}^a\cdot(\overline{y}+j\overline{\beta})\,da = 0 \qquad 3.30$$

For a "shunt" slot with a symmetric voltage excitation ($V_1=V_2=V$), the equivalent network is bisected with an open circuit, that is, $I_1 = -I_2 = I$ and the integral equation, Eqn. 3.30 becomes:

$$-jY_o\ V(\underline{h}_o \sin\gamma_o z + j\underline{h}_{zo}\cos\gamma_o z) = \iint_A \underline{n}\times\underline{E}^a \cdot (\bar{y}+j\bar{\beta})\,da \qquad 3.31$$

whilst the current discontinuity equation is:

$$2I = jY_o \iint_A \underline{n}\times\underline{E}^a \cdot \underline{h}_{zo}\ \cos\gamma_o z \qquad 3.32$$

A variational solution for the shunt impedance is arrived at by taking the scalar product of Eqn. 3.31 and $\underline{n} \times \underline{E}^a$, integrating over the aperture (to give 2VI) and dividing by the square of Eqn. 2.31 to yield V/2I, which is the normalised shunt impedance Z_s. The final expression is:

$$Z_s = \frac{\iint\iint \underline{n}\times\underline{E}^a \cdot (\bar{y}+j\bar{\beta}) \cdot \underline{n}\times\underline{E}^a\ da\,da}{Y_o^2\left[\iint \underline{n}\times\underline{E}^a \cdot \underline{h}_{zo}\cos\gamma_o z\,da\right]^2} \qquad 3.33$$

An interpretation of this expression and its evaluation for various slot configurations will be given in the next section. Now, the derivation of the equivalent circuit of the slot cut in the end wall will be considered.

The end wall slot is somewhat easier to analyse than the side wall slot in that it lies entirely in a transverse plane. An equivalent circuit can be obtained from the infinite waveguide equations derived above by suitable choice of the symmetry of the overall excitation. A more direct approach has been described by Harrington [25] and his analysis is employed here.

In a semi-infinite waveguide region (such as a waveguide terminated in a slot) it is convenient to represent the dominant mode voltages and currents on a scattering basis.

For a wave incident in the positive z direction, a possible solution of the source free transmission line equations is:

$$V_o(z) = A(z')\ (e^{-j\gamma_o(z-z')} + \Gamma(z')e^{+j\gamma_o(z-z')})$$

$$I_o(z) = Y_o A(z')(e^{-j\gamma_o(z-z')} - \Gamma(z')e^{+j\gamma_o(z-z')}) \qquad 3.34$$

where $\Gamma(z')$ is the voltage reflection coefficient and is given by $\frac{B(z')}{A(z')}$ where $B(z')$ is the amplitude of the reflected wave.

At $z = z'$, the voltage relation is:

$$V_o(z') = A(z')\ (1+\Gamma) \qquad 3.35$$

Therefore, Eqns. 3.34 may be re-written as:

$$V_o(z) = \frac{V(z')}{1+\Gamma(z')}\ (e^{-j\gamma_o(z-z')} + \Gamma(z')e^{j\gamma_o(z-z')})$$

$$I_o(z) = Y_o\ \frac{V(z')}{1+\Gamma(z')}(e^{j\gamma_o(z-z')} - \Gamma(z')e^{j\gamma_o(z-z')}) \qquad 3.36$$

The higher order mode voltages and currents are given by:

$$V_i(z) = B_i(z')\ e^{j\gamma_i(z-z')}$$

$$I_i(z) = -Y_i B_i(z')\ e^{j\gamma_i(z-z')} \qquad 3.37$$

The total tangential electric and magnetic fields are:

$$\underline{E}_t(z) = V_o(z)\,\underline{e}_o + \sum_{i,i=0} V_i(z)\,\underline{e}_i$$

$$\underline{H}_t(z) = I_o(z)\,\underline{h}_o + \sum_{i,i=0} I_i(z)\,\underline{h}_i \qquad 3.38$$

For an aperture in the end wall as shown in Figure 3.8, Eqns. 3.35, 3.37 and 3.38 reduce to the following at the plane of the slot, $z = z' = 0$:

$$\underline{E}_t = V_o\underline{e}_o + \sum_i V_i\underline{e}_i$$

$$\underline{H}_t = Y_o \frac{1-\Gamma}{1+\Gamma}\, V_o\underline{h}_o - \sum_i Y_i V_i \underline{h}_i \qquad 3.39$$

The mode voltages at the plane of the slot are defined by:

$$V_i = \iint_A \underline{E}^a \cdot \underline{e}_i \, da \qquad 3.40$$

A variational solution for the slot admittance may be obtained by conserving the "flux of reaction" through the slot. That is,

$$\iint_{\substack{\text{interior}\\ \text{surface of A}}} \underline{E}^a \times \underline{H} \, da = \iint_{\substack{\text{exterior}\\ \text{surface of A}}} \underline{E}^a \times \underline{H} \, da \qquad 3.41$$

Since we have assumed $\underline{E}^a$ in the slot, this is another statement of the continuity of $\underline{H}$ at the slot and, if $\underline{E}^a$ is real, Eqn. 3.41 also implies conservation of complex power through the slot. In the latter case, an aperture admittance, y_s, can be defined

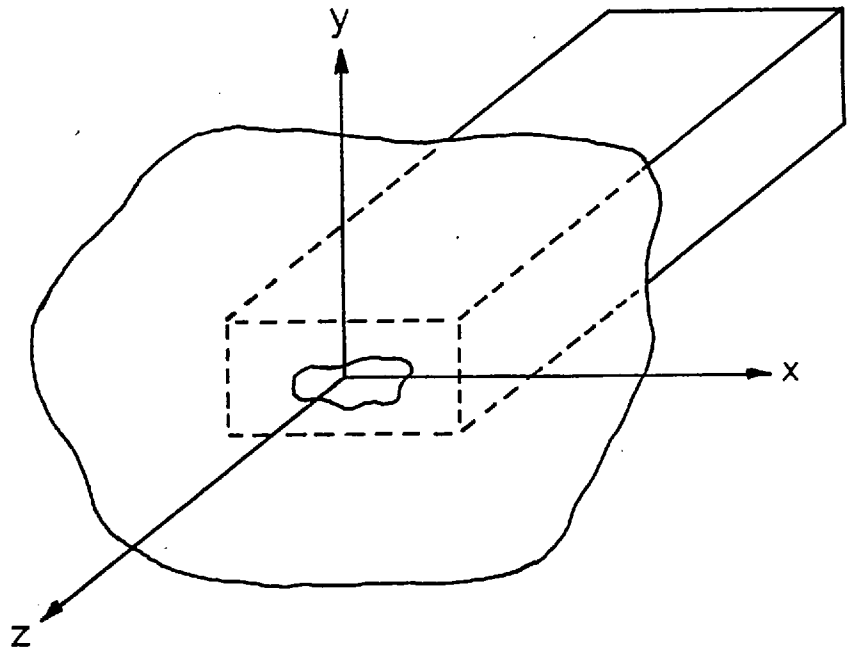

Fig. 3.8: Aperture in the end wall of cylindrical waveguide.

such that

$$v^2 y_s = \iint_{\text{exterior}} \underline{E}^a \times \underline{H} \, da \qquad 3.42$$

where v is an arbitrary voltage defined in the slot.

Substituting Eqns. 3.42 and 3.39 into Eqn. 3.41 yields:

$$\frac{1-\Gamma}{1+\Gamma} \; V_o^2 Y_o - \sum_i V_i^2 Y_i = v^2 y_s \qquad 3.43$$

The admittance presented to the TE_{10} mode is:

$$Y = \frac{1-\Gamma}{1+\Gamma} = \frac{\sum V_i^2 Y_i + v^2 y_s}{V_o^2 Y_o} \qquad 3.44$$

The calculation of Y for various slot shapes is considered in section 3.4.

3.3. THE EQUIVALENT CIRCUIT OF A SLOT IN THE SIDE WALL OF A RECTANGULAR WAVEGUIDE

The normalised shunt impedance of a slot in the side wall of rectangular waveguide, z_s, is defined in Eqn. 3.33. The numerator may be split into two integrals, one with an integrand including $\bar{\beta}$ and the other with an integrand including $\bar{y}$. This second integral is just:

$$\iint_A \underline{H}.\underline{n}\times\underline{E}^a \, da \qquad 3.45$$

which may be re-arranged to give:

$$\iint_A \underline{E}^a \times \underline{H} \, da = v^2 y_s \qquad 3.46$$

as defined for the end wall slot.

If v is defined to be the voltage across the slot centre and if the assumed electric field in the slot, $\underline{E}^a$, is normalised to this voltage, V^2 may be factorised from the integral expression in the denominator. Z_s can then be expressed as:

$$Z_s = \frac{Y_s}{K^2} + jX \qquad 3.47$$

where $K^2 = Y_o^2 [\iint_A \underline{n} \times \underline{E}^a, \underline{h}_{zo} \cos\gamma_o z \, da]^2$

and $$jX = \frac{\iint \iint \underline{n} \times \underline{E}^a . j\overline{\beta} . \underline{n} \times \underline{E}^a \, da \, da}{Y_o [\iint \underline{n} \times \underline{E}^a . \underline{h}_{zo} \cos\gamma_o z \, da]^2}$$

Eqn. 3.47 may be represented by the network shown in Figure 3.3.

3.3.1. Narrow Rectangular Slots

Consider the slot shown in Figure 3.9. For a single slot near half-wave resonance, a good approximation for the electric field is (with the necessary normalisation):

$$\underline{E}^a = \frac{1}{\omega} \cos \frac{\pi z}{2\ell} \hat{\underline{y}} \qquad 3.48$$

where ω is the slot width

2ℓ is the slot length

and $\hat{y}$ is a vector in the y direction.

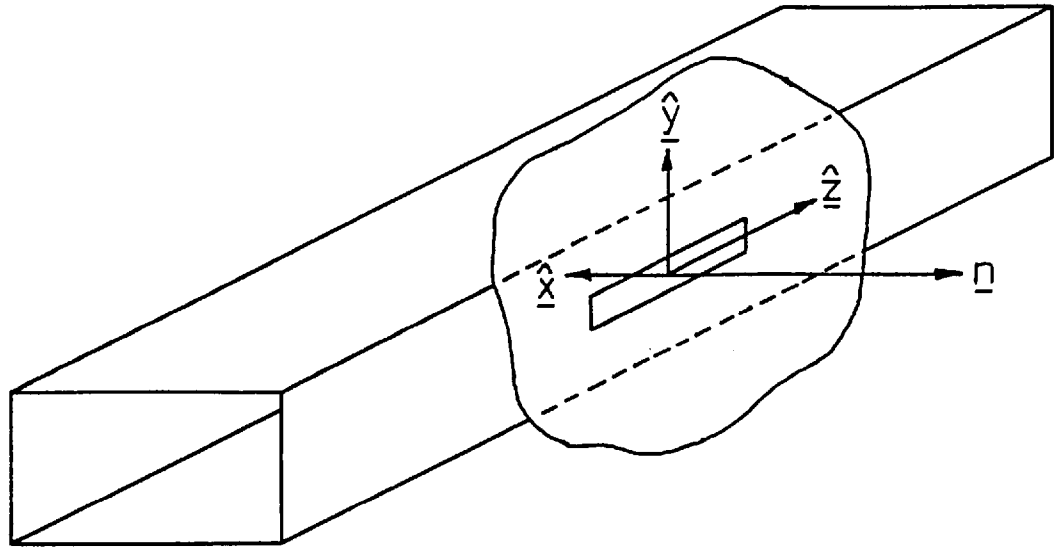

Fig. 3.9: Longitudinal straight slot in the side wall of a rectangular waveguide.

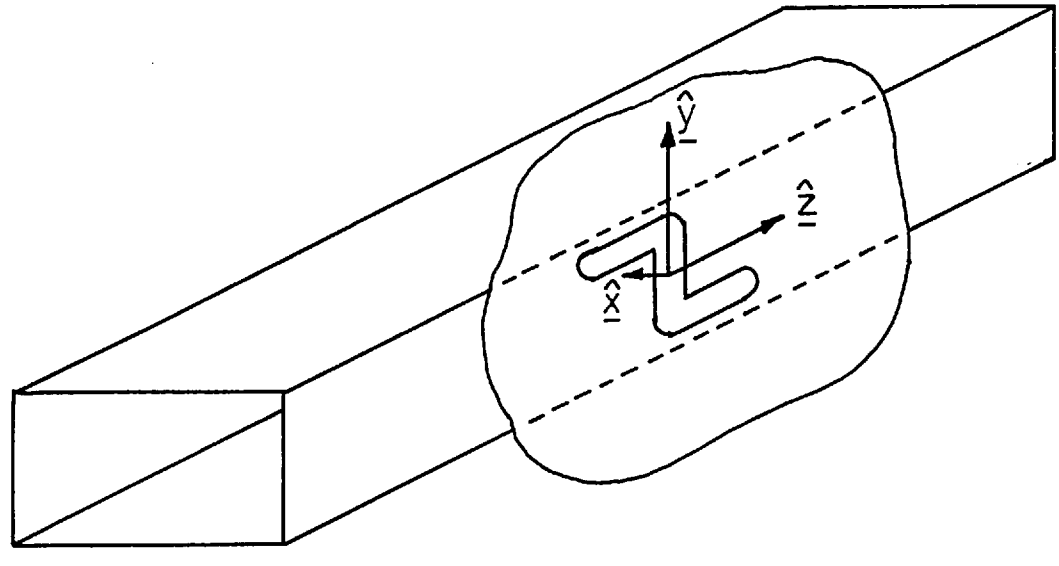

Fig. 3.10: 7 shaped slot in the side wall of rectangular waveguide.

Then,

$$\underline{n} \times \underline{E}^a = -\frac{1}{\omega} \cos \frac{\pi z}{2\ell} \hat{\underline{z}} \qquad 3.49$$

For the TE_{10} mode:

$$\underline{h}_{zo} = \frac{2}{ab} \frac{\pi}{a\gamma_o} \cos \frac{\pi x}{a} \qquad 3.50$$

K^2 is then given by

$$K^2 = Y_o \left| \iint_A \frac{1}{\omega} \frac{2}{ab} \frac{\pi}{a\gamma_o} \cos\gamma_o z \cos \frac{\pi z}{2\ell} \, da \right|^2$$

$$K^2 = \frac{2Y_o \pi^4 \cos^2\gamma_o \ell}{a^3 b \gamma_o^2 \ell^2 (\frac{\pi^2}{4\ell^2} - \gamma_o^2)^2} \qquad 3.51$$

3.3.2. Narrow "Z" Slots

The geometry of the slot is shown in Figure 3.10. This slot is one of the configurations, developed at Imperial College to reduce the coupling losses incurred with some compact slots.[1]. Here it is assumed that the discontinuity at the corners is small such that the field distribution remains essentially co-sinusoidal. That is, the electric field in the horizontal arms (which provide the only contribution to the coupling to the TE_{10} waveguide mode) may be expressed as:

$$\underline{E}^a = \frac{1}{\omega} \cos \frac{\pi(\ell + |z|)}{2(d+\ell)} \hat{\underline{y}} \qquad 3.52$$

where d is the effective length of the horizontal arms

and 2ℓ is the effective length of the vertical centre section.

Then, following the procedure used for the straight slot

$$K^2 = \frac{2\gamma_o \pi^4 (\cos\gamma_o d - \sin\frac{\pi\ell}{2(d+\ell)})^2}{a^3 b \gamma_o^2 (d+\ell)^2 (\frac{\pi^2}{4(d+\ell)^2} - \gamma_o^2)^2} \qquad 3.53a$$

3.3.3. Narrow 'I' shaped slots

The I shaped slot was developed from the Z-shaped slot to provide a variable coupling to the TE_{10} waveguide mode.[1] The resonant frequency can be estimated by considering the equivalent transverse network with the arms represented by equivalent transmission lines. The effective lengths have been established empirically as ℓ_a, ℓ_b and ℓ_c as shown in Figure 3.11. At the tee-junctions the electric fields in the end arms are generated in opposition as depicted in Figure 3.11. and their input impedances are in series across the end of the centre section. Then, for resonance,

$$\tan \beta\ell_a + \tan \beta\ell_b = \cot \beta\ell_c \qquad 3.53b$$

where β is the propagation constant of the equivalent transmission line.

The electric fields in the end arms, assuming a sinusoidal distribution in the slot, and, with a unit voltage across the centre of the slot, may be expressed as:

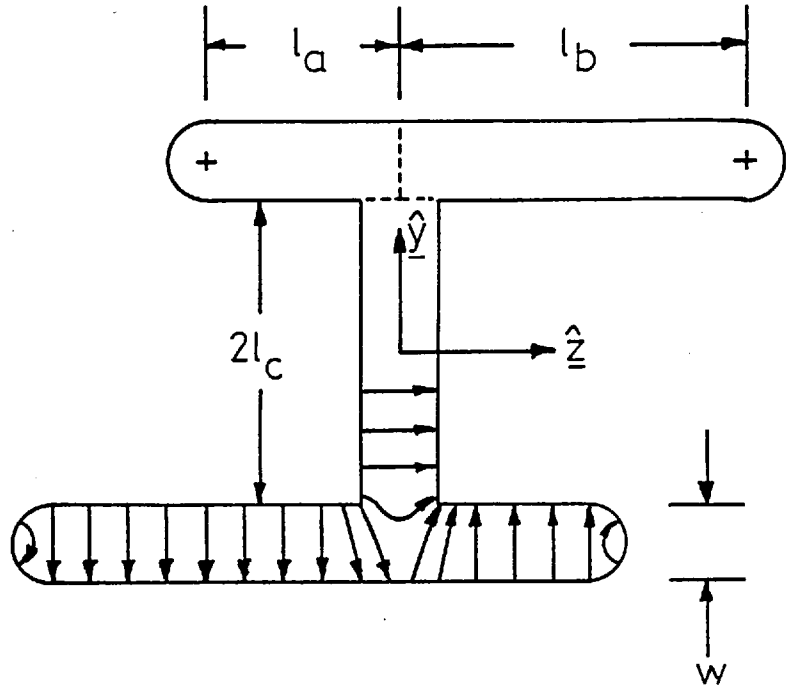

Fig. 3.11: Electric fields in I shaped slots.

$$\underline{E}_a^a = \frac{1}{\omega} \frac{\sin \beta\ell_c}{\cos \beta\ell_a} \sin \beta(\ell_a - |z|)$$

$$\underline{E}_b^a = -\frac{1}{\omega} \frac{\sin \beta\ell_c}{\cos \beta\ell_b} \sin \beta(\ell_b - |z|) \qquad 3.54$$

where the subscripts refer to the arms labelled in Figure 3.11.

Then, using the procedure described in section 3.3.1:

$$K^2 = \frac{\gamma Y_o \pi^2 \beta^2 \sin^2 \beta\ell_c}{a^3 b \gamma_o^2 (\gamma_o^2 - \beta^2)^2} \left\{ \frac{\cos \gamma_o \ell_b}{\cos \beta\ell_b} - \frac{\cos \gamma_o \ell_a}{\cos \beta\ell_a} \right\}^2 \qquad 3.55$$

3.4. THE EQUIVALENT CIRCUIT OF A SLOT IN THE END WALL OF A RECTANGULAR WAVEGUIDE

The expression for the normalised admittance of an end wall slot suggests the equivalent circuit shown in Figure 3.2. From Eqn. 3.44:

$$n^2 = \frac{v^2}{V_o^2 Y_o} \qquad 3.56$$

$$jB = \frac{\Sigma Y_i V_i^2}{V_o^2 Y_o}$$

3.4.1. Narrow Rectangular slot

The slot is positioned as shown in Figure 3.12. For the TE_{10} mode:

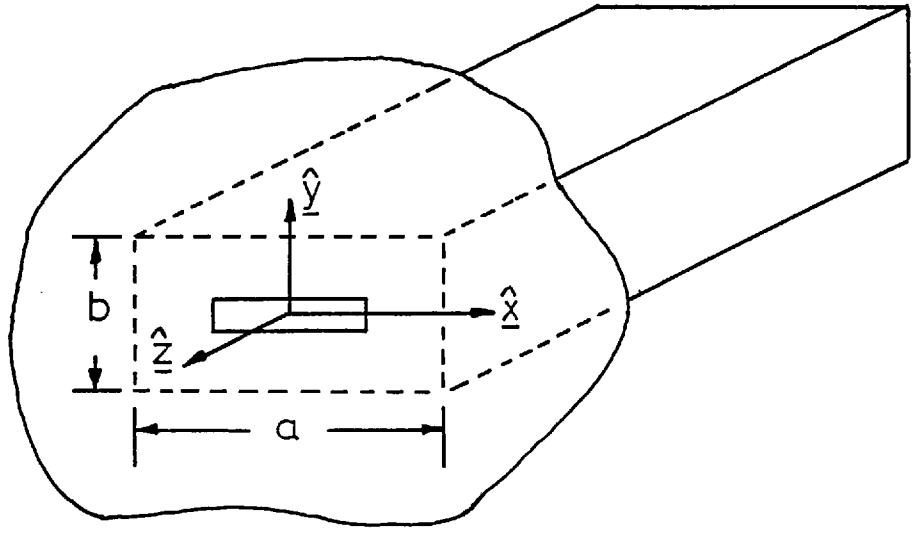

Fig. 3.12: Straight slot in the end wall of rectangular waveguide.

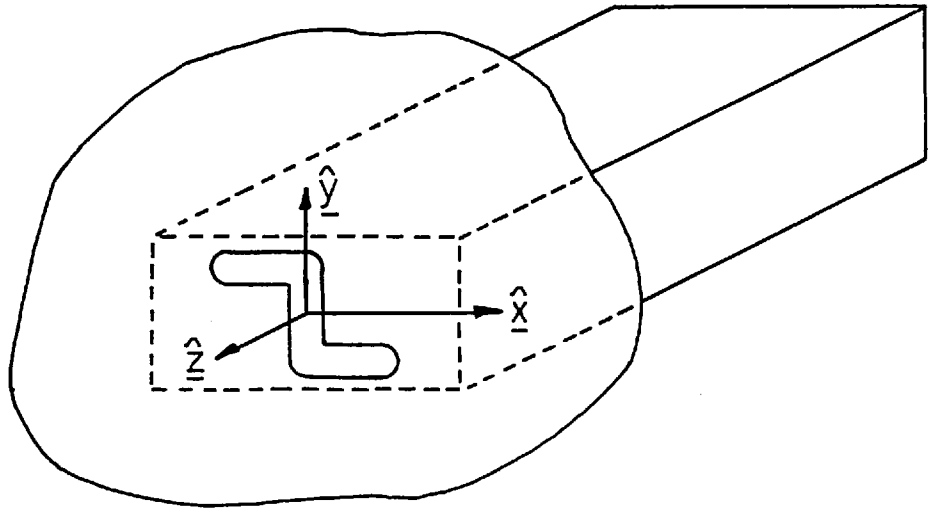

Fig. 3.13: Z shaped slot in the end wall of rectangular waveguide.

$$\underline{e}_o = \frac{2}{ab} \cos \frac{\pi x}{a} \hat{\underline{y}} \qquad 3.57$$

Assuming a slot field of the same form as in the side wall slot, let:

$$\underline{E}^a = \frac{v}{\omega} \cos \frac{\pi x}{2\ell} \hat{\underline{y}} \qquad 3.58$$

Then,

$$V_o = \iint_A \frac{v}{\omega} \frac{2}{ab} \cos \frac{\pi x}{a} \cos \frac{\pi x}{2\ell} \, da \qquad 3.59$$

This gives:

$$n^2 = \frac{\pi^2 ab\ell^2}{2Y_o \cos^2(\frac{\pi\ell}{a})} \left\{ \frac{1}{4\ell^2} - \frac{1}{a^2} \right\}^2 \qquad 3.60$$

3.4.2. Narrow Z slot

The slot configuration is depicted in Figure 3.13. The same assumptions concerning the electric field in the Z slot in the side wall may be made here. Then the electric field in the end arms can be expressed as:

$$\underline{E}^a = \frac{v}{\omega} \cos \frac{\pi(d+|x|)}{2(d+\ell)} \hat{\underline{y}} \qquad 3.61$$

Following the procedure used in the previous section

$$V_o = \iint_A \frac{2}{ab} \frac{v}{\omega} \cos \frac{\pi x}{a} \cos \frac{\pi(d+|x|)}{2(d+\ell)} \, da \qquad 3.62$$

This yields

$$n^2 = \frac{ab\ell^2\pi^2}{2Y_o\left(\cos\frac{\pi\ell}{a} - \sin\frac{\pi\ell}{2(d+\ell)}\right)^2}\left\{\frac{1}{4(d+\ell)^2} - \frac{1}{a^2}\right\}^2 \qquad 3.63$$

3.4.3. Narrow I slot

For the slot shape of Figure 3.11 and with the fields in the end arms as described in Eqns. 3.59, n^2 is given by:

$$n^2 = \frac{ab\left(\frac{\pi^2}{a^2} - \beta^2\right)^2}{\gamma Y_o \beta^2 \sin^2\beta\ell_c\left\{\frac{\cos\frac{\pi\ell_b}{a}}{\cos\beta\ell_b} - \frac{\cos\frac{\pi\ell_a}{b}}{\cos\beta\ell_a}\right\}^2} \qquad 3.64$$

3.5. EXPERIMENTAL INVESTIGATIONS OF SLOT EQUIVALENT CIRCUITS

The validity of the equivalent circuits derived for straight and Z shaped slots has been examined experimentally. For convenience, measurements have been made at X-band, with the slots milled in WG16 rectangular waveguide. The dimensions of the slots, which are resonant around 9 GHz, are provided in Figure 3.14. For ease of manufacture the ends of the slots are rounded. This may be allowed for in the calculation of the equivalent circuit coupling parameters by using effective slot lengths determined empirically from measurements of the resonant frequencies of

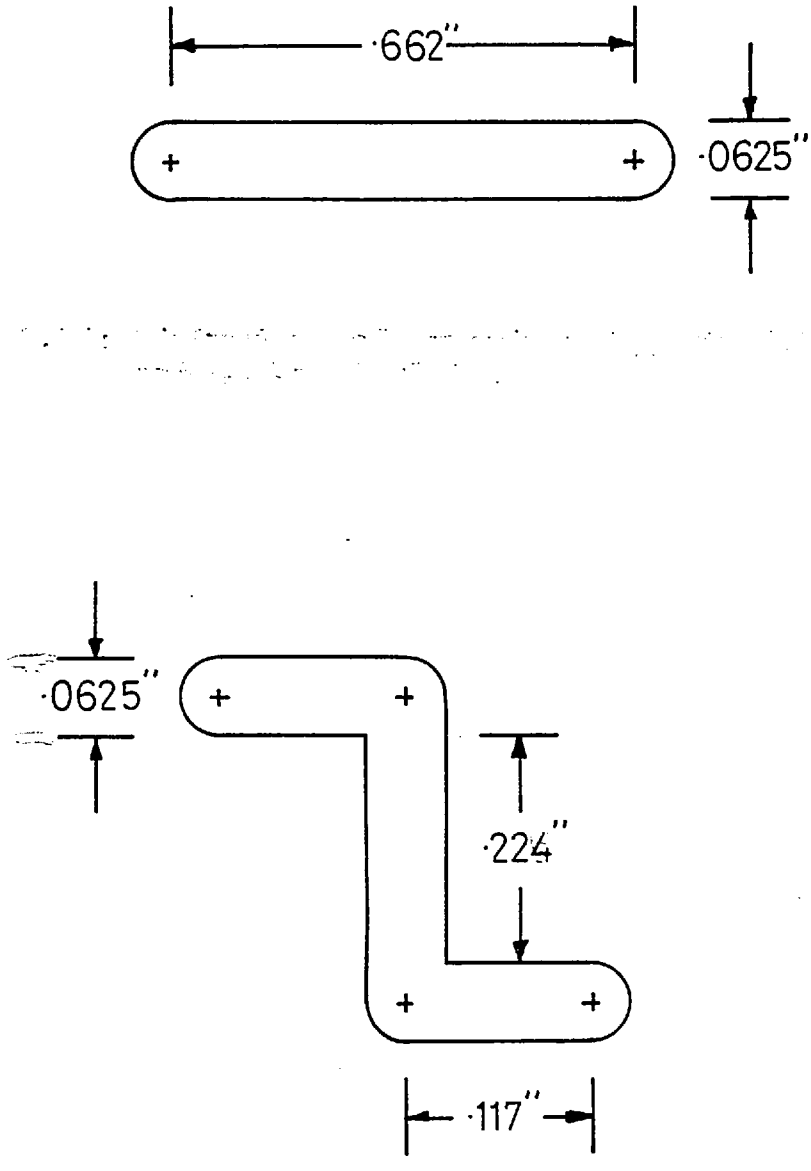

Fig. 3.14: Dimensions of experimental straight and Z shaped slots.

the various slots. Values of n^2 and K^2 are plotted in Figure 3.15 as a function of frequency for the slots shown in Figure 3.14.

The finite thickness of the slot (here the thickness of the waveguide wall) was not accounted for in the theoretical analyses. Its effect may be included in the equivalent circuits by treating the slot as a short length of waveguide [21]. It is assumed that the only significant coupling arises from the dominant mode; as the thickness involved is very small, this is obviously very approximate. The modified equivalent circuit is shown in Figure 3.15 for the case of the end fed slot, the side wall slot may be similarly modified. Approximate values for the transmission line properties of rectangular waveguide with rounded side walls are given in Reference 31 and have been used in admittance calculations of the straight slots. The inclusion of this effect had an insignificant effect on the results and it was not considered necessary to treat the more complicated 'Z' shaped slot in the same fashion.

It was noted in Section 3.2. that the calculation of B and X is generally very difficult and here the quantities were measured experimentally. The measurement of B is quite straightforward, being half the susceptance of the equivalent iris. X is more difficult to evaluate, but can be obtained by measuring the shunt impedance of a tee-network coupling through the slot in question. The arrangement is shown in Figure 3.17, for which the equivalent circuit is that drawn in Figure 3.18. The only unknown parameter in Figure 3.18 (assuming theoretical values for n^2 and K^2) is X.

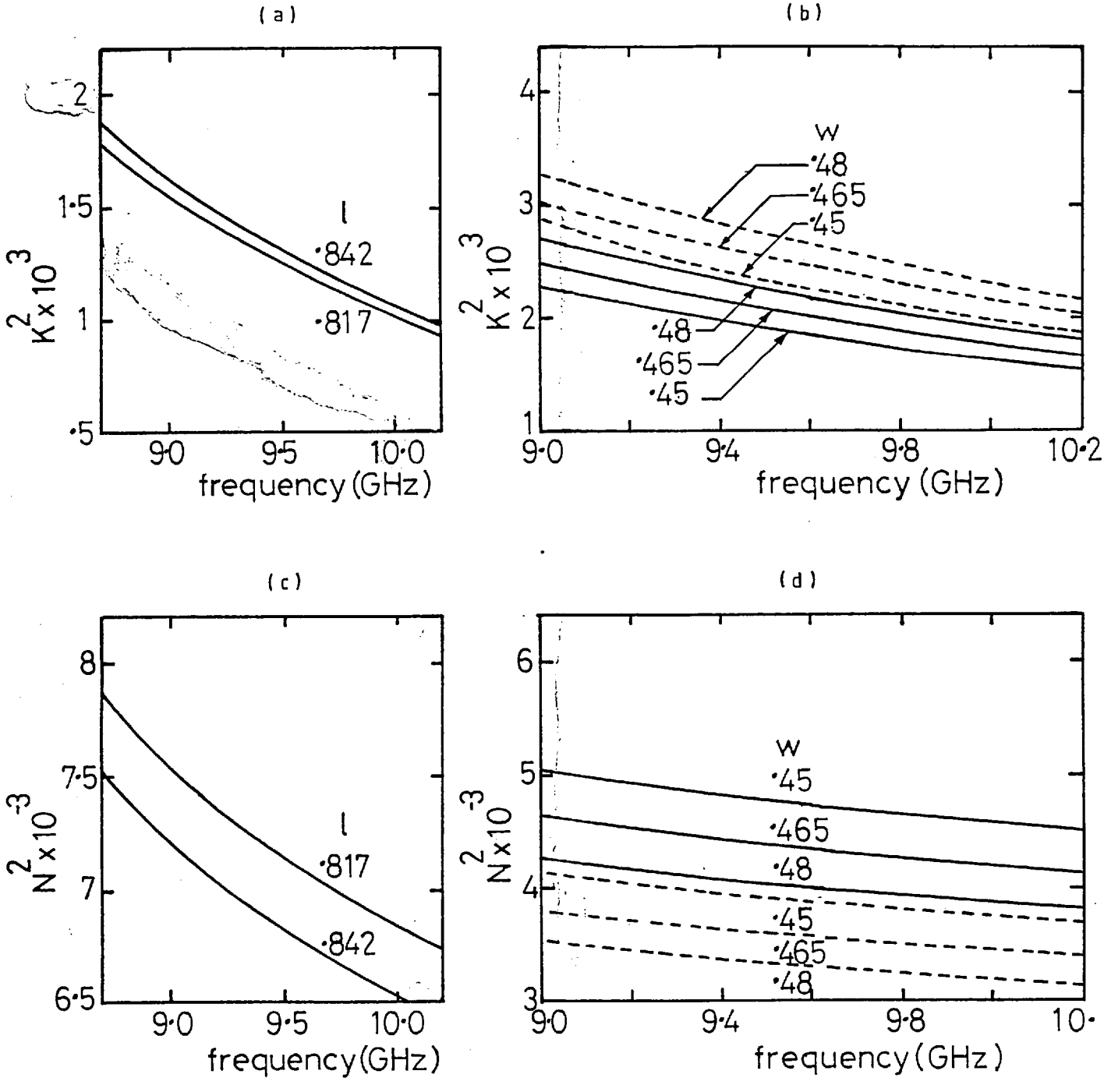

Fig. 3.15: Waveguide coupling parameters as a function of frequency.

(a) K^2 for straight slot in side wall of rectangular waveguide.

(b) N^2 for straight slot in end wall of rectangular waveguide.

(c) K^2 for Z shaped slot in side wall of rectangular waveguide.

(d) N^2 for Z shaped slot in end wall of rectangular waveguide.

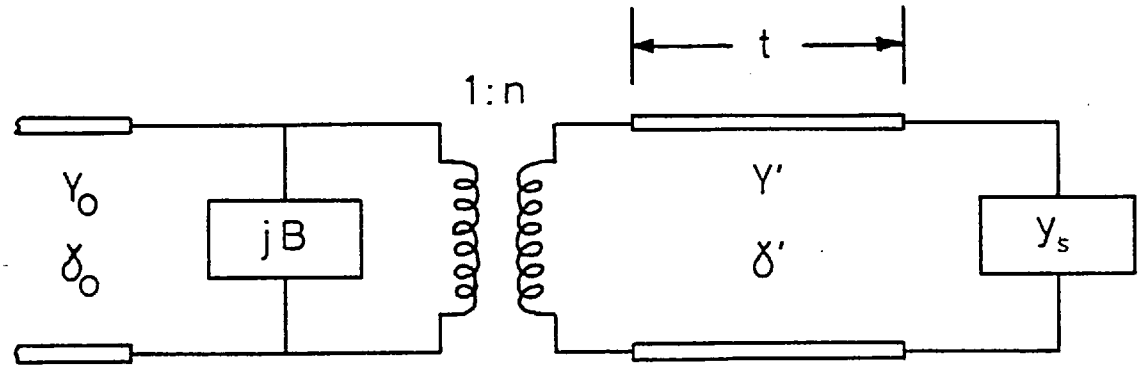

Fig. 3.16: Equivalent circuit of an end wall slot with finite wall thickness.

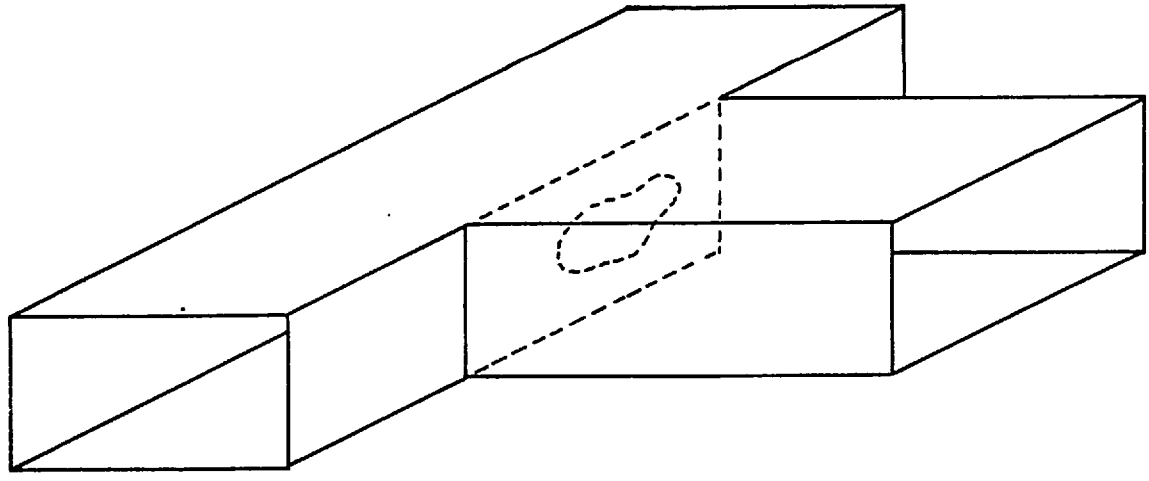

Fig. 3.17: Tee network.

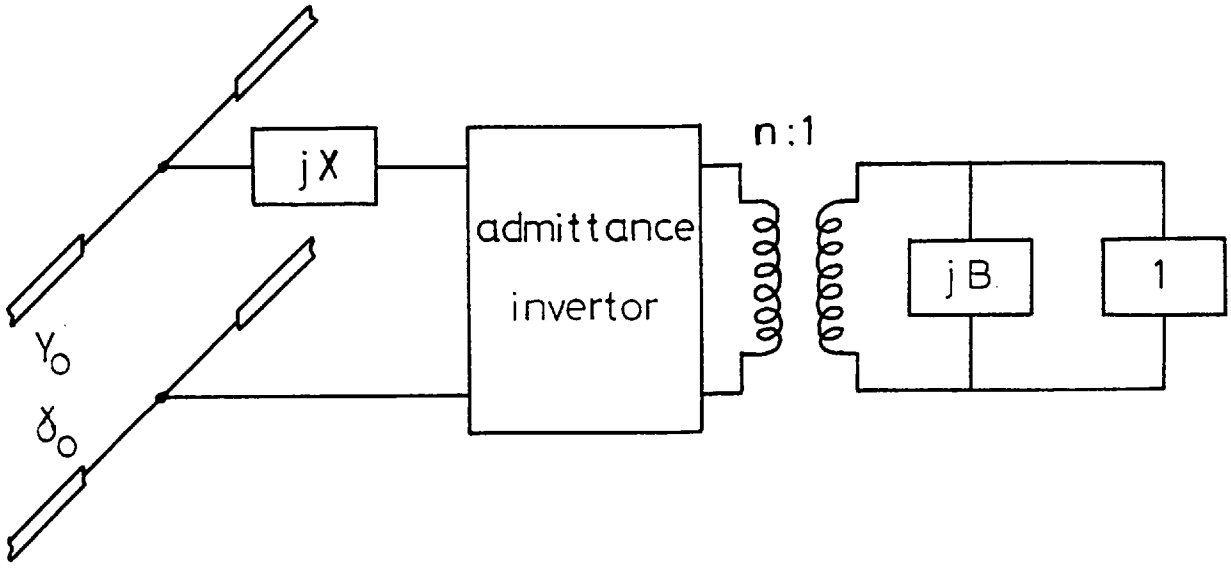

Fig. 3.18: Equivalent circuit of a tee-network.

The normalised slot admittances (or impedances) were measured using standard slotted line techniques. The slot position in the side wall case was established by setting up a large standing wave in the waveguide with a moveable short circuit such that the power radiated by the slot was a minimum. Since the slot is a shunt element in the dominant mode transmission line, this corresponds to a minimum in the voltage standing wave. The position of the standing wave detector probe could then be accurately related to the slot position as a function of the guide wavelength. In the measurement of the end wall slot, the slot position was established directly by shorting out the slot with conducting adhesive aluminium tape.

All measurements were carried out with metal sheets placed flush with the waveguide wall to form a ground plane. The joints were taped over to ensure reasonable electrical continuity. The sheets were approximately three wavelengths square; any increase in their size had no noticeable effect on the slot impedance and it was thus assumed that the ground plane was sufficiently large to simulate an infinite baffle.

The results are presented in two sections, dealing with straight slots and 'Z' shaped slots separately.

3.5.1. Straight slots

The results are summarised in Figures 3.19, 3.20 and 3.21. First, it may be noted that the slot in the side wall is resonant at a significantly higher frequency than that in the end wall. This suggests a higher internal reactance associated with the side wall slot in the region of the resonant

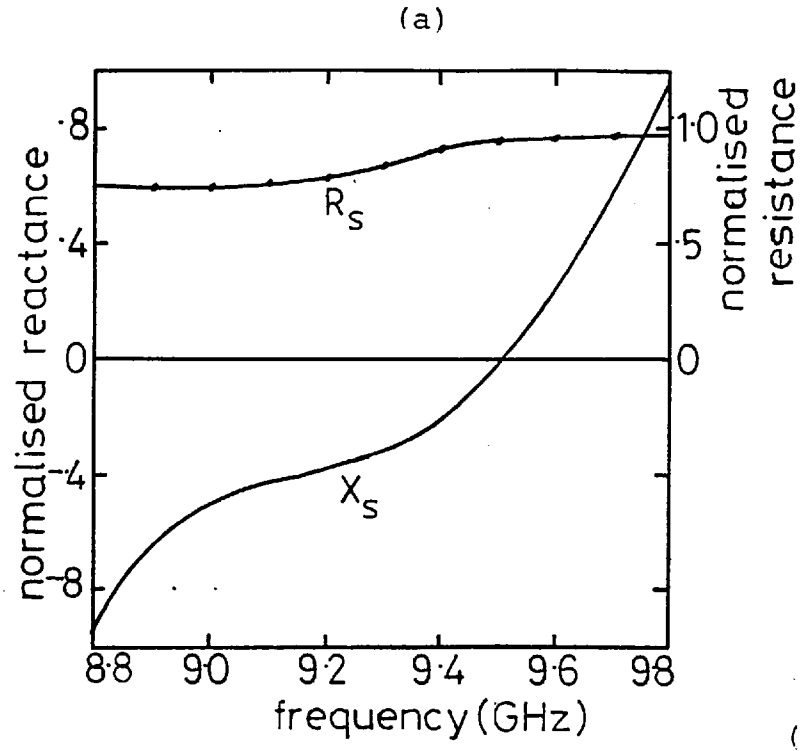

Fig. 3.19: Impedance characteristics of straight slot in a side wall and associated tee-network.

(a) slot in side wall
(b) tee-network.
(c) equivalent reactance of side arm of tee-network and derived internal reactance of slot (corresponding to energy stored in main guide).

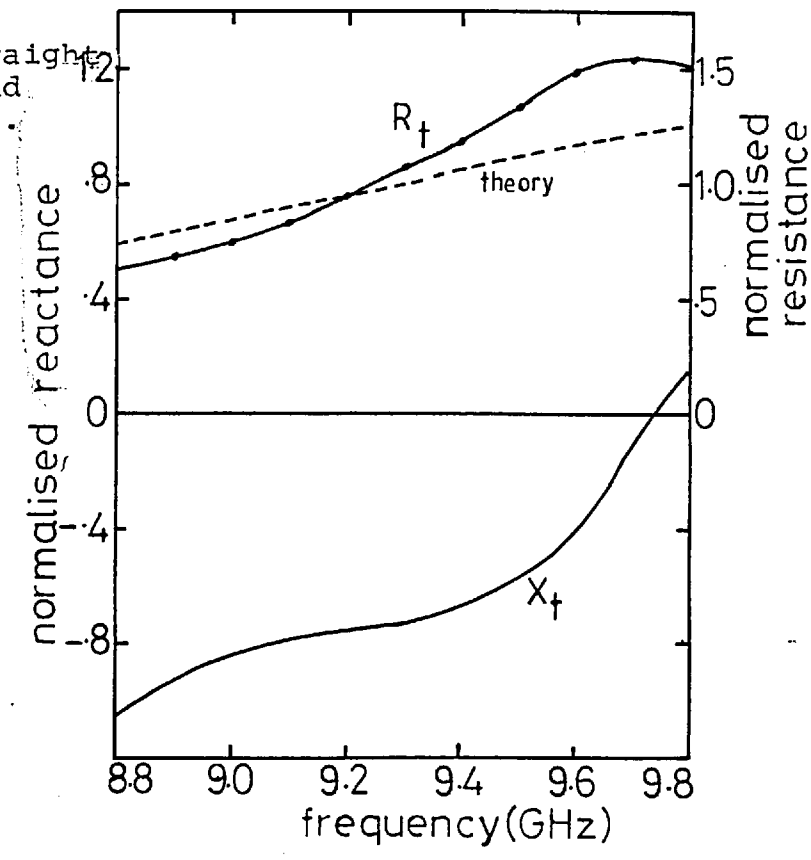

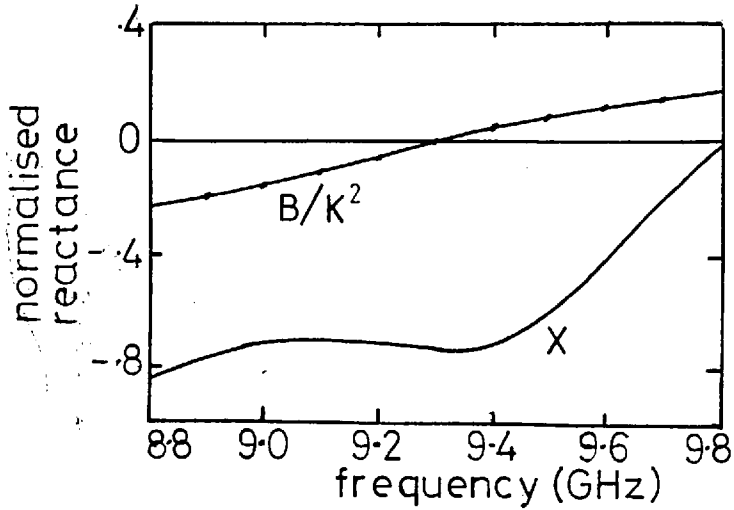

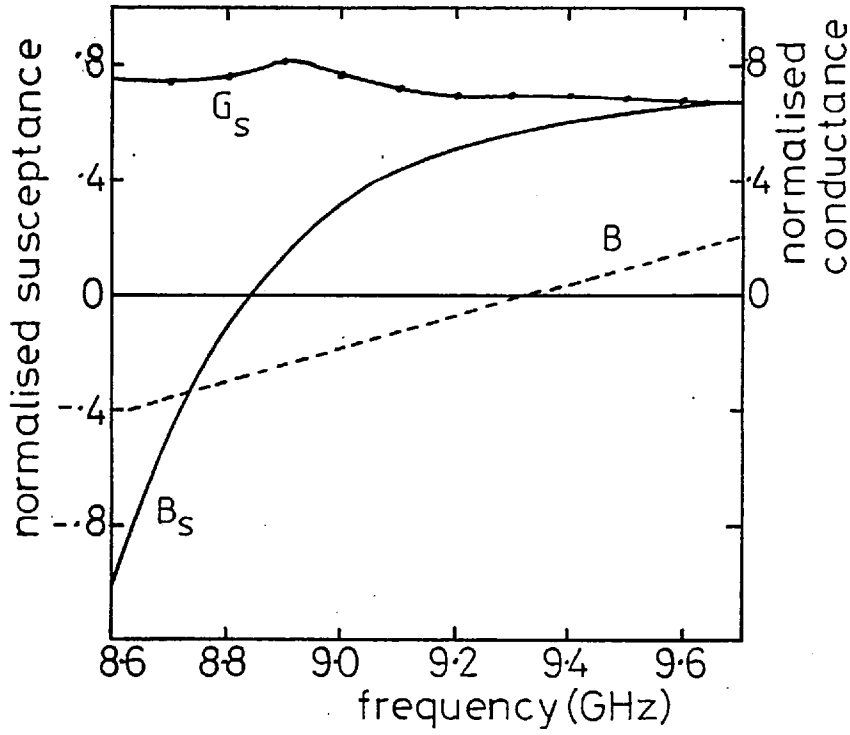

Fig. 3.20: Admittance characteristics of straight slot in end wall.

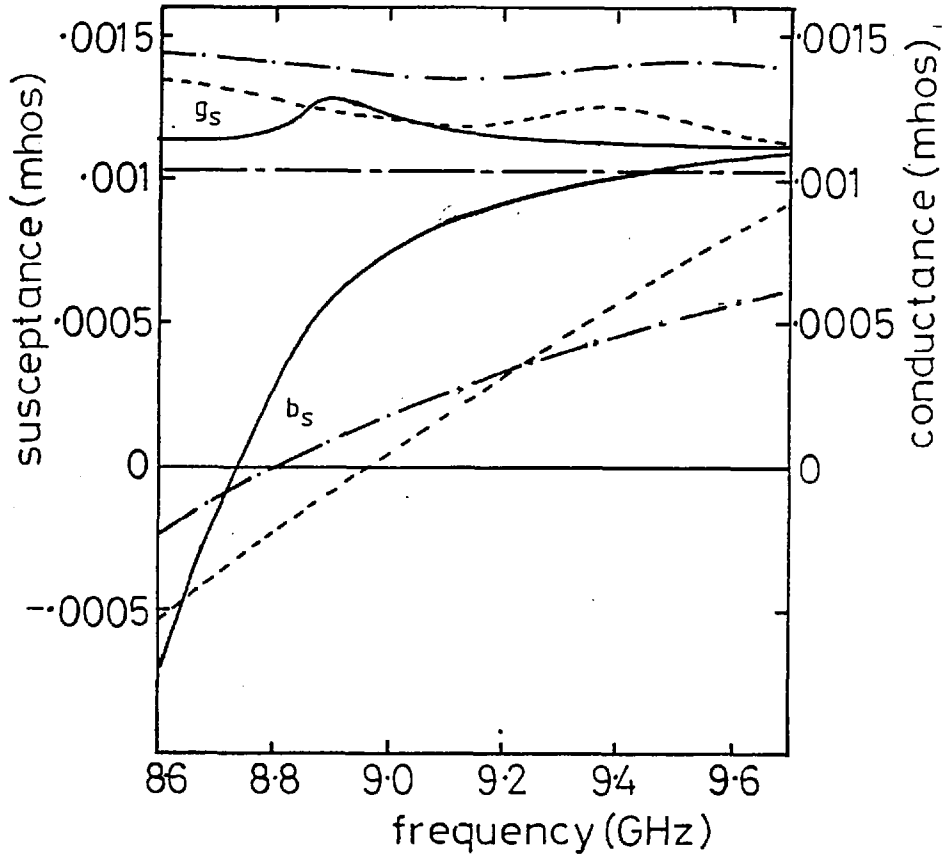

Fig. 3.21: Admittance characteristics of isolated straight slot.

- - - - - - - - - side wall.

———————— end wall slots.

———·———·— Putnam's results for rectangular slot, scaled to provide a resonant frequency at 8.8GHz (width/length = .114)

———- ——— conductance obtained by Babinet's principle from equivalent dipole.

frequency of the isolated slot, this is in fact the case as seen in Figure 3.19c)which includes a plot of the internal reactance, derived from the tee-network. Figure 3.21 shows the comparison between the values of the admittance obtained for the isolated slot from the two sets of waveguide measurements. A comparison is also made with Putnam's results [28] which were obtained for a UHF rectangular slot fed with a twin wire transmission line connected across the centre of the slot. Here the slots have been scaled to an arbitrary resonant frequency of 8.8 GHz. As expected the conductance values are reasonably constant through resonance and well correlated although the waveguide derived results are lower than those obtained by Putnam. It is thought that the difference is due mainly to the inherent difficulties associated with Putnam's measurement, the system is extremely prone to scattering from the transmission line structure. Also, the ratios n^2 and K^2 are not exact as can be seen from a comparison of the theoretical and experimental plots of the resistance of the tee-network. The susceptance curves differ both in slope and resonant frequency, the difference in the latter being approximately 200 MHz. These are, however, to be expected, with the difficulty in reproducing the slot dimensions exactly in the three experimental assemblies and the possible errors in the measurement.

3.5.2. Z shaped slots

The corresponding results for the Z shaped slots are given in Figures 3.22, 3.23 and 3.24. It may be noted that the waveguide susceptances are all monotonic, although the internal susceptance derived for the side wall slot does not pass

(a) slot in side wall

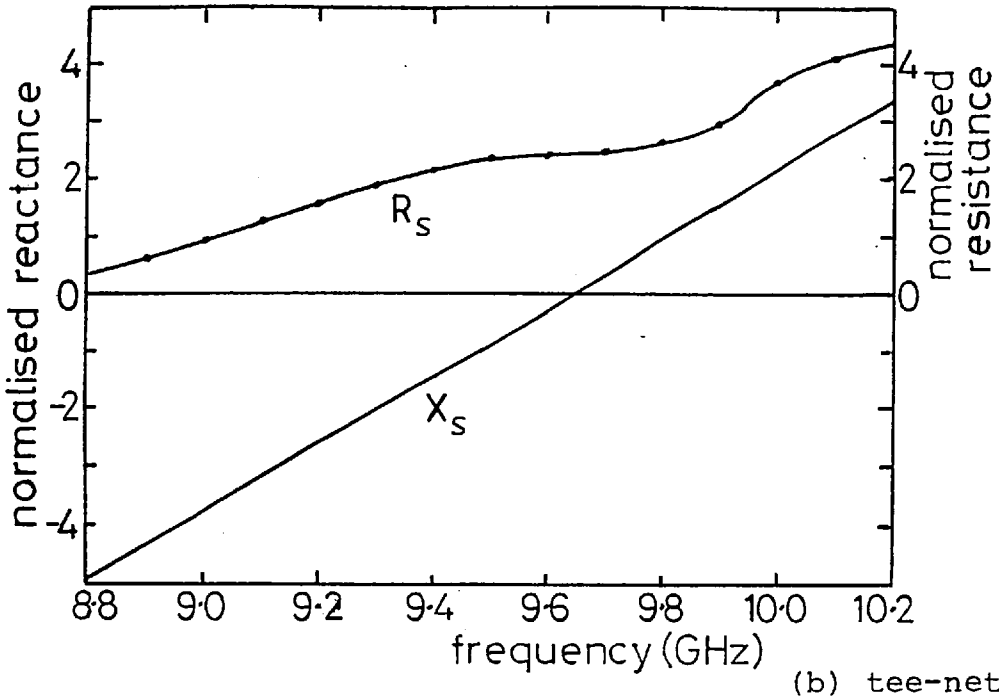

(b) tee-network.

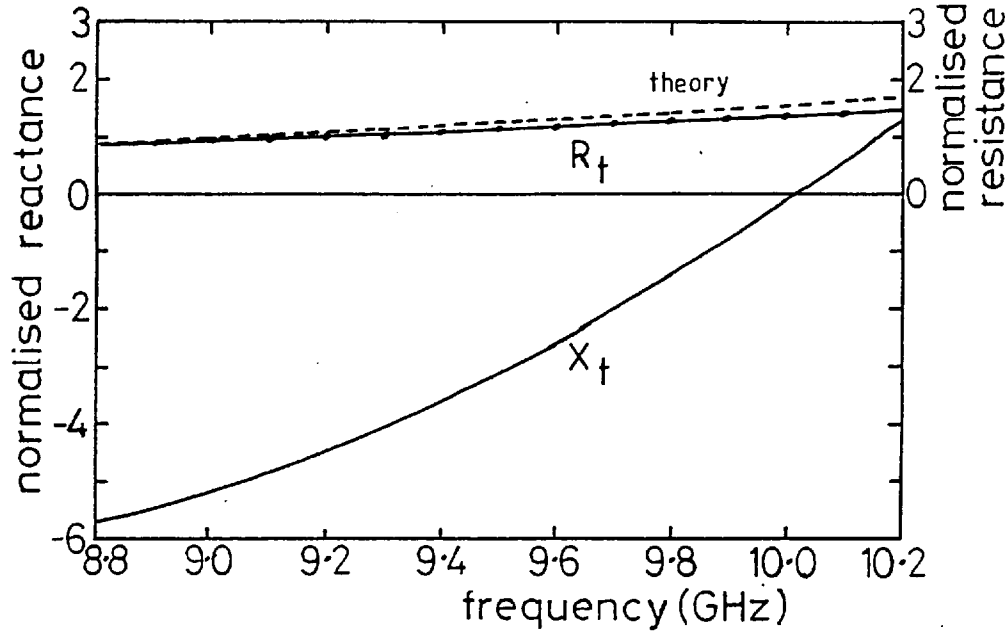

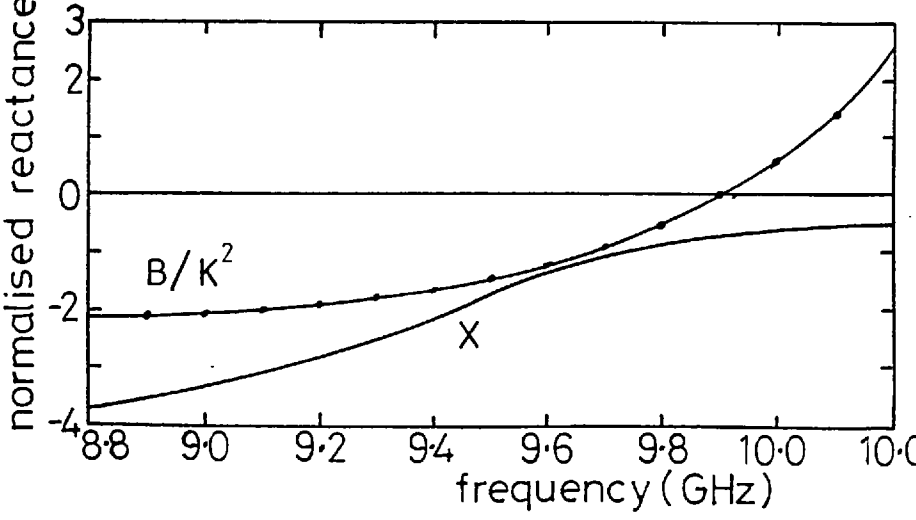

(c) equivalent reactance of side arm of tee-network and derived internal reactance of slot

Fig. 3.22: Impedance characteristics of Z shaped slot in side wall and associated tee-network.

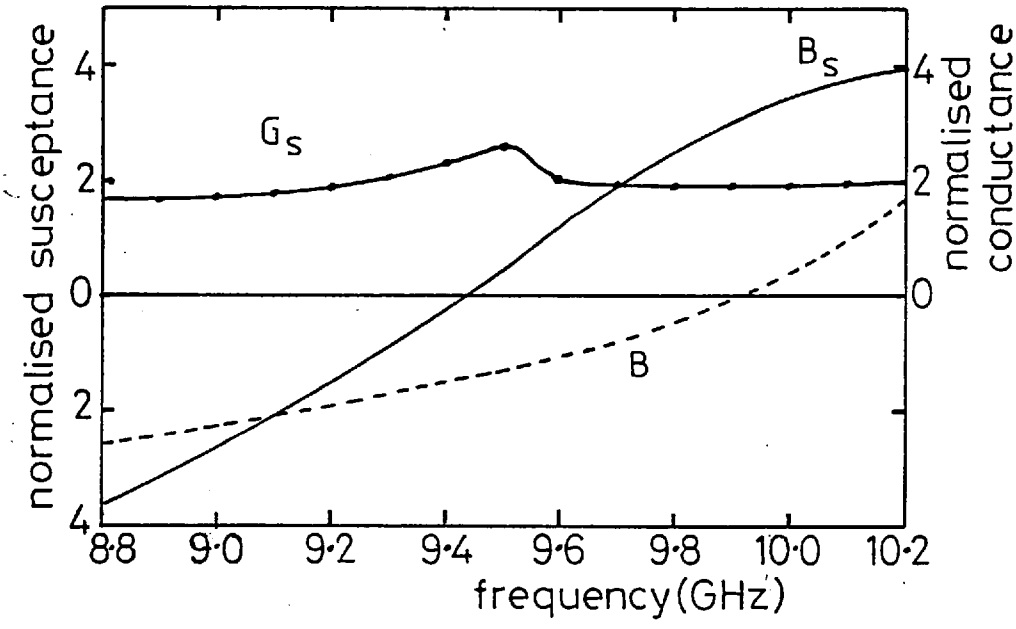

Fig. 3.23: Admittance characteristics of Z shaped slot in end wall.

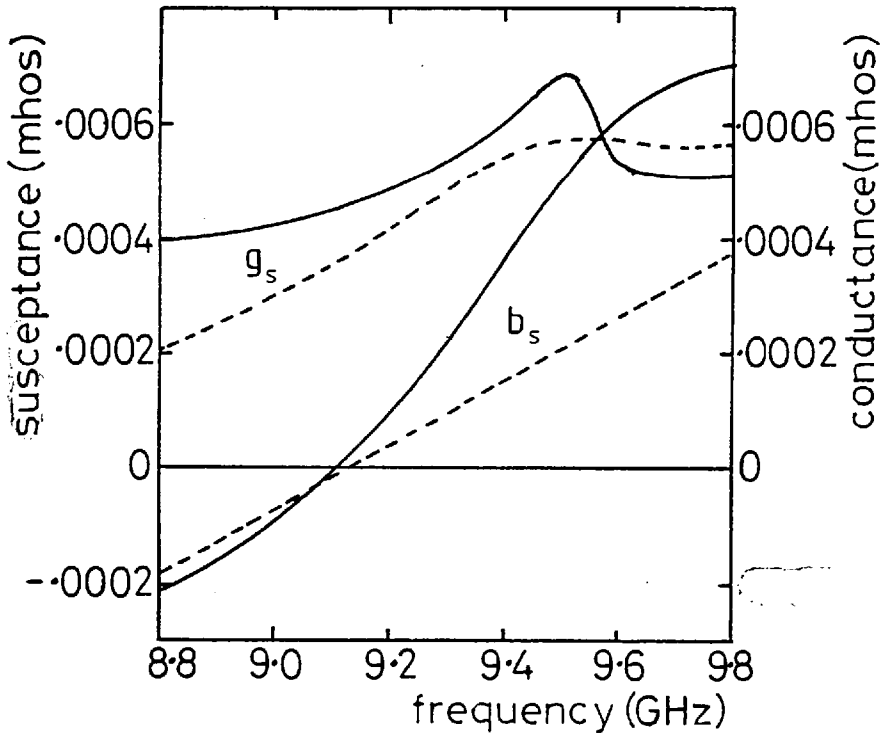

Fig. 3.24: Admittance characteristics of isolated Z shaped slot.

———— end wall slot

-------- side wall slot

through zero in the region of interest. The admittance of the isolated slots derived from the two sets of measurements are compared in Figure 3.24. Again there is a discrepancy in the slopes of the susceptance components although the resonant frequencies are only 20 MHz apart. The conductance curves are well correlated although there is a sharp peak in the end wall case. This is most likely due to measurement errors.

3.6. SUMMARY

Equivalent circuits which are valid about half-wave resonance have been derived theoretically for end and side wall slots. They have been used with experimental data to deduce the admittances of the isolated slots. Considering the accuracy of the measurements, the results are sufficiently well correlated to allow the equivalent circuits to be used with a good degree of confidence in mutual coupling models. The results for the Z shaped slots also provide some validation of the field representations used in the slot.

4. MUTUAL COUPLING MODELS IN WAVEGUIDE SLOT ARRAYS

4.1. SIMPLIFICATION OF THE MUTUAL COUPLING PROBLEM

Following a survey of the techniques available for the treatment of mutual coupling it was concluded in Chapter 2 that an admittance representation is most suited to the problem under consideration. For a two-dimensional array of stacked slotted waveguides the current i_{mn} associated with the m^{th} slot in the n^{th} waveguide is related to the voltages of the remaining slots by Eqn. 2.2 and is given by:

$$i_{mn} = \sum_p \sum_q y_{mn,pq} \, v_{pq} \qquad 4.1$$

where the double sum is taken over all the slots v_{pq} is the 'total' voltage on the (pq)th element as implied by the forced excitation concept (see section 2.2.1) and is the parameter which defines the radiation pattern of the array. $y_{mn,mn}$ is termed the self-admittance of the (mn)th slot and $y_{mn,pq}$ $(mn \neq pq)$ is termed the mutual admittance.

A major difficulty in using the mutual admittance approach is that the condition of forced excitation is rarely met and for most feed systems v is not independent of i. The complete network representation must then take account of the feed structure and the solution becomes extremely difficult except for very small arrays as the sum is slowly convergent. For many large arrays infinite array techniques have been used to obtain, either theoretically or experimentally (using a waveguide simulator), a value for the active admittance

$Y_{mn,pq}$ which is valid for slots not close to the array edge. As stated in secton 2.2.2, such a procedure is not valid for the aperture distributions used in the monopulse array and so alternative approximations must be sought to make the problem tractable.

The initial assumptions used to simplify the mutual coupling model were deduced from the geometry of the array face and using data obtained by Chignell [1]. To suppress the large cross polarised fields radiated by the end (horizontal) arms of the I shaped slots developed for the array, baffles were placed on the array surface. These were placed transverse to the axis of the waveguides to form parallel plate regions which are cut-off to the cross polarised fields as shown in Figure 4.1. Such baffles were incorporated in the several prototype linear arrays constructed using I shaped slots. The slots were milled in special reduced height waveguide (with internal dimensions 1.270" × .590") at spacings of 1.50" and were designed for resonance at 5.70 GHz (when covered with a thin layer of PTFE waterproofing tape). With .625" square baffles between the slots it was found that the mutual coupling had no significant effect on the aperture illumination. It was found, however that the mutual coupling between slots in adjacent waveguides and sharing the same trough formed by the baffles was not negligible. In an attempt to reduce this mutual coupling, chokes were placed on the top of the baffles to provide a better match at the array aperture and hence reduce the energy coupled back into the slots. It was found, however, that any reduction in the mutual coupling between slots in the transverse direction was accompanied by a corresponding increase

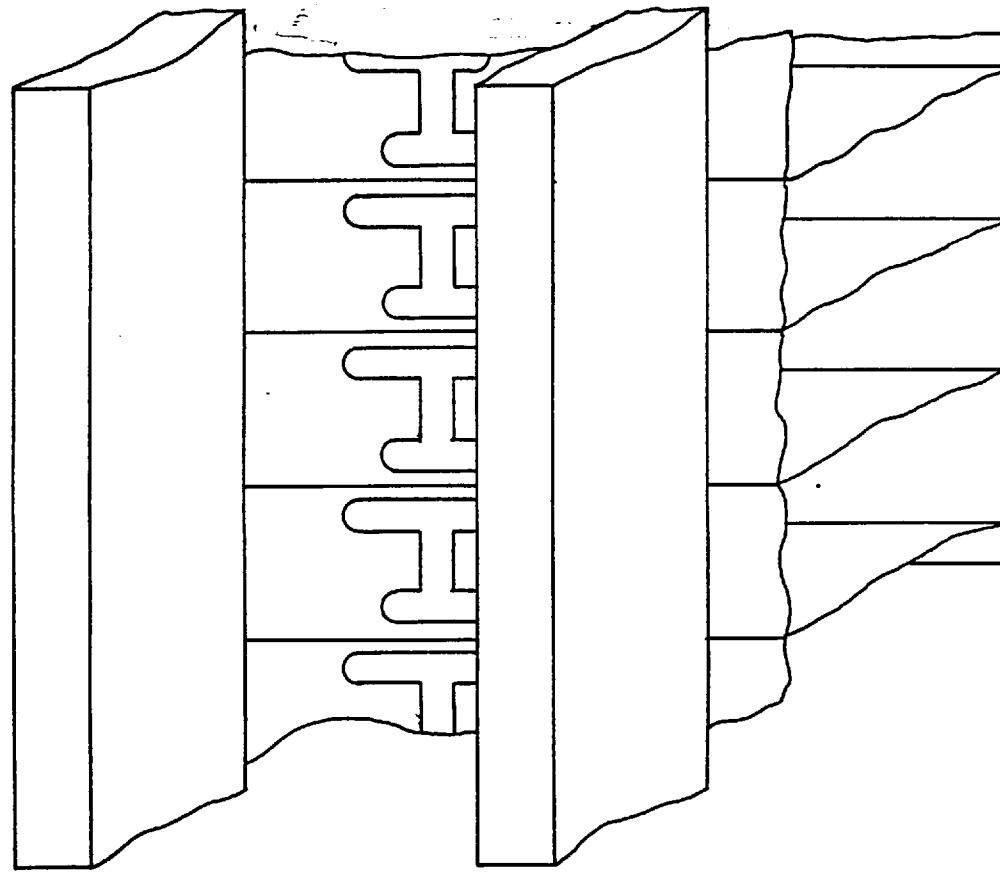

Fig. 4.1: Cross polarisation suppressors on slotted waveguide array.

in the mutual coupling over the baffles in the longitudinal direction. It was also observed from radiation pattern measurements that certain baffle configurations supported a leaky wave mode propagating in the direction of the baffles. Although only a small fraction of the radiated energy was coupled into the mode, it had the effect of increasing the effective aperture and reducing the element pattern beamwidth in the transverse plane. This would result in an unacceptable gain loss when phase scanning in this plane. Theoretical calculations confirmed that a channel type leaky wave mode could not be supported by the .625" square baffles and so these were retained in the final design, even though they do not provide optimum suppression of the cross polarisation. It did mean, however, that the mutual coupling problem was considerably simplified, in that only mutual coupling in the transverse direction need be considered. In the final array, only 8-waveguides are stacked and so the impedance sub-matrices (for each column of slots) for that case are only (8×8) matrices which are easily manipulated with digital computers.

In the following section the equivalent circuits developed in Chapter 3 for the isolated slot are used to examine the mutually coupled power between two waveguide-fed slots shown typically in Figure 4.2. and the effect of choosing different terminal positions.

4.1.2. MUTUAL COUPLING EQUIVALENT CIRCUIT WITH TERMINALS AT THE DOMINANT MODE TRANSMISSION LINE

It was shown in the previous chapter that a slot in the side wall of rectangular waveguide could be represented as

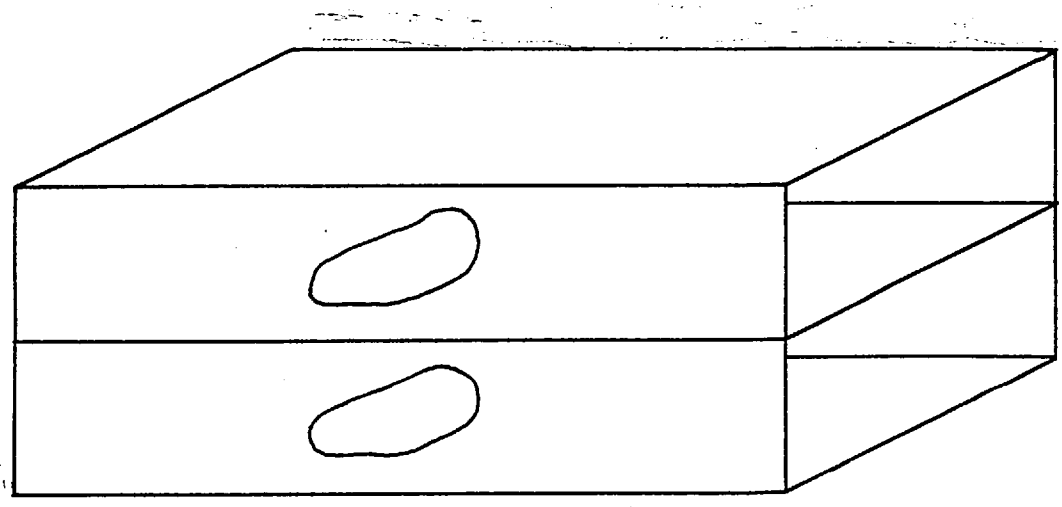

Fig. 4.2: Mutual coupling situation in adjacent slotted waveguides.

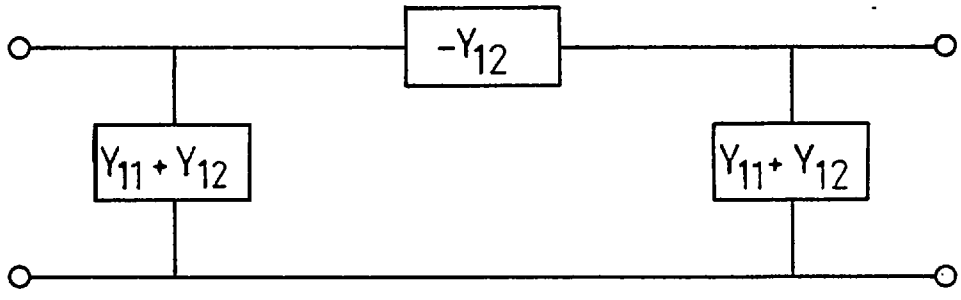

Fig. 4.3: Mutual admittance equivalent and terminal network.

a lumped element shunted across the equivalent transmission line of the waveguide. Choosing terminals across this element, the matrix equations defining the mutual coupling are:

$$\begin{pmatrix} I_1 \\ I_2 \end{pmatrix} = \begin{bmatrix} Y_{11} & Y_{12} \\ Y_{21} & Y_{22} \end{bmatrix} \begin{pmatrix} V_1 \\ V_2 \end{pmatrix} \qquad 4.1$$

where the two coupled slots are labelled 1 and 2.

The use of the upper case letters signifies that the quantities are normalised to the equivalent waveguide transmission line. If the mutual coupling is reciprocal:

$$Y_{12} = Y_{21} \qquad 4.2$$

and Eqn. 4.1 may be represented by the four terminal network of Figure 4.3. With a matched generator feeding one waveguide port, a matched detector at the output port of the second waveguide, and the remaining ports matched, the equivalent circuit for the complete system is that shown in Figure 4.4. It is assumed that the two slots are identical and $Y_{11} = Y_{22}$.

Consider now, the voltage relations between the source and detector. These may be obtained using cascade matrices which are defined for an arbitrary two port network as:

$$\begin{pmatrix} V_1 \\ I_1 \end{pmatrix} \begin{bmatrix} A & B \\ C & D \end{bmatrix} \begin{pmatrix} V_2 \\ I_2 \end{pmatrix} \qquad 4.3$$

where, by convention, I_1 flows into the network and I_2 flows out.

The values of the matrix elements for specific networks are tabulated in Reference 4. Using these, the relationships between V_1, I_1 and V_2, I_2 in Figure 4.4. is:

$$\begin{pmatrix} V_1 \\ I_1 \end{pmatrix} = \begin{bmatrix} 1 & 1 \\ 0 & 1 \end{bmatrix} \begin{bmatrix} 1 & 0 \\ 1+Y_{11}+Y_{12} & 1 \end{bmatrix} \begin{bmatrix} 1 & -1/Y_{12} \\ 0 & 1 \end{bmatrix} \begin{bmatrix} 1 & 0 \\ 2+Y_{11}+Y_{12} & 1 \end{bmatrix} \begin{pmatrix} V_2 \\ I_2 \end{pmatrix}$$

$$= \begin{bmatrix} A & B \\ C & D \end{bmatrix} \begin{pmatrix} V_2 \\ I_2 \end{pmatrix} \qquad 4.4$$

With $I_2 = 0$, $V_1 = AV_2$.

Multiplying out:

$$A = \frac{(2+Y_{11}+Y_{12})\ (2+Y_{11}-Y_{12})}{-Y_{12}} \qquad 4.5$$

Therefore,

$$\frac{V_2}{V_1} = \frac{-Y_{12}}{(2+Y_{11})^2 - Y_{12}^2} \qquad 4.6$$

If the mutual coupling is small,

$$Y_{12}^2 << (2+Y_{11})^2 \qquad 4.7$$

and

$$\frac{V_2}{V_1} = \frac{-Y_{12}}{(2+Y_{11})^2} \qquad 4.8$$

This expression is termed the voltage coupling coefficient and is useful for characterising the mutual coupling of identical slots. The formulation in terms of Y_{11} and Y_{12} given above, however, is limited since both Y_{11} and Y_{12} are strongly dependent on the slot dimensions, and, with resonant slots, the frequency.

4.2. MUTUAL COUPLING EQUIVALENT CIRCUIT WITH TERMINALS ACROSS THE CENTRE OF THE SLOT

The equivalent circuits developed in Chapter 3 allow the admittance of an isolated slot relative to imaginary terminals across its centre, y_{11}, to be referred to the dominant mode transmission line. That is, the normalised shunt impedance, z_{in}, is given by

$$z_{in} = \frac{Y_{11}}{K^2} \qquad 4.9$$

where y_{11} is now taken to include the internal susceptance of the slot in the waveguide. It should be noted that quantities referred to the slot terminals are written in lower case.

In terms of voltages and currents, this becomes:

$$\frac{V_{in}}{I_{in}} = \frac{1}{K^2} \left(\frac{i_s}{v_s}\right) \qquad 4.10$$

where v_s and i_s are, respectively, the equivalent voltage and current at the slot terminals.

To represent the coupling through the slot with a cascade matrix, it may be arbitrarily assumed that:

$$V_{in} = \frac{i_s}{K} \qquad 4.11$$

and $I_{in} = Kv_s$

Thus the admittance invertor may be represented by the cascade matrix equation:

$$\begin{pmatrix} V_{in} \\ I_{in} \end{pmatrix} = \begin{bmatrix} 0 & 1/K \\ K & 0 \end{bmatrix} \begin{pmatrix} v_s \\ i_s \end{pmatrix} \qquad 4.12$$

The equivalent circuit corresponding to that shown in Figure 4.4. is drawn in Figure 4.5, with the self and mutual admittances now referred to terminals across the centres of the slots. The cascade matrix relating the input and output quantities can be constructed in similar fashion to that described in Section 4.1, and the matrix element, A, calculated to obtain the voltage coupling coefficient. This is:

$$\frac{V_2}{V_1} = \frac{-K^2 y_{12}}{4(y_{11}^2 - y_{12}^2) + K^4 + 2K^2 y_{11}} \qquad 4.13$$

The relationship between the slot voltages, v_{s1} and v_{s2}, is easily deduced from a consideration of just part of the network in Figure 4.5. and is given by:

$$\frac{v_{s2}}{v_{s1}} = \frac{-y_{12}}{y_{11} + \frac{K^2}{2}} \qquad 4.14$$

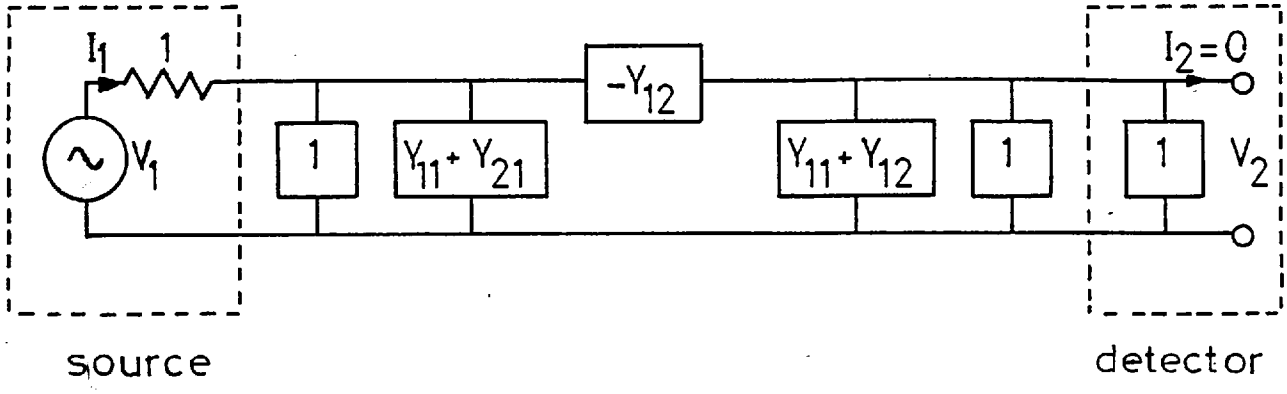

Fig. 4.4: Equivalent network of two mutually coupled slots in adjacent waveguides.

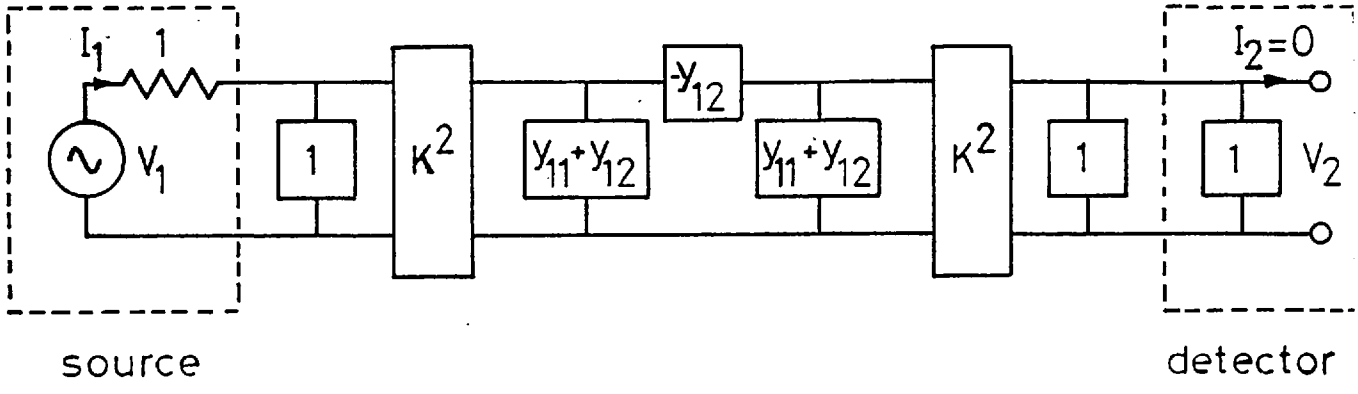

Fig. 4.5: Alternative equivalent network of two mutually coupled slots in adjacent waveguides with terminals across the slot centres.

For the slots cut in a groundplane and the waveguides removed, the voltage relation is:

$$\frac{V_{s2}}{V_{s1}} = - \frac{y_{12}}{y_{11}} \qquad 4.15$$

Thus the $\frac{K^2}{2}$ term in the denominator of 3.14 represents the effect of the waveguide loading. If the two slots are resonant, the self-admittance y_{11} is a pure conductance, g_{11}. The conductance presented across the dominant mode transmission line, G, by a single slot is:

$$G = \frac{K^2}{g_{11}} \qquad 4.16$$

The denominator of Eqn. 4.14, D can then be expressed as:

$$D = g_{11}(1+ \frac{G}{2}) \qquad 4.17$$

The waveguide loading is thus given by the bracketed term. Its reciprocal has been plotted in Figure 4.6 as a function of G. In any slotted waveguide design, the normalised slot conductances are limited to prevent excessive mismatches in the waveguide and are generally not greater than .1. It can be seen from Figure 4.6. that for conductances less than .2 the loading effect is less than 10% and to a good approximation, the slots may be considered to be open circuited and the mutual coupling calculated in isolation from the waveguide.

It has been shown that if the mutual coupling is small ($y_{12} << y_{11}$) it may be expressed in terms of the slot

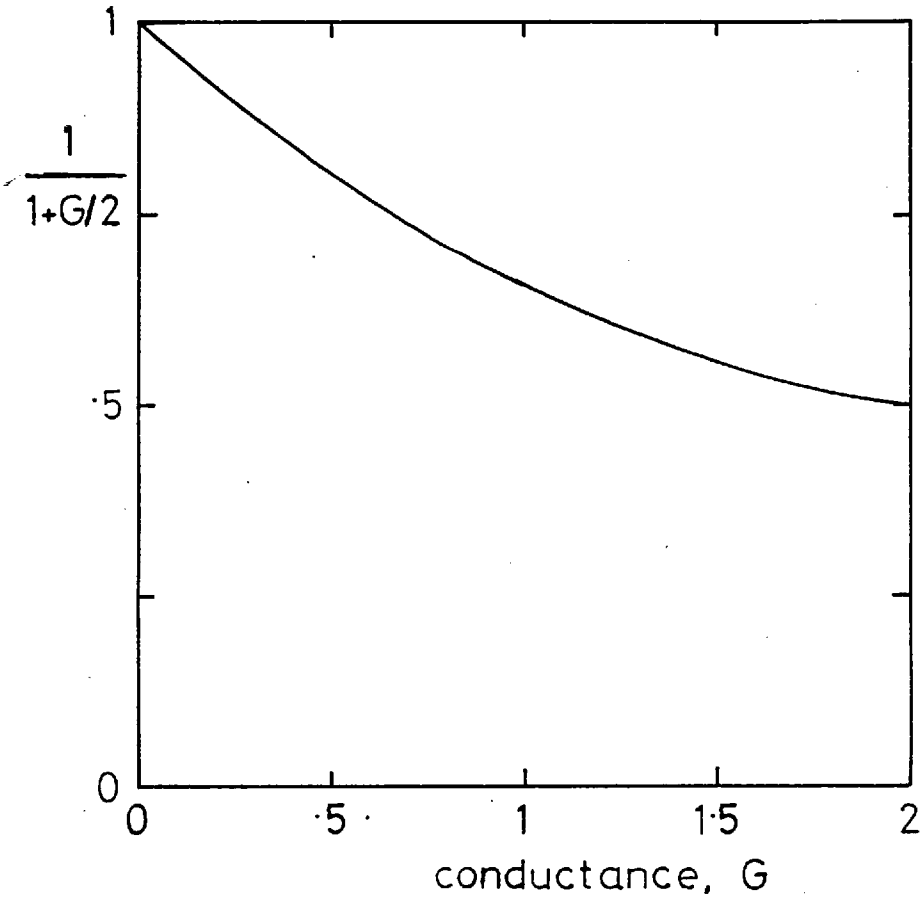

Fig. 4.6: The loading effect of waveguide feeds on two mutually coupled slots as a function of the normalised shunt conductance presented to the TE_{10} mode.

voltage coupling coefficients. At resonance these are defined from Eqn. 4.15 as:

$$\frac{V_{2s}}{V_{1s}} = \frac{-Y_{12}}{g_{11}} \qquad 4.18$$

With the I slots used in the array, the centre (vertical) arm length is held constant and the coupling to the waveguide is adjusted by varying the dimensions of the end (horizontal) arms. The large amount of experimental waveguide conductance data obtained from the prototype linear arrays has been used by Chignell [1] to derive values for the self conductance, g_{11}, using theoretical values for the coupling to the TE_{10} mode. It was found that g_{11} remains virtually constant with changes in the end arm dimensions and thus, from Eqn. 4.18, the slot voltage coupling coefficient is directly related to the mutual admittance. It also implies that the external admittance matrix is simplified in that the diagonal elements are independent of the coupling to the waveguide. In the following Chapters the mutual coupling between pairs of slots is examined to determine the off-diagonal elements of the matrix.

5. MUTUAL COUPLING CHARACTERISTICS OF STRAIGHT AND 'Z' SHAPED SLOTS

5.1. INTRODUCTION

The study of mutual coupling between waveguide excited slots has been largely confined to narrow rectangular slots located longitudinally in the broad waveguide wall. This configuration is used in a large number of slotted waveguide planar arrays and, also, it is the simplest case to study theoretically. Ehlrich and Short [32] measured the scattering matrix of the two rectangular waveguides in broad wall contact, with narrow rectangular slots cut in the side walls such that, external to the waveguides, the geometry corresponded to two longitudinal slots cut in the broad wall (either side of the centre line). The scattered waves in each waveguide are related to the electric fields in the respective slots. The results are then applied to the actual case of the slots located in the broad wall and the active impedance of one slot deduced. Similar cases have been investigated by Kay and Simmons [33] (using the theory of Stevenson [17]) and Das and Sengal [34]. A later paper by Yee [24] has considered an infinite array simulator to secure a value for the active admittance of a longitudinal slot in a planar array.

This chapter describes the development of measuring techniques which are suitable for characterising complex shaped slots. The existing methods available for waveguide fed slots are reviewed and the most appropriate technique chosen and implemented. The accuracy of the measurements is assessed by

first considering narrow rectangular slots and comparing the results with theoretical values. Z shaped slots are then investigated and a general confirmation of the measurements is obtained by radiation pattern measurement of small parasitic slot arrays.

5.2. THE MEASUREMENT OF MUTUAL COUPLING

Several high frequency techniques have been developed for measuring the mutual coupling between antenna pairs. Those which are based on an impedance or admittance approach have been critically reviewed by Iisuka [35]. Since these measurements are dependent on the variation in the reflection coefficient of the antennas, the mutual coupling is invariably determined as the difference of two larger quantities and the calculation is thus inherently sensitive to measurement inaccuracies, particularly when the mutual coupling is small. In such cases a more satisfactory approach is to feed one antenna and compare the coupled signal in the second antenna with that incident on the excited antenna. The comparison may be made using a microwave bridge although the phase calibration is extremely difficult. Mailloux and LaRuse [36] described a technique for measuring the phase, in which anti-symmetric excitation is established using a probe positioned exactly half-way between the radiators. This is quite difficult to set up in practice, particularly if the mutual coupling is to be measured at various antenna spacings. Due to the complexity of this system it was decided to use a standard microwave bridge in the present investigations and establish the absolute phase of the coupling in a separate experiment, as described in section 5.3. and 5.4.

5.2.1. MUTUAL COUPLING COEFFICIENTS

When using a bridge measurement technique it is appropriate to express the mutual coupling in terms of scattering matrices as these are obtained directly. If required, the scattering matrix can be related to the mutual admittance or impedance. When comparing different types of antennas, it is convenient to define a power coupling coefficient, C_p, [37], as:

$$C_p = \frac{p_r}{p_t} \tag{5.1}$$

where p_r is the power received in one antenna
and p_t is the power transmitted by the other.

The coupling between two identical linear antennas may be represented by the equivalent circuit shown in Figure 5.1. which is analogous to the admittance based circuits discussed in Chapter 4. It is assumed that the coupling is reciprocal such that $Z_{12} = Z_{21}$. The power transmitted by antenna 1 is:

$$P_t = \mathrm{Re}(VI^*) = |I_1|^2 \, \mathrm{Re}(Z_1) \tag{5.2}$$

where Z_1 is the impedance looking into terminals 1 1'
and Re( ) denotes the real part.

The power received by antenna 2 is:

$$P_r = \mathrm{Re}(V_2 I_2^*) = |I_2|^2 \, \mathrm{Re}(Z_2) \tag{5.3}$$

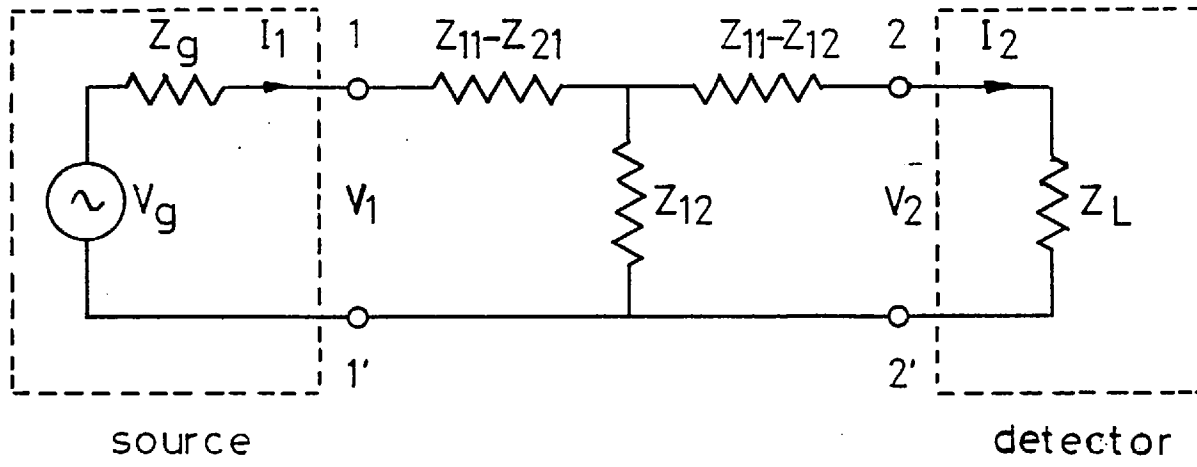

Fig. 5.1: Impedance based equivalent circuit for the mutual coupling between two identical antennas.

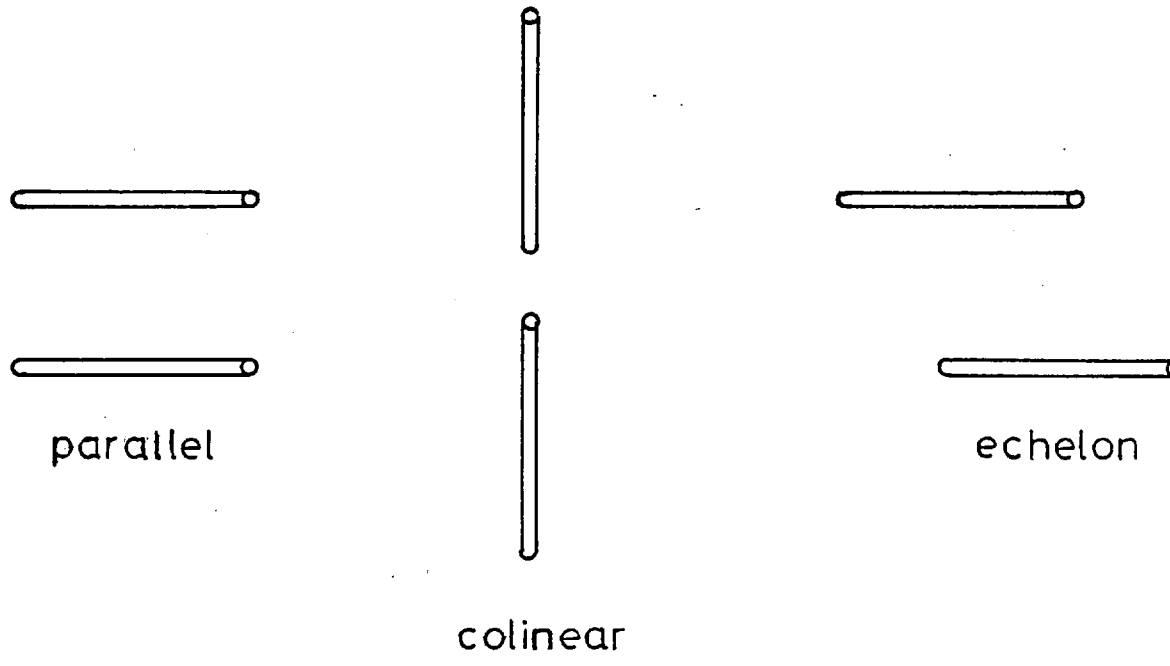

Fig. 5.2: Arrangements of pairs of dipoles.

If $|Z_{12}| << |Z_{11}|$ and the input and output ports are conjugately matched, then it can be shown that:

$$C_p = \frac{|Z_{12}|^2}{4[\mathrm{Re}(Z_{11})]^2} \tag{5.4}$$

With the above conditions, a voltage coupling coefficient, C_v, may be defined:

$$C_v = \frac{|Z_{12}|}{2\mathrm{Re}(Z_{11})} \tag{5.5}$$

The power coupling coefficient, C_p, is a convenient parameter to use here because it enables a direct comparison to be made between waveguide-fed slots and their dual dipoles and also gives an indication of the relative mutual coupling between differently shaped slots.

It is interesting from a measurement viewpoint to note the fractional error, E_p, introduced into the power coupling coefficient when the two antennas are conjugately matched in isolation, rather than with the other slot present as implied in Eqn. 5.4. This is given by:

$$E_p = \frac{\mathrm{Re}(Z_{12})^2}{2[\mathrm{Re}(Z_{11})]^2} \tag{5.6}$$

The error is only significant when the elements are closely spaced and Z_{12} is comparable with Z_{11}. For the majority of cases considered in this investigation it may be ignored.

5.2.2. DUALITY BETWEEN SLOTS AND THEIR COMPLEMENTARY DIPOLES

The radiation characteristics of a slot can be obtained by recognising its duality with a flat dipole of the same dimensions and transforming the corresponding results. The equivalence relationships between the two cases is well established, a particularly straightforward derivation of the equation relating the slot self-admittance, y^s_{11}, to the self-impedance of its complimentary dipole, z^d_{11} is given in Reference 19. It is:

$$y^s_{11} = z^d_{11} \frac{4}{z_o^2} \tag{5.7}$$

where z_o is the intrinsic impedance of free space.

The corresponding relation for the mutual coupling parameters is not given in Reference 19. However, it may be easily derived by using the equivalent field quantities defined there and the following expressions for the mutual impedance between dipole pairs and the mutual admittance between complementary slot pairs, defined in terms of reaction [25]:

$$z^d_{12} = -\frac{1}{i^d_1 i^d_2} \int_{\text{surface of dipole}} \underline{E}^d_1 \cdot \underline{J}^d_2 \, da$$

$$y^s_{12} = -\frac{1}{v^s_1 v^s_2} \int_{\text{surface of slot}} \underline{H}^s_1 \cdot \underline{M}^s_2 \, da \tag{5.8}$$

where subscripts 1 and 2 refer to the two coupled antennas

i^d is the dipole loop current

and v^s is the equivalent voltage across the centre of the slot.

The result is the same as that relating the isolated antenna parameters:

$$y_{12} = z^d_{12} \frac{4}{z_o^2} \qquad (5.9)$$

With the slots radiating into a half-space, the admittances given in Eqns. 4.8 and 4.9 are simply halved. Thus the power coupling coefficient, C_p, as defined by Eqn. 5.4 is identical for slots and their complementary dipoles, irrespective of whether the slots are radiating into full or half space.

Theoretical methods for determining the mutual impedance of thin wire dipoles will now be discussed.

5.2.3. MUTUAL COUPLING BETWEEN THIN WIRE, HALF WAVE DIPOLES

Using the relationships derived in the previous section, theoretical results available for the mutual coupling between thin wire dipoles may be applied to the complementary slot configuration. Although the correct complementary form to a slot cut in a groundplane is a thin flat dipole, for half wave radiators it has been found that calculations of infinitesimally thin dipoles yield very good results for narrow slots. The theory employed here is that due to Carter [10]

who used an induced E.M.F. method to calculate the self and mutual impedances. As the results are well known they are not discussed in detail here; a complete summary may be found elsewhere [37]. The arrangements considered by Carter , designated parallel, colinear and echelon, are shown in Figure 5.2. More recently, numerical techniques have been applied to include cylindrical (non-vanishing thickness) dipoles [38]. These studies indicated that the mutual coupling between dipoles in colinear or echelon arrangements can generate strong anti-symmetric components of current which would result in large discrepancies between measured data and predicted values based on first order sinusoidal approximations for the currents as used in Carter's formulation. It was expected, however, that these effects are not significant for thin half-wave dipoles and, by duality, narrow resonant slots.

5.2.4. EXPERIMENTAL INVESTIGATION OF THE MUTUAL COUPLING BETWEEN NARROW RECTANGULAR SLOTS IN THE END WALL

Measurements were initially carried out at X band (8.2 - 12.4 GHz), although the design frequency of the final array is 5.75 GHz. The components required in a bridge network were available in this frequency band and, if necessary, the results are readily scaled to thedesign frequency. The slots were milled in the end wall of WG16 rectangular waveguide as shown in Figure 5.3. About resonance the slot fields are practically independent of the method of excitation; thus the external mutual coupling should not be significantly

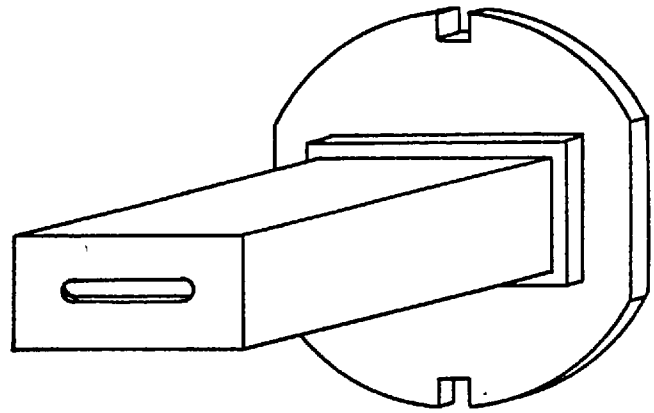

Fig. 5.3: Straight slot in the end of rectangular waveguide.

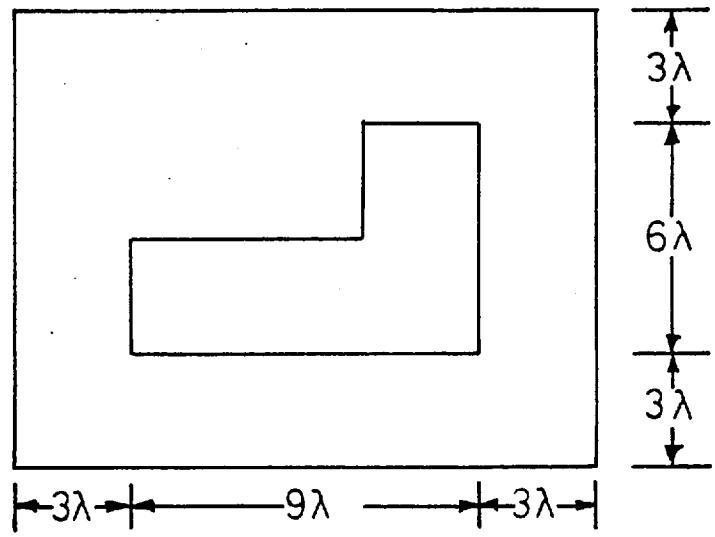

Fig. 5.4: Groundplane configuration used in mutual coupling investigations.

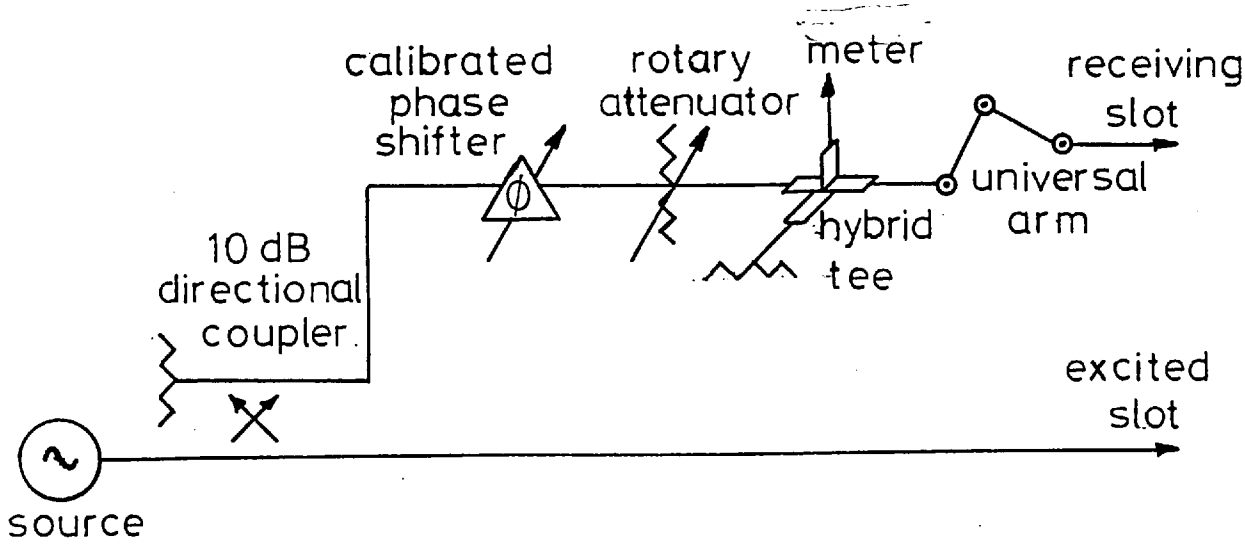

Fig. 5.5: Schematic diagram of microwave bridge.

different for the end and side wall located slots. By matching the slots to the incident TE_{10} mode in the waveguide (consistent with the definition of the power coupling coefficient, C_p), the power transmitted by the slot is maximised and thus the measurement sensitivity. Employing end wall slots also allows a greater flexibility in the spacing and orientation of the slots. The slot dimensions were those given in Figure 3.14.

The ground plane (Figure 5.4) was cut from copper sheet and backed with blockboard (to keep it planar) supported by a metal frame. The size of the groundplane was such that, for any slot position, the effect of the edges could be ignored. A clamping arrangement beneath the groundplane held the slots, emerging through the 'L' shaped hole cut in the centre of the groundplane, flush with its top surface. The gaps in the groundplane were then covered with copper sheet and electrical continuity was ensured by covering the joints with conducting adhesive aluminium tape. The slot spacing was measured using a travelling microscope.

The microwave bridge arrangement is shown schematically in Figure 5.5. As the maximum coupled power measured was approximately -15dB, a -10dB directional coupler was found suitable to split the power between the reference and test arms. In order to make precise measurements of therelative phase of the coupling as the slot separation was varied, it was necessary to construct a universal arm connecting the coupled waveguide to the input port of the test arm. This consisted of two lengths of waveguide coupled with coaxial rotating

joints (manufactured by Sivers Ltd., Sweden). Tests on the arm showed that the phase of the transmitted wave varied by less than ± 2 degrees as the position of the arms was varied. The phase shifter in the reference arm was of the trombone type, utilising a 'U' section of waveguide with internal dimensions 1" × .5" which is a sliding fit over WG16 waveguide. A full range of 360° was available with a negligible change in the insertion loss. A rotary attenuator with a useful range of 50dB was used as the reference attenuator and further steps of attenuation were provided with standard waveguide attenuators whose phase shift had been calibrated at specific attenuation levels.

The measurement procedure was as follows:

1. The slot admittances, referred to the end wall plane, were measured against frequency to establish the resonant frequency.

2. The bridge was calibrated for amplitude measurements by joining the two measuring arms with a short length of waveguide.

3. The slotted waveguides were then connected to the measurement arms and the groundplane completed. Their separation was measured using a travelling microscope.

4. Each slot was matched using a standard four stub tuner.

5. The bridge was balanced by adjustment of the calibrated phase shifter and rotary attenuator. The coupled signal to the second slot could then be determined.

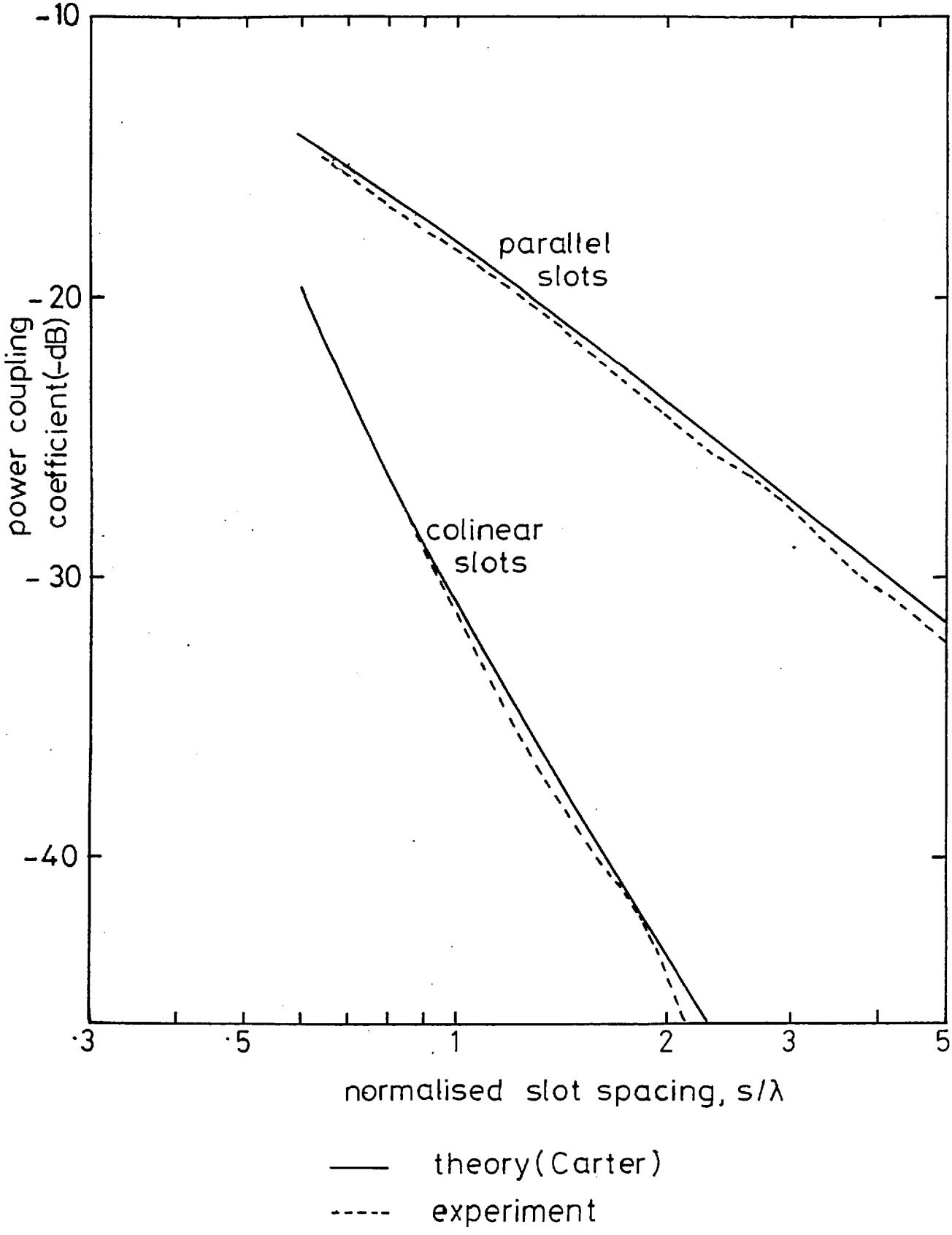

Fig. 5.6: Amplitude of mutual coupling coefficients for half-wave slots.

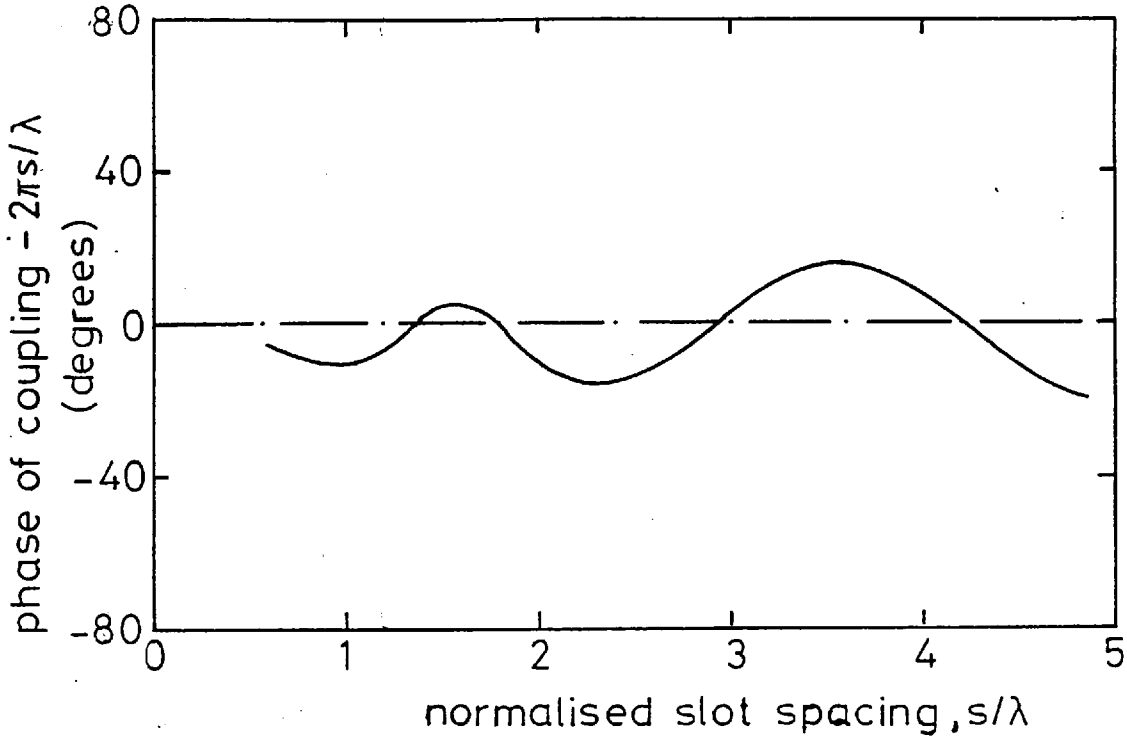

Fig. 5.7: Phase of mutual coupling coefficients for arrangement of half-wave slots.

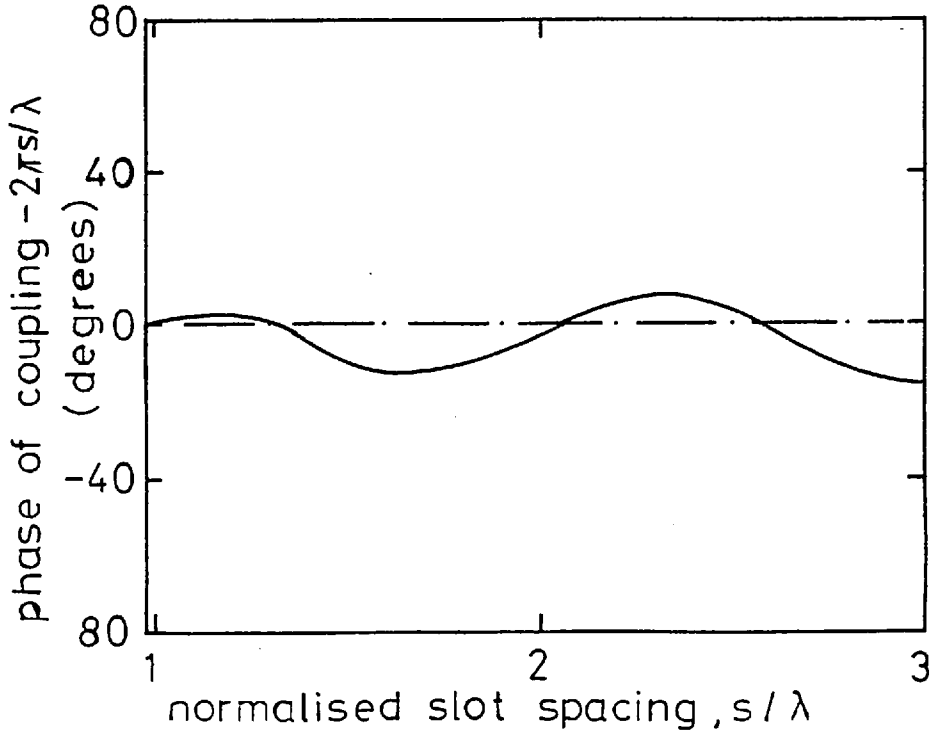

Fig. 5.8: Phase of mutual coupling coefficients for collinear arrangement of half wave slots.

5.2.5. RESULTS

The mutual coupling between parallel and colinear pairs of slots have been investigated. Graphs of the magnitude and relative phase of the power coupling coefficients against spacing, s, are reproduced in Figures 5.6., 5.7 and 5.8. The results have been compared with those obtained theoretically using Carter's formulation for the mutual impedance of infinitesimally thin wire dipoles as discussed in section 5.2.3. It should be noted that the phase variations are relative to an arbitrary reference which was chosen to provide the best fit to the free space law predicted by Carter.

The amplitude results show a good correlation between the theoretical and experimental values although the latter are consistently lower which suggests the presence of a small calibration error. Tests with narrower slots and thinner end walls (which better approach the theoretical models) had no significant effect on the results. The power coupling coefficients vary as $1/s^2$ for parallel slots and $1/s^4$ for colinear slots, a result which is predicted by theory. The ripple on the results is due to mismatches within the measurement system. Although it is of a form which is consistent with the presence of reflections, extending the groundplane to change the position of the edges and placing radio-absorbant material on the ceiling had no effect on the value obtained. The same ripple occurs in the phase plots of Figures 5.7. and 5.8. which, however, have the predicted free space dependence. The discrepancy between the theoretical and measured amplitudes of the coupling coefficient is less

than .5dB. This corresponds to a 5% difference in the values of mutual admittance which is considered satisfactory, particularly for the colinear configuration where the theoretical model is known to be less accurate.

5.3. MUTUAL COUPLING BETWEEN Z SHAPED SLOTS

The 'Z' shaped slot is a member of the class of complex shaped slots developed at Imperial College to overcome the high loss associated with the inclined 'H' slot used in the prototype slotted waveguides which are to be incorporated in the ASWE monopulse antenna. As it is the simplest of the various configurations, it was chosenfor the initial investigations of mutual coupling. The cross polarisation suppressor design had not been finalised at this stage and the slots were located in a large groundplane. Thus the results obtained here are not directly applicable to the final array design, but should provide valuable insight into the mutual coupling mechanisms present. To provide some confirmation ofthe experimental results the mutual coupling has been examined theoretically. This is discussed in the following section.

5.3.1. A FIRST ORDER THEORY OF MUTUAL COUPLING BETWEEN 'Z' SHAPED SLOTS

The discontinuities which exist at the two corners of the 'Z' shaped slot make it difficult to accurately predict the form of the equivalent magnetic current distribution in the slot, which is required in a calculation of the mutual coupling. However, it is well-known that the mutual coupling

particularly at large spacings, is not strongly dependent on the current distribution. So, as a first approximation, it is assumed that the magnetic current is of a sinusoidal form at frequencies about resonance. Chignell [1] has established empirically that the resonant frequency of a 'Z' shaped slot whose dimensions are defined in Figure 5.9(a) is approximately the same as that of the straight slot shown in Figure 5.9 (b). Neglecting the width and thickness of the slot, the Z shaped slot can then be represented by the continuous sinusoidal magnetic line current shown in Figure 5.10.

In order to remain consistentwith the theoretical treatment of straight slots, the dual of the above slot model, the infinitesimally thin wire 'Z' shaped dipole will be considered. An induced E.M.F. method is used to calculate the mutual coupling between two such dipoles. This method has received much attention in the literature, particularly in respect to its use in calculating antenna self impedances [29]. After making the assumption of the current distribution, the method becomes exactly equivalent to alternative techniques such as the Poynting Vector Method.

Consider the two dipoles shown in Figure 5.11 which are confined to the x, z plane, corresponding to the situation in planar arrays. Results are presented only for the case where the centre sections are parallel although the analysis is quite general. The dipoles shown in Figure 5.11 are referred to as being "of the same hand"; the alternative orientation where one of the dipoles is rotated about the z-axis by 180° is referred to as dipoles "of opposite hand".

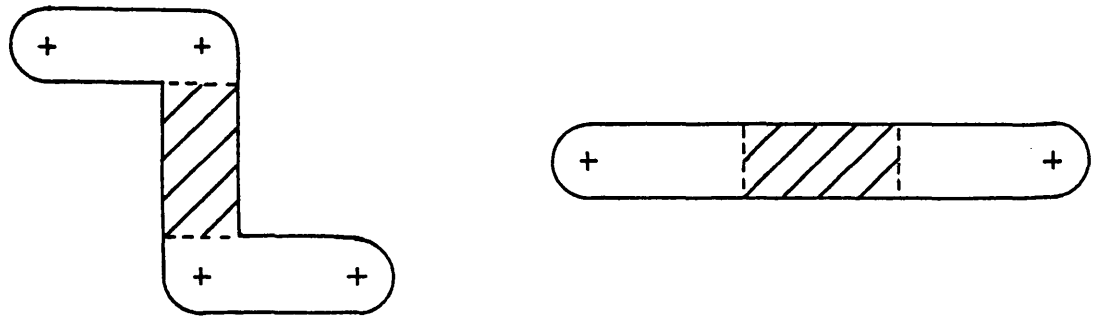

Fig. 5.9: Z shaped slot and its equivalent straight slot.

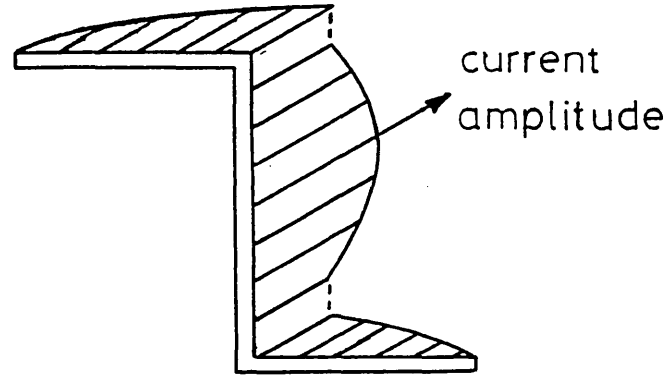

Fig. 5.10: Equivalent Z shaped dipole.

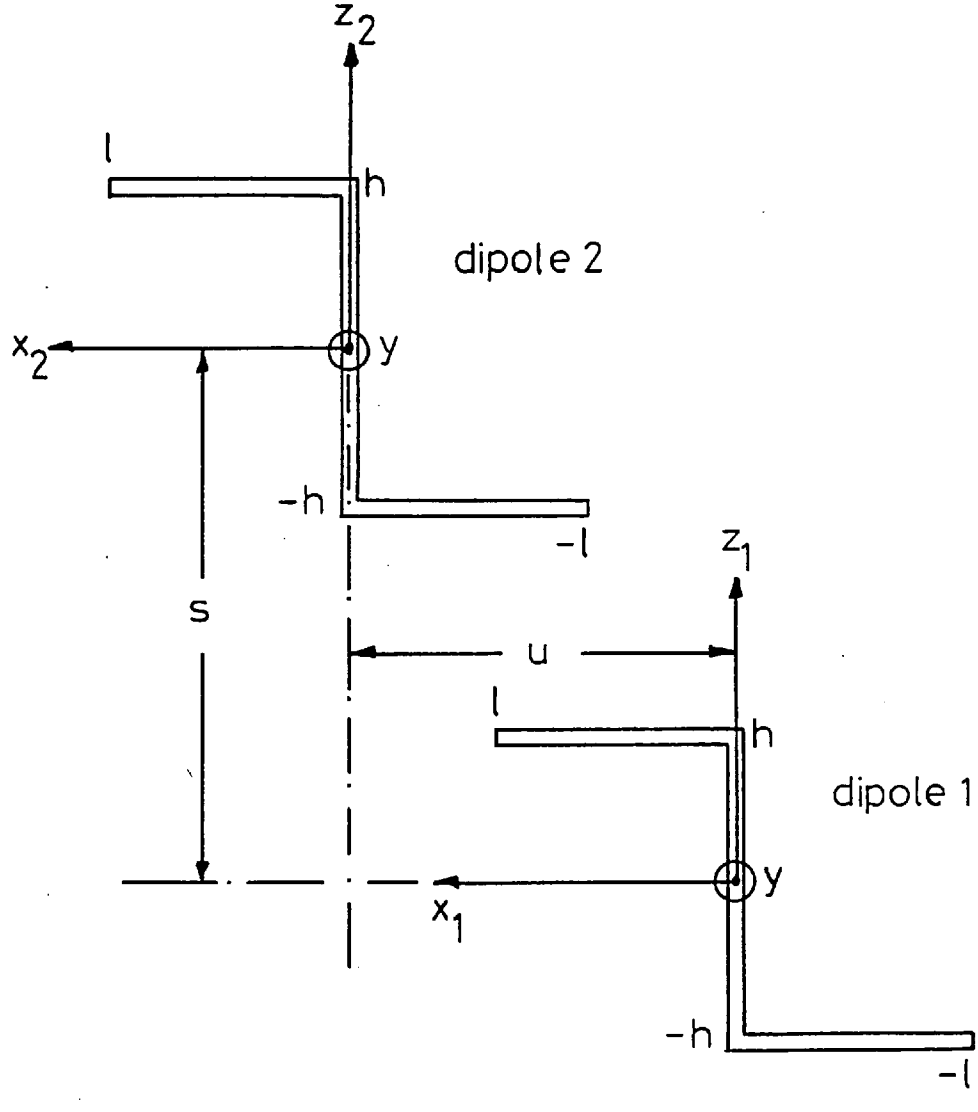

Fig. 5.11: Two mutually coupled z dipoles

Let dipole 1 (defined in Figure 5.11) be excited with a current equivalent to the magnetic current of the dual slot shown in Figure 5.10. For this analysis it is convenient to express the fields radiated by dipole 1 in cartesian (x,y,z) co-ordinates. Then, for the above case where the dipoles are contained in the y = 0 plane, the component of the electric field parallel to the sections of dipole 2 is either the x or z component. To calculate these electric field components, first consider an elementary electric dipole placed at the origin and orientated in the z-direction as drawn in Figure 5.12. With a current, i_o, along the dipole, the radiated electric field in the required directions at point P are:

$$E_x = \frac{j\omega\mu i_o dz}{4\pi k^2} e^{-jkr} \left\{ \frac{k^2}{r^3} - \frac{3jk}{r^4} - \frac{3}{r^5} \right\} xz \qquad (5.10)$$

$$E_z = \frac{j\omega\mu i_o dz}{4\pi k^2} e^{-jkr} \left\{ -\frac{k^2}{r} + \frac{jk}{r^2} + \frac{[1+k^2z^2]}{r^3} - \frac{3jkz^2}{r^4} - \frac{3z^2}{r^5} \right\}$$

where k, ω and μ have their usual meaning.

If it is assumed that the centre arm of dipole 1 is made up of elementary dipoles of infinitesimal length, the electric field at a point P, defined in Figure 5.13, is given by the integrals:

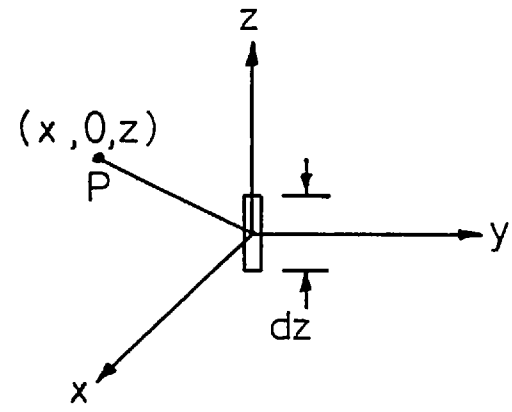

Fig. 5.12: Elementary dipole and co-ordinate system.

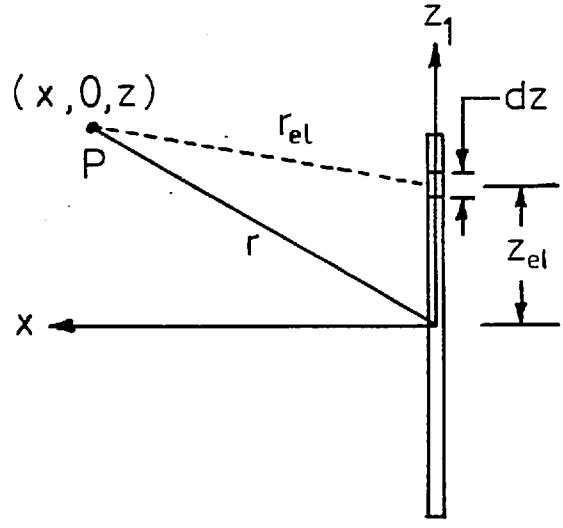

Fig. 5.13 : Centre arm of Z shaped diple and co-ordinate system.

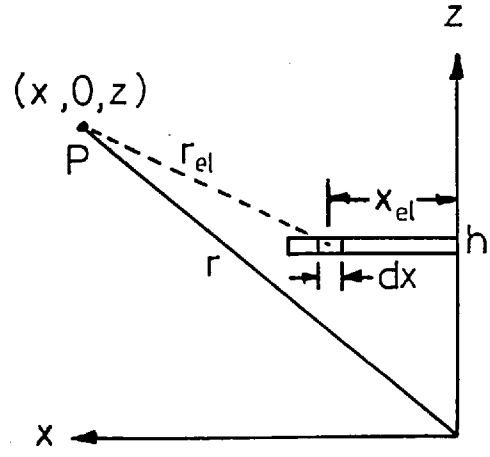

Fig. 5.14: End arm of Z shaped dipole and co-ordinate system.

$$E_{x1} = \frac{j\omega\mu}{4\pi k^2} \int_{-\ell}^{\ell} i(z_{el})\, e^{-jkr_{el}} \left\{ \frac{k^2}{r_{el}^3} - \frac{3jk}{r_{el}^4} - \frac{3}{r_{el}^5} \right\} x(z_1 - z_{el})\, dz_{el}$$

(5.11)

$$E_{z1} = \frac{j\omega\mu}{4\pi k^2} \int_{-\ell}^{\ell} i(z_{el})\, e^{-jkr_{el}} \left\{ \frac{k^2}{r_{el}} + \frac{jk}{r_{el}^3} + \frac{[1+k^2(z_1-z_{el})^2]}{r_{el}^4} - \right.$$

$$\left. \frac{3jk(z_1-z_{el})^2}{r_{el}^4} - \frac{3(z_1-z_{el})^2}{r_{el}^5} \right\} dz_{el}$$

The fields radiated by the end arms of dipole 1 can be expressed in a similar manner after transformation of the coordinate system. For the end arm of Figure 5.14, it can be shown that the electric field at point (x_1, z_1) is given by:

$$E_{x1} = \frac{j\omega\mu}{4\pi k^2} \int_{0}^{d} i(x_{el}) e^{-jkr_{el}} \left\{ \frac{k^2}{r_{el}} + \frac{jk}{r_{el}^2} + \frac{[1+k^2(x_1-x_{el})^2]}{r_{el}^3} \right.$$

$$\left. - \frac{3jk(x_1-x_{el})^2}{r_{el}^4} - \frac{3(x_1-x_{el})^2}{r_{el}^5} \right\} dx_{el}$$

(5.12)

$$E_{z1} = -\frac{j\omega\mu}{4\pi k^2} \int_{0}^{d} i(x_{el}) e^{-jkr_{el}} \left\{ \frac{k^2}{r_{el}^3} - \frac{3jk}{r_{el}^4} - \frac{3}{r_{el}^5} \right\}$$

$$(h-z_1)(x-x_{el})\, dx_{el}$$

where the additional parameters are defined in Figure 5.14.

A similar expression can be derived for the other end arm of dipole 1 and the total field at any point in the y = 0 plane obtained by summing the contribution from the three sections.

The mutual impedance between the two dipoles is defined

by the EMF method as:

$$Z_{12} = -\frac{1}{I_1} \iint_{\text{dipole 2}} E_{21}(x,z) f_2(x,z)\,dx\,dz \qquad (5.13)$$

where I_1 is the loop current on dipole 1

$E_{21}(x,z)$ is the electric field radiated by dipole 1 at dipole 2

and $I_2 f_z(x,z)$ is the assumed current distribution on dipole 2 where I_2 is the loop current.

From the geometry of Figure 5.11, this becomes:

$$Z_{12} = -\frac{1}{I_1}\left[\int_{-d}^{0} E_x(u+x_2, s-\ell) f_2(x_2,-\ell)\,dx + \int_{\ell}^{\ell} E_z(u, s+z_2) f_2(o,z_2)\,dz_2 + \int_{0}^{d} E_x(u+x_2, s+\ell) f_2(x_2,\ell)\,dx_2\right] \qquad (5.14)$$

Substituting for the electric field using Eqns. 5.11 and 5.12 yields the complete expression for the mutual impedance in terms of a sum of integrals, each integral representing the coupling between two sections, one of each antenna. Several of these integrals can be combined from a consideration of the geometry of Figure 5.11. With the individual sections labelled as in Figure 5.15 and the integrals between sections m and n denoted by I_{mn}, the mutual impedances for the two orientations are: For slots of the same hand:

$$Z_{12} = -\frac{j\omega\mu}{4\pi k^2}\{2I_{14}+2I_{15}+I_{16}+2I_{24}+I_{25}+I_{34}\} \qquad (5.15)$$

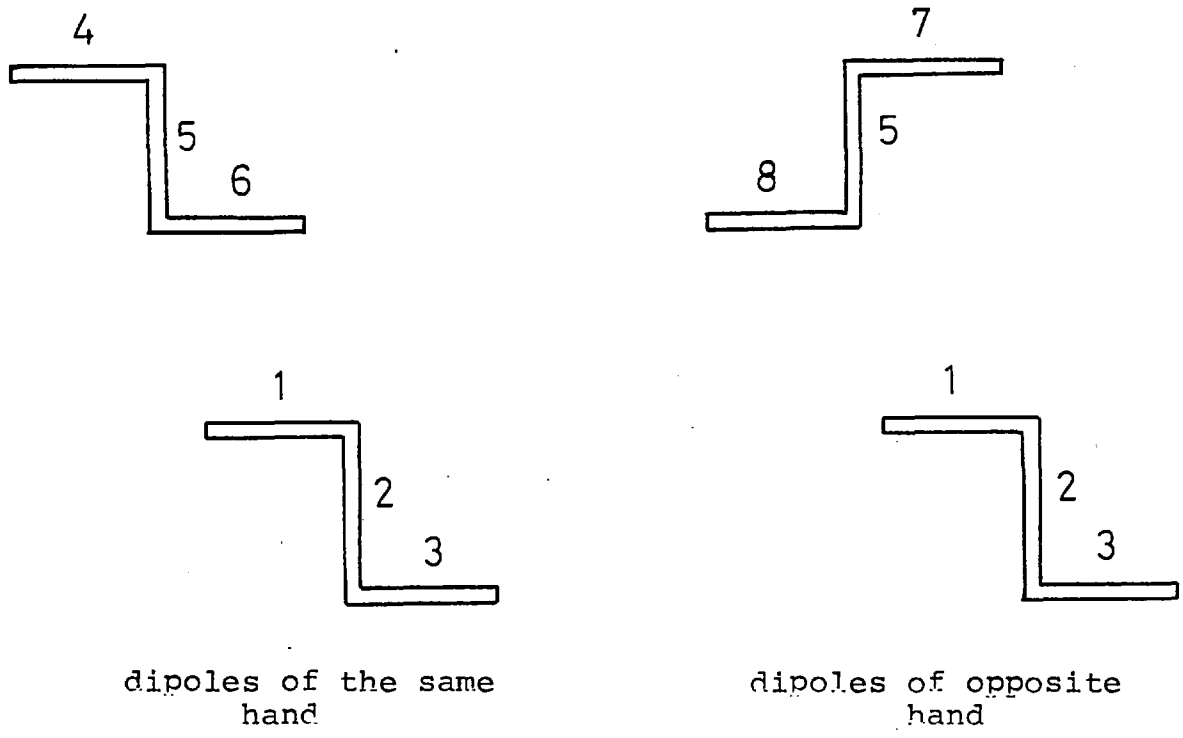

Fig. 5.15: Section designation of two mutually coupled Z shaped dipoles.

For slots of opposite hand:

$$Z_{12} = \frac{-j\omega\mu}{4\pi k^2} \{I_{15} + I_{17} + I_{18} + I_{25} + I_{27} + I_{28} + I_{35} + I_{37} + I_{38}\} \tag{5.16}$$

The integrals are of two types, corresponding to a parallel or orthogonal orientation of the coupled sections. The expressions for all of the integrals are not presented here; only one of each type, I_{14}, I_{15}, are given as examples:

$$I_{14} = \int_0^d \int_0^d e^{-jkr_{el4}} \cos \frac{\pi(h+x_{e1})}{2(d+\ell)} \cos \frac{\pi(h+x_{e2})}{2(h+\ell)} \{\frac{-k^2}{r_{el4}} + \frac{jk}{r_{el4}^2} + \frac{[1+k^2t^2]}{r_{el4}^3} - \frac{3jkt^2}{r_{el4}^4} - \frac{3t}{r_{el4}^5}\} dx_{e1}\, dx_{e2} \tag{5.17}$$

where $t = x_{e2} + u - x_{e1}$

and $r_{el4}^2 = t^2 + s^2$.

$$I_{15} = \int_{-\ell}^{\ell} \int_0^d e^{-jkr_{15}} \cos \frac{\pi(h+x_1{}_e)}{2(d+\ell)} \cos \frac{\pi z_2{}_e}{2(h+\ell)} \{+\frac{k^2}{r_{el5}^3} - \frac{3jk}{r_{el5}^4} - \frac{3}{r_{el5}^5}\}(s+z_{e2}-\ell)(x_{e1}-u)\, dx_{e1}\, dx_{e2} \tag{5.18}$$

where $r_{el5}^2 = (u-x_{e1})^2 (s-z_{e2}-\ell)^2$.

The mutual impedance for the two orientations has been calculated with the aid of a computer. The integrals were evaluated numerically using a Simpson's Rule integration sub-routine. To ascertain the dominant coupling mechanisms the components of the mutual impedance associated with each section of the dipoles, $\frac{-j\omega\mu}{4\pi k^2} I_{mn}$, have been plotted in Figures 5.16, 5.17, 5.18 and 5.19 as a function of spacing for the cases where the centre sections are colinear. The corresponding curves for the total mutual impedances for the two arrangements are shown in Figure 5.20. It may be noted from Figure 5.16 that at small spacings the principal coupling components are those between the collinear centre sections and between the centre sections and their nearest neighbour horizontal sections (corresponding to the integrals I_{25} and $2I_{15}$). These components are common to both configurations. However, it can be seen from Figure 5.20 that the remaining components still modify the net mutual coupling such that the mutual impedances are quite different for the two arrangements. At larger spacings, outside the inductive field region the coupling is dominated by the components between the centre sections and between the parallel horizontal sections. From the coupling behaviour of collinear and parallel straight dipoles, the significant role played by the former component was somewhat surprising; its high value relative to the other components is due to the higher field excitation in the centre sections.

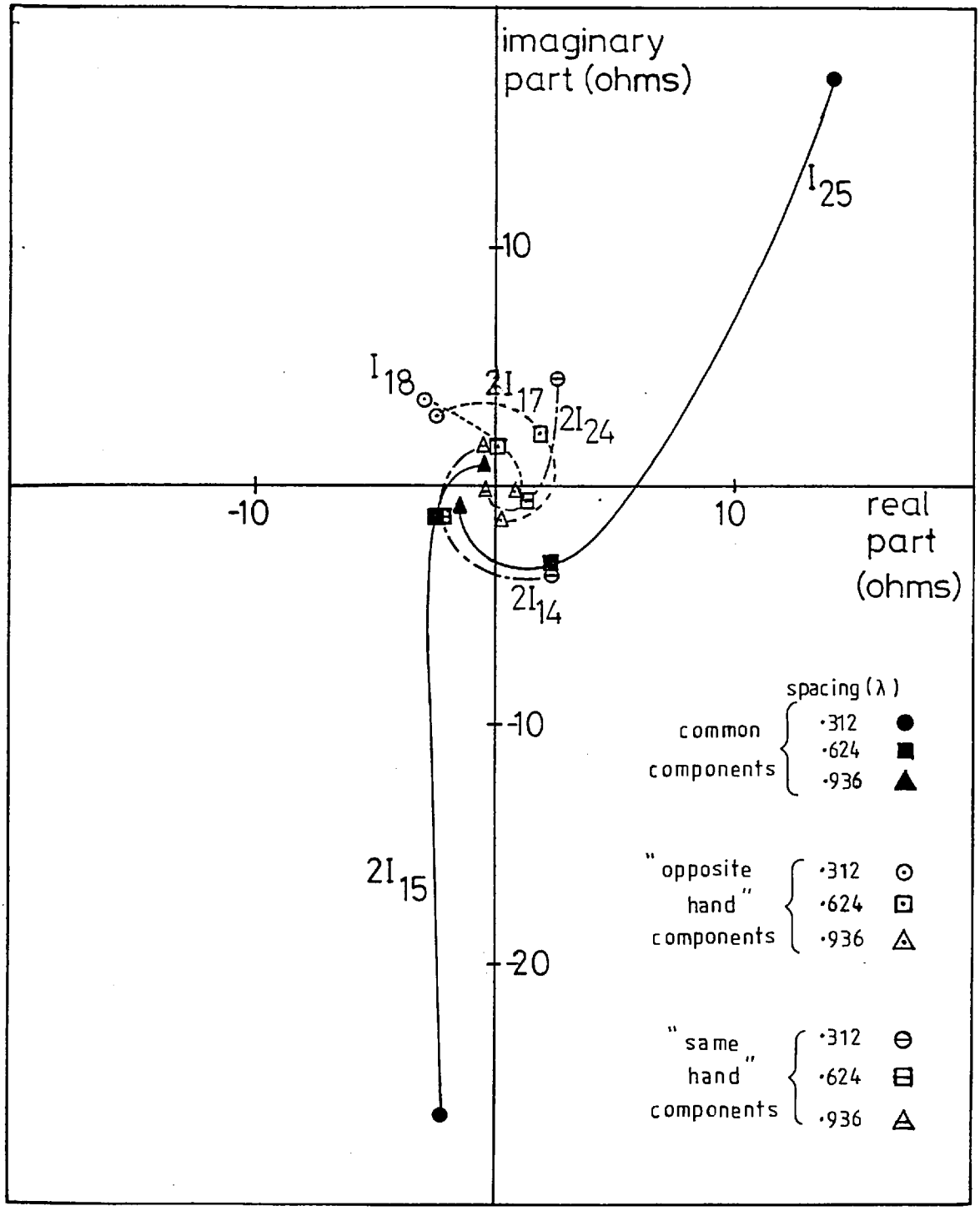

Fig. 5.16: Variation of major mutual impedance components at close spacings.
Components are identified by subscripts corresponding to sections labelled in Fig. 5.15.

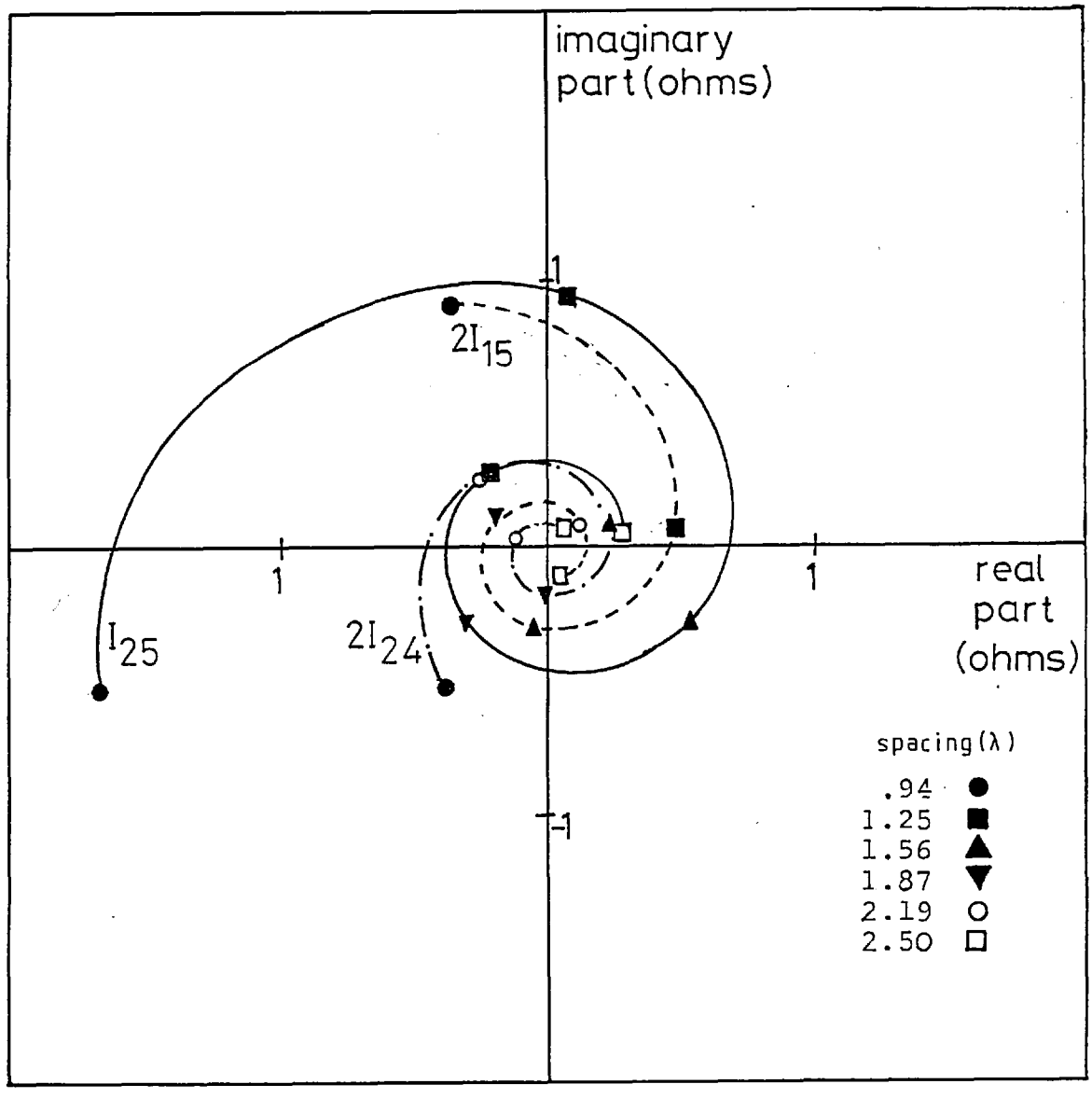

Fig. 5.17: Variation of mutual impedance components common to both configurations with spacing.

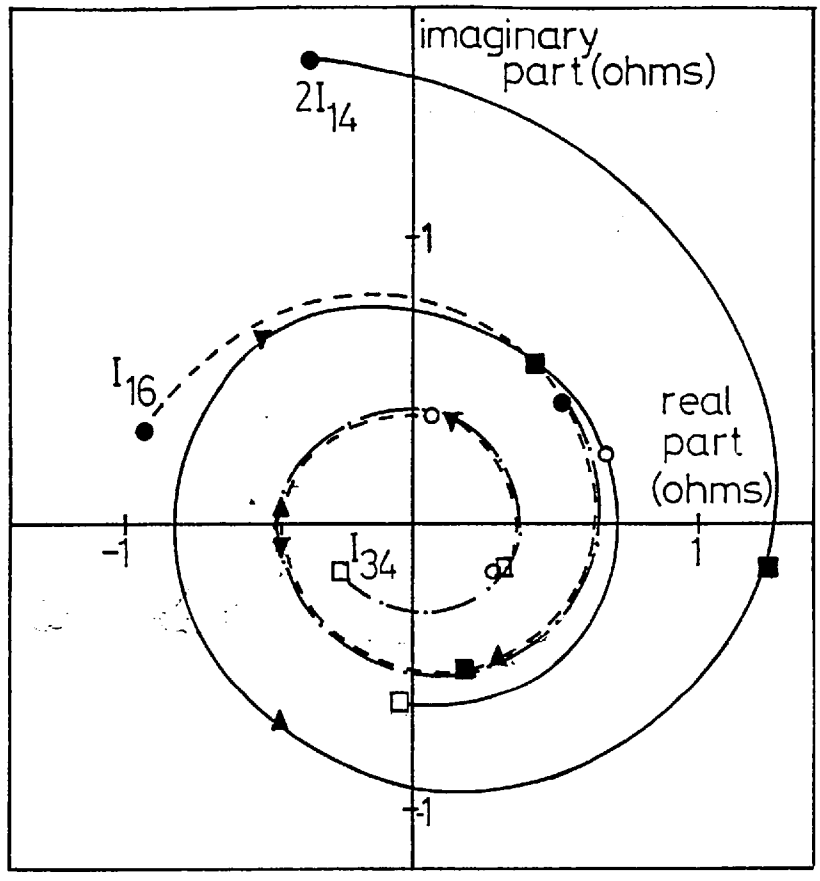

Fig. 5.18: Variation of mutual impedance components between parallel sections of dipoles of the same hand with spacing.

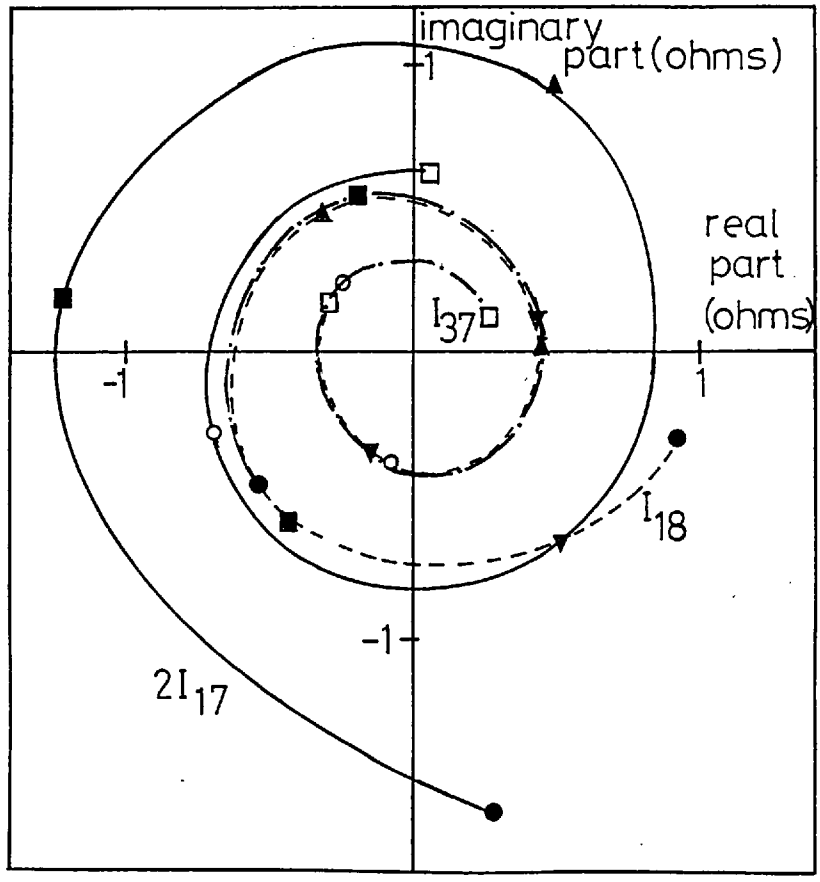

Fig. 5.19:

Variation of mutual impedance between parallel sections of dipoles of opposite hand with spacing.

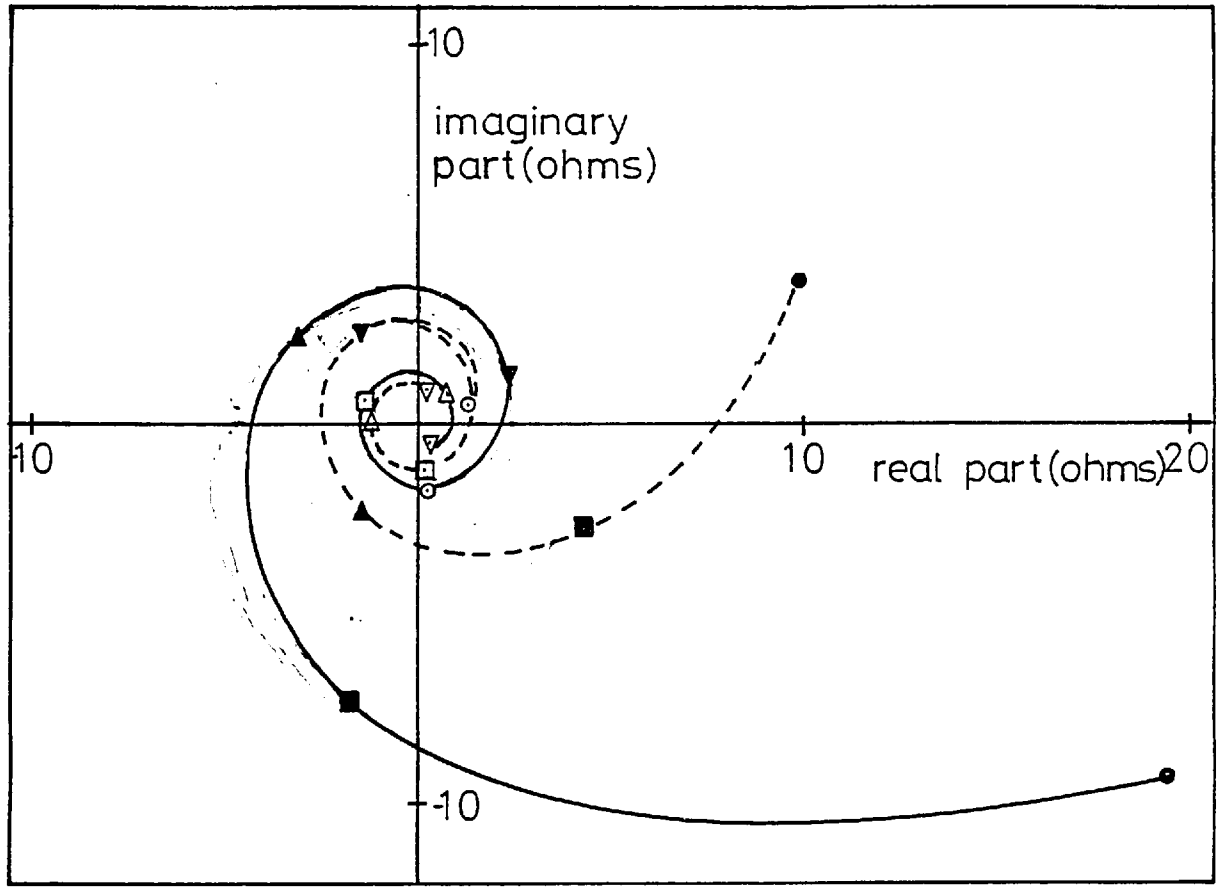

Fig. 5.20: Variation of total mutual impedance with spacing.

.312	●
.624	■
.94	▲
1.25	▼
1.56	⊙
1.87	⊡
2.19	△
2.50	▽

——————slots of opposite hand

– – – – – –slots of the same hand

5.3.2. EXPERIMENTAL INVESTIGATION

Measurements of the mutual coupling coefficients of Z slots with collinear centre sections as a function of spacing have been performed using the bridge network described in section 5.2. The dimensions of the slots are those defined in Figure 3.14. The slot self-admittances were measured in isolation and the resonant frequency determined. The measurements were carried out at this frequency, following the procedure outlined in section 5.2. The power coupling coefficients of the two configurations are plotted in Figure 5.21. The corresponding phase of the voltage coupling coefficients are plotted in Figure 5.22. The theoretical curves have been computed using the mutual impedances plotted in Figure 5.20. The calculations also require a value for the resistance of the equivalent dipole at resonance. This has been obtained empirically by Chignell [1] and his value is used here. The measured results for the phase variations with spacing are again relative due to the difficulty in calibrating the bridge. In the graph they have been shown normalised to the theoretical value for slots of opposite hand at the closest spacing considered in the experiment. (This value has been labelled R in Figure 5.22).

5.3.3. DISCUSSION OF RESULTS

Although quite large ripples are present in the experimental data there is reasonable agreement with the theoretical curves which tend to provide the upper envelope of the experimental curves. The ripple was first thought to be associated with the

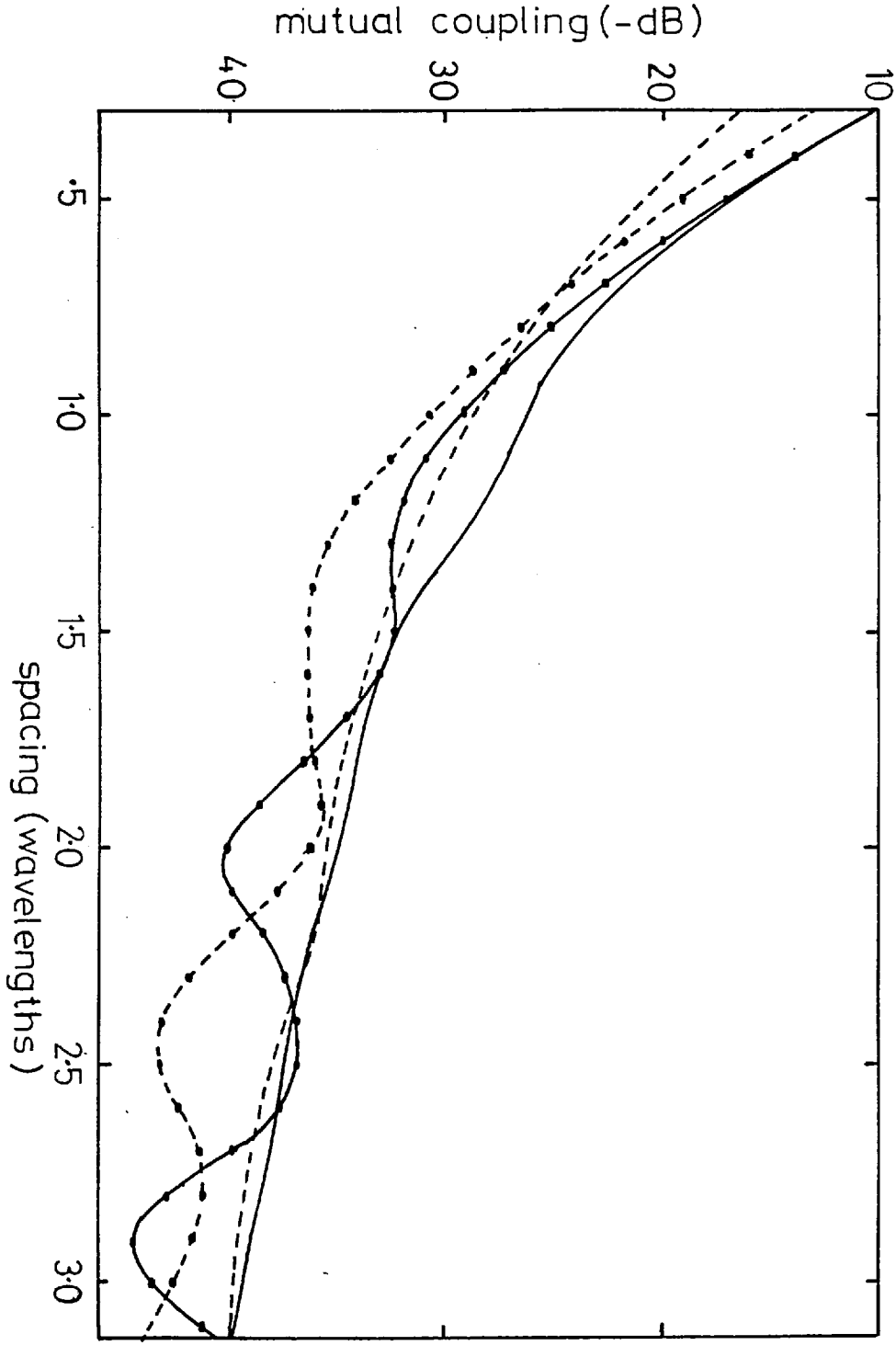

Fig. 5.21: Variation of the mutual coupling coefficient with spacing.

theory
experiment
} slots of same hand
results given in Table 5.1

theory
experiment
} slots of opposite hand
results given in Table 5.1

Fig. 5.22: Variation of the phase of the mutual coupling coefficient with spacing.

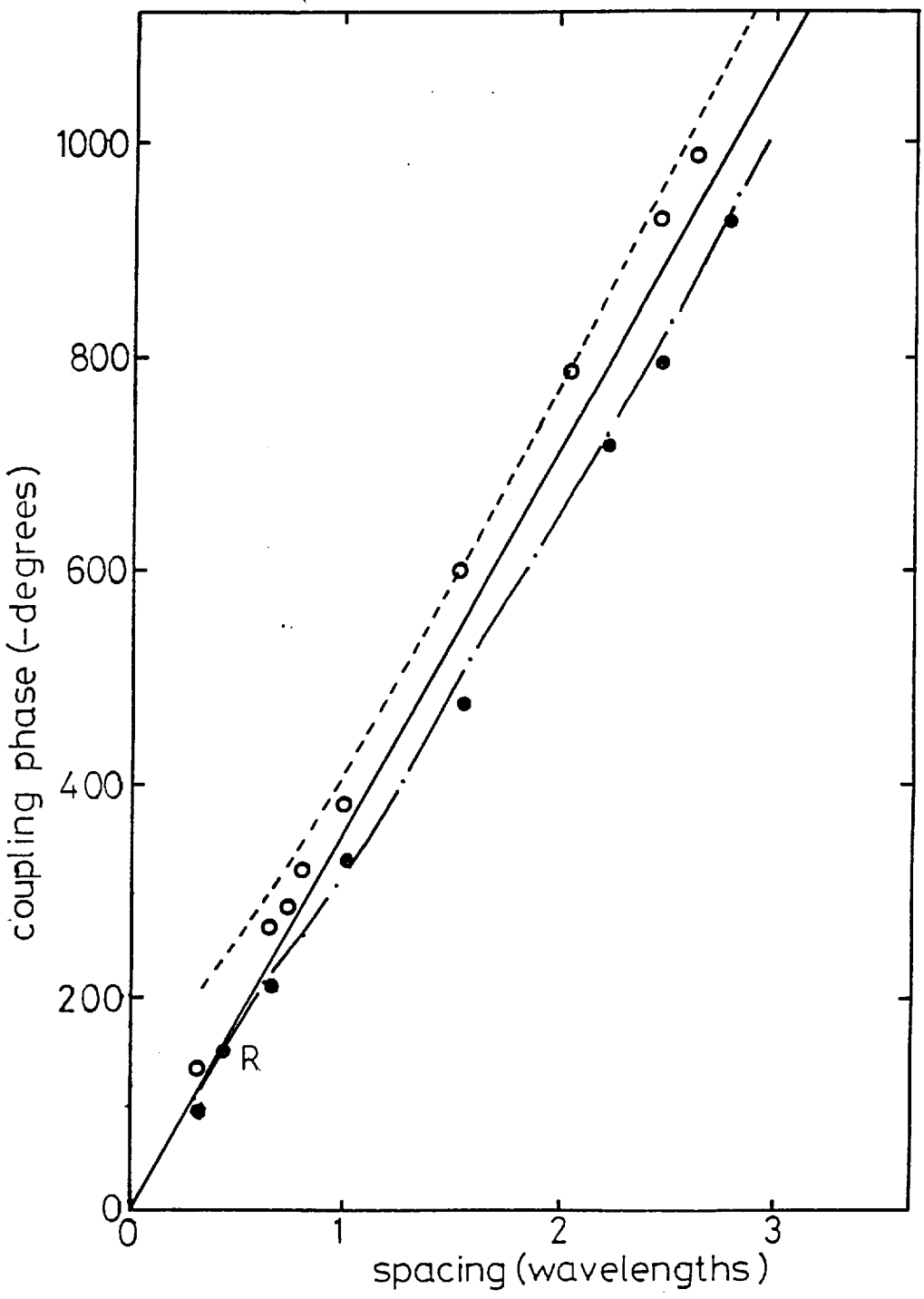

——— free space variation R-reference phase (see text)

—·—·— theory
● experiment
results given in
Table 5.1 (absolute values)
} slots of opposite hand

---- theory
○ experiment
results given in
Table 5.1 (absolute values)
} slots of the same hand.

finite size of the ground plane; modifications to the edges, however, failed to perturb the results significantly. Also, the effect is not consistent with a mismatch error in the measurement arm. It was concluded that the ripple is due to scattering between the arms of the slots.

At close spacings the mutual coupling falls away rapidly as expected with the predominant inductive coupling predicted by theory. At extended spacings, where the coupling between the parallel end arms becomes significant, the rate of decay is reduced in accordance with the theoretical curves. In general, the agreement is better for slots of the same hand. The results, for small spacings (provided by measurements of slots milled in the side walls of adjacent reduced height waveguide as described in the following section) show that, for slots of opposite hand, the experimental values of coupling are significantly larger than the theoretical values. This is thought to be due to the close proximity of the two adjacent end arms in which situation the theory is not accurate.

In contrast to the amplitude of the amplitude of the mutual coupling, the experimental values of the phase of the mutual coupling plotted in Figure 5.22 are in good agreement with theory for slots of opposite hand, whilst there is a marked divergence between the corresponding curves for slots of the same hand at small spacings. It is well known, however, that the first order theory used here does not in general provide accurate predictions of the coupling phase.

At extended spacings the experimental values are in good agreement with the theoretical curves for the

two configurations. Both tend towards a free space law as expected. It should be remembered, however, that the experimental results plotted in Figure 5.22 are only relative due to the difficulty in calibrating the phase of the bridge. Absolute values for thephase of the coupling will be established in the next section.

5.4. MUTUAL COUPLING BETWEEN Z SHAPED SLOTS IN THE SIDE WALL

5.4.1. DERIVATION OF THE RELATIVE SLOT EXCITATIONS IN MUTUALLY COUPLED SLOTS IN THE SIDE WALLS OF ADJACENT WAVEGUIDES

In order to determine the absolute phase of the mutual coupling between Z shaped slots, the arrangement shown in Figure 5.24 was considered. The slots are milled in the side wall of separate waveguides which are positioned such that the slots are adjacent.

Consider one such slotted waveguide with a fundamental TE_{10} mode wave of unit amplitude incident on the slot as shown in Figure 5.23. This excites an electric field in the slot which, in turn, generates secondary TE_{10} mode waves, travelling to the left and right of the slot and also a radiated wave. The amplitude and phase of these waves will be directly related to the voltage excited across the centre of the slot provided that the slot is single moded. The latter assumption has been substantiated by the admittance measurements documented in Chapter 3. For a resonant shunt slot the generated waves will be equal in both directions and in antiphase with the incident wave. Then, provided that the higher order waveguide modes are evanescent, conservation of energy demands:

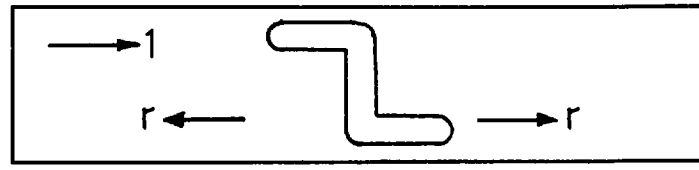

Fig. 5.23: Scattering of waves by a slot in a waveguide.

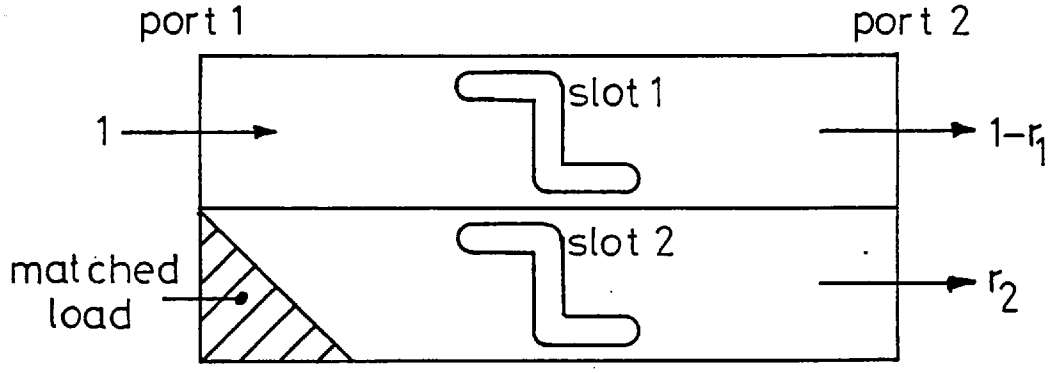

Fig. 5.24: Scattered waves in mutually coupled waveguide slots.

$$1 = r_1^2 + (1-r_1)^2 + \text{(energy radiated)} \qquad (5.19)$$

where r_1 is the amplitude of the secondary waves. Now, with thesecond slotted waveguide placed adjacent to the excited slot, a wave of amplitude r_2, say, is generated in this waveguide due to the mutual coupling between the slots as depicted in Figure 5.24. When the Z shaped slots are identical in size and of the same hand, then the relative amplitudes and phases of the generated waves in the two waveguides will be directly related to the corresponding slot excitations. That is,

$$\frac{v_1^s}{v_2^s} = \frac{r_1}{r_2} e^{j\phi_{12}} \qquad (5.20)$$

where ϕ_{12} is the relative phase of the secondary waves in the two waveguides.

If identical slots of opposite hand are considered, then the phase relationship is different by π radians. That is,

$$\frac{v_1^s}{v_2^s} = - \frac{r_1}{r_2} e^{j\phi_{12}} \qquad (5.21)$$

In an actual measurement, the signals at ports 2 and 4 (see Figure 5.24) are compared, that is, $(1-r_1)$ and r_2. Although r_1 is not determined explicitly it may be derived separately, either from an impedance measurement, or a measurement of the attenuation past the slot. In the latter case, the attenuation at resonance in dB, A, is defined by:

$$A = 20 \log_{10} (1-r_1) \qquad (5.22)$$

If the mutual coupling is small and the scattering from the parasitic slot can be ignored, the attenuation can be measured with the slot isolated. Ideally, however, the resonant frequency and attenuation should be established with the second slot parasitic.

The relative phase of the waves generated in the two waveguides can be determined directly from the signals at ports 2 and 4, provided that the slots are resonant. If the electrical lengths of the waveguides relative to the slot positions are equal, then the relative phase, ϕ, of the waves $(1-r_1)$ and r_2 at the slot centres are preserved at ports 2 and 4. ϕ_{12} is thus given by ϕ for slot of opposite hand and $(\phi \pm \pi)$ for slots of the same hand.

5.4.2. EXPERIMENTAL INVESTIGATION

The Z shaped slots were milled in the special reduced height waveguide (internal dimensions 1.27" × .67") which was to be used in the final array design. The dimensions of the slots are given in Figure 5.25 and are directly scaled from those used in the X-band experiments so that they are resonant around 5.6 GHz. The reduced height waveguide allows the measurement of mutual coupling to be made at a slightly smaller electrical spacing than that possible with standard waveguide.

To provide clearance for the waveguide flanges with the waveguides adjacent, double-mitred joints were used to angle the input arms of one slotted waveguide as depicted in Figure 5.26.

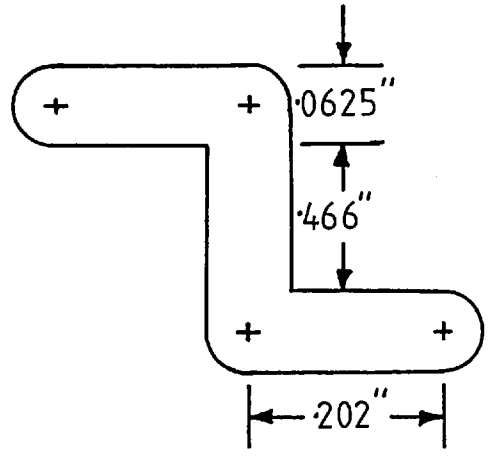

Fig. 5.25: Dimensions of Z shaped slots for operation at 5.6GHz.

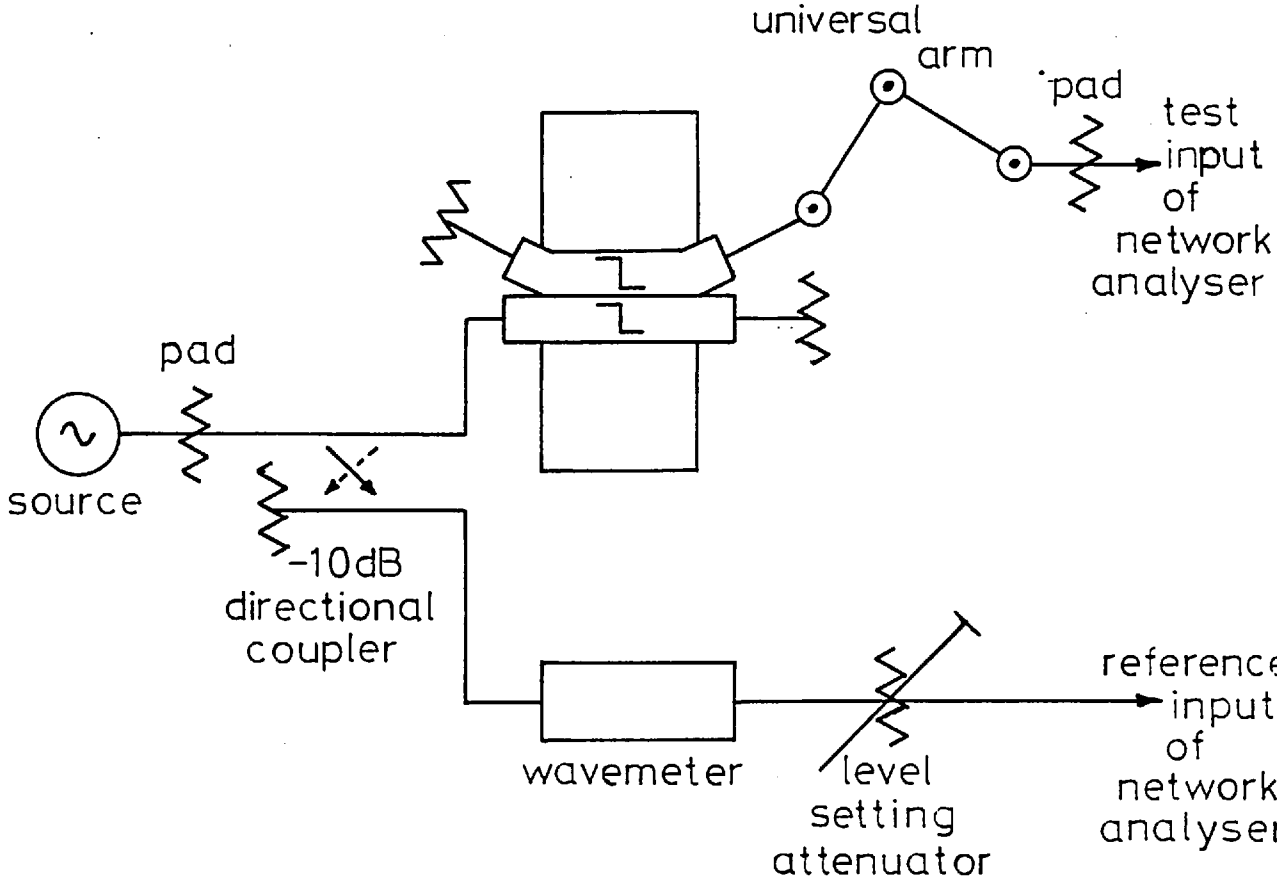

Fig. 5.26: Schematic diagram of mutual coupling measurement bench for slots in the side wall.

With the slot in this waveguide shorted with conducting adhesive aluminium tape and a high quality matched load (VSWR < 1.03) at one output port, the input VSWR was less than 1.07 over the band of interest, demonstrating that the corners do not introduce any serious mismatch. The difference in electrical lengths from the slot to the measurement port in the two waveguides was compensated for when establishing the phase relationship of the two slot excitations. The difference was measured by connecting a variable short circuit to the two measurement ports in turn and adjusting it to minimise the radiated power, at which point the voltage minimum of the standing wave is positioned at the slot centre.

The slotted-waveguides were clamped in an experimental jig and aluminium sheets placed either side of the waveguides, flush with the wall containing the slot to form a groundplane. Electrical continuity was ensured by sealing over the joints with conducting adhesive aluminium tape. The sheets extended approximately five wavelengths either side of the slots.

The signals at ports 2 and 4 were compared using a Hewlett-Packard network analyser, model no. 8102A. The phase error associated with this instrument is specified to be not greater than ±2 degrees. Phase variations produced in the receiving channel as the detector was moved from one measurement port to the other was reduced by using the co-axial universal arm described earlier. Allowing for possible errors due to the variation in phase through the rotating joint with rotation, the total uncertainty in phase is approximately ±4 degrees. The uncertainty in the amplitude measurements was estimated to be no greater than ±.2dB. A schematic diagram of the complete

measuring system is given in Figure 5.26.

The calibration of r_1 was obtained from a measurement of the insertion loss of the slotted waveguides. A swept frequency measurement was made over the band 5.25-6.00GHz; plots of the insertion loss for three nominally identical Z shaped slots, each measured in isolation, is reproduced in Figure 5.27. The plots labelled 1 and 2, corresponding to two slots of the same hand, are well correlated and their frequency of peak attenuation, 5.60 GHz, was taken to be the resonant frequency. (This has been shown by Chignell [1] to be a valid assumption). The third slot (plot 3), which is of opposite hand to the other two slots, has a lower peak value of insertion loss occurring at a slightly higher frequency. The reactance introduced when the slot is operated off-resonance at 5.60 GHz is, not, however, large enough to introduce any significant errors in the phase measurements. At 5.60 GHz, the presence of an adjacent slot had a negligible effect on the measurement of attenuation and the isolated levels were taken for a calculation of r_1.

The mutual coupling was measured for one, two and three waveguide spacings (one waveguide spacing = $.332\lambda_o$) of slots of opposite hand and of the same hand. The results are presented in Table 5.1. Also included in Table 5.1 are the equivalent values of the mutual coupling coefficient defined earlier. The derivation of these values from the side wall slot measurements is described in Appendix 3. These results and the values for the phase of the mutual coupling are superimposed on the curves of Figures 5.21 and 5.22 for comparison.

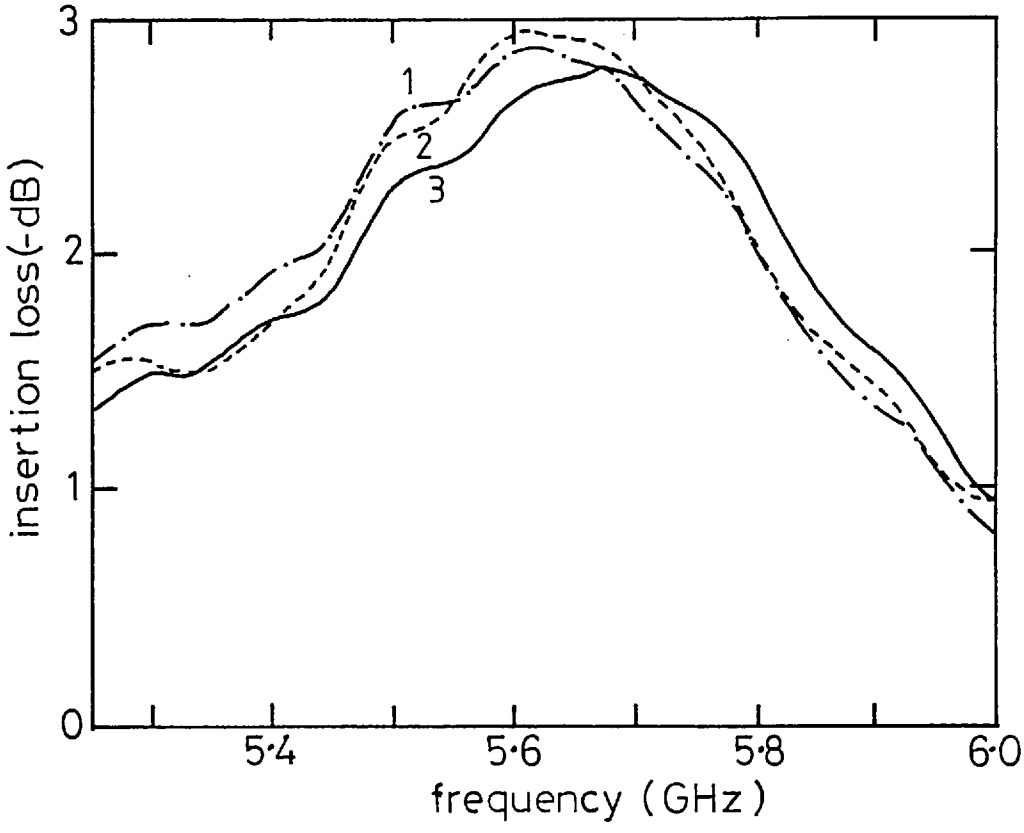

Fig. 5.27: Insertion loss of Z shaped slots in the side wall.

Table 5.1

Slot configuration	Spacing (waveguide widths)	Signal at Port 4 relative to that at Port 2		Magnitude of r_1	Relative slot excitation		Mutual Coupling Coefficient
		$r_2^2/(1-r_1^2)$ dB	phase (deg)		magnitude	phase (deg)	amplitude (dB)
slots of the same hand	1	-14.0	+48	.302	.462	-132	-10.3
	2	-25.0	-85	.302	.141	+ 95	-21.3
	3	-33.1	+161	.302	.051	- 19	-29.4
slots of opposite hand	1	-18.4	-95	.284	.302	- 95	-14.4
	2	-27.2	-208	.284	.110	-208	-23.2
	3	-34.1	+36	.284	.050	+ 36	-30.1

Note: one waveguide width = .332λ.

The phase of the mutual coupling between slots of opposite hand are in good agreement with the theoretical values. With slots of the same hand, however, the experimental curve for the phase variation with spacing diverges from the theoretical curve at close spacings, although it is consistent with the end wall measurement. The amplitudes of the mutual coupling coefficient are generally well correlated with the corresponding end wall measurements.

To confirm the experimental results presented in Table 5.1 the radiation patterns of arrays of two slots were measured. These are described in the following section.

5.5. RADIATION PATTERN ANALYSIS OF MUTUAL COUPLING IN Z SHAPED SLOT SUB-ARRAYS

It may be noted from Table 5.1 that the relative magnitude of the voltage excited across the centre of a coupled slot is quite large at small spacings. It was realised that the effect of the coupled (or parasitic) slot on the radiation pattern of a single fed slot would be significant enough to give a good indication of the phase of the coupled voltage and provide some confirmation of the results obtained in the above investigation. As the second slot is parasitic, the power dividing network of a fully excited array is not required and the measurement is greatly simplified.

5.5.1. RADIATION PATTERN OF AN END-LOADED DIPOLE

The principal polarized fields radiated by a Z shaped slot are due only to the equivalent magnetic current in the centre section. To remain consistent with theprevious theoretical

analyses, we will determine the E plane radiation pattern of the centre section of the equivalent end loaded dipole. The corresponding end loaded slot radiation pattern is identical from duality considerations.

The far fields of an elemental dipole of length dz' aligned along the z axis and at the origin of the co-ordinate system defined in Figure 5.28 are given by:

$$E_\theta = \frac{j\omega\mu_o I_o dz' e^{-jkr}\sin\theta}{4\pi r} \qquad (5.23)$$

$$H_\phi = \frac{E_\theta}{Z_o} \qquad (5.24)$$

where I_o is the amplitude of the current.

and Z_o is the intrinsic impedance of free space.

The current distribution along the end loaded diple I(z') is given, as before, by:

$$I(z') = I_o \cos\left(\frac{\pi z'}{2\ell}\right) \qquad (2.25)$$

where ℓ is the equivalent height of the dipole.

Assuming the dipole to be made up of elemental dipoles, each with a uniform current distribution along its length, the contribution of one element at z' to the total electric field at a point P in the far field is :

$$dE_\theta = \frac{j\omega\mu\sin\theta}{4\pi r} I_o \cos\frac{\pi z'}{2\ell} e^{-jk(r-z'\cos\theta)} dz' \qquad (5.26)$$

where r is defined in Figure 5.28.

The total electric field radiated by the centre section will then be:

$$E_\theta = \frac{j\omega\mu\sin\theta}{4\pi r} I_o e^{-jkr} \int_{-h}^{h} \cos\frac{\pi z'}{2\ell} e^{jkz'\cos\theta} dz' \qquad (5.27)$$

$$E_\theta = \frac{j\omega\mu I_o e^{-jkr}}{2\pi kr} \left\{ \frac{\sin(\frac{\pi h}{2\ell})\cos(k\cos\theta.h) - \cos\theta\cos(\frac{\pi h}{2\ell})\sin(k\cos\theta.h)}{\sin\theta} \right\} \qquad (5.28)$$

With Eqn. 3.25, the power E plane radiation pattern of the dipole (and the dual slot) is proportional to the square of the function included in the brackets in Eqn. 5.28. This has been computed for the slot dimensions defined in Figure 5.25 and is used for comparison with experimentally derived patterns.

5.5.2. CALCULATION OF THE ARRAY PATTERNS

The calculation of the array pattern is a standard problem and has been discussed in Chapter 1. If the radiators are identical (or produce identical radiation patterns) the total radiation pattern is simply the product of the radiation pattern or one element and the array factor. For the two slot array considered here, the array factor, $F(\theta)$, is given by:

$$F(\theta) = 1 + \frac{v_2^s}{v_1^s} e^{j(ks\cos\theta+\phi_{21})} \qquad (5.29)$$

where s is the slot separation

and ϕ_{21} is the phase of the parasitic slot excitation relative to the excited slot.

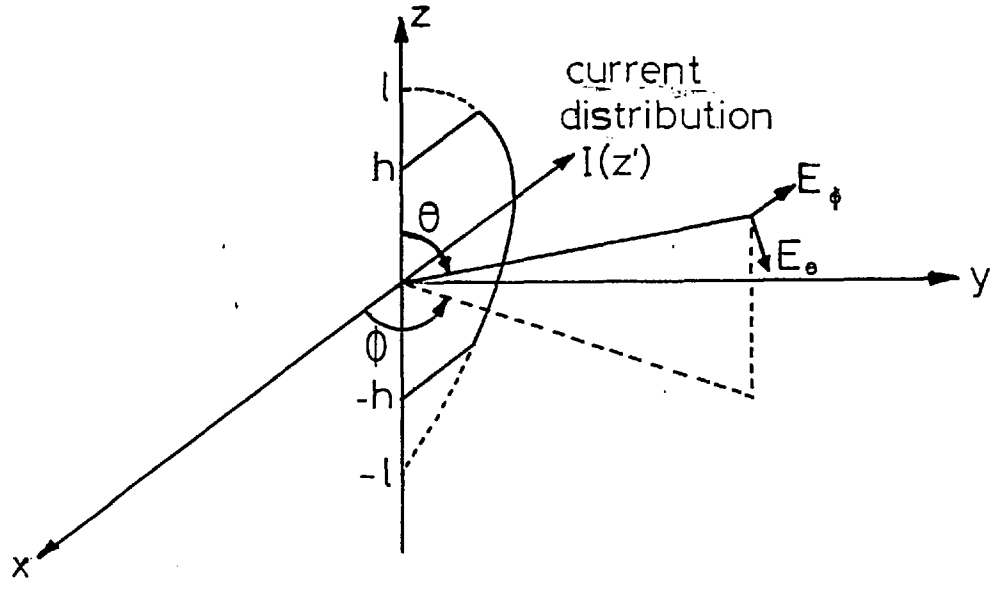

Fig. 5.28: End loaded dipole and co-ordinate system.

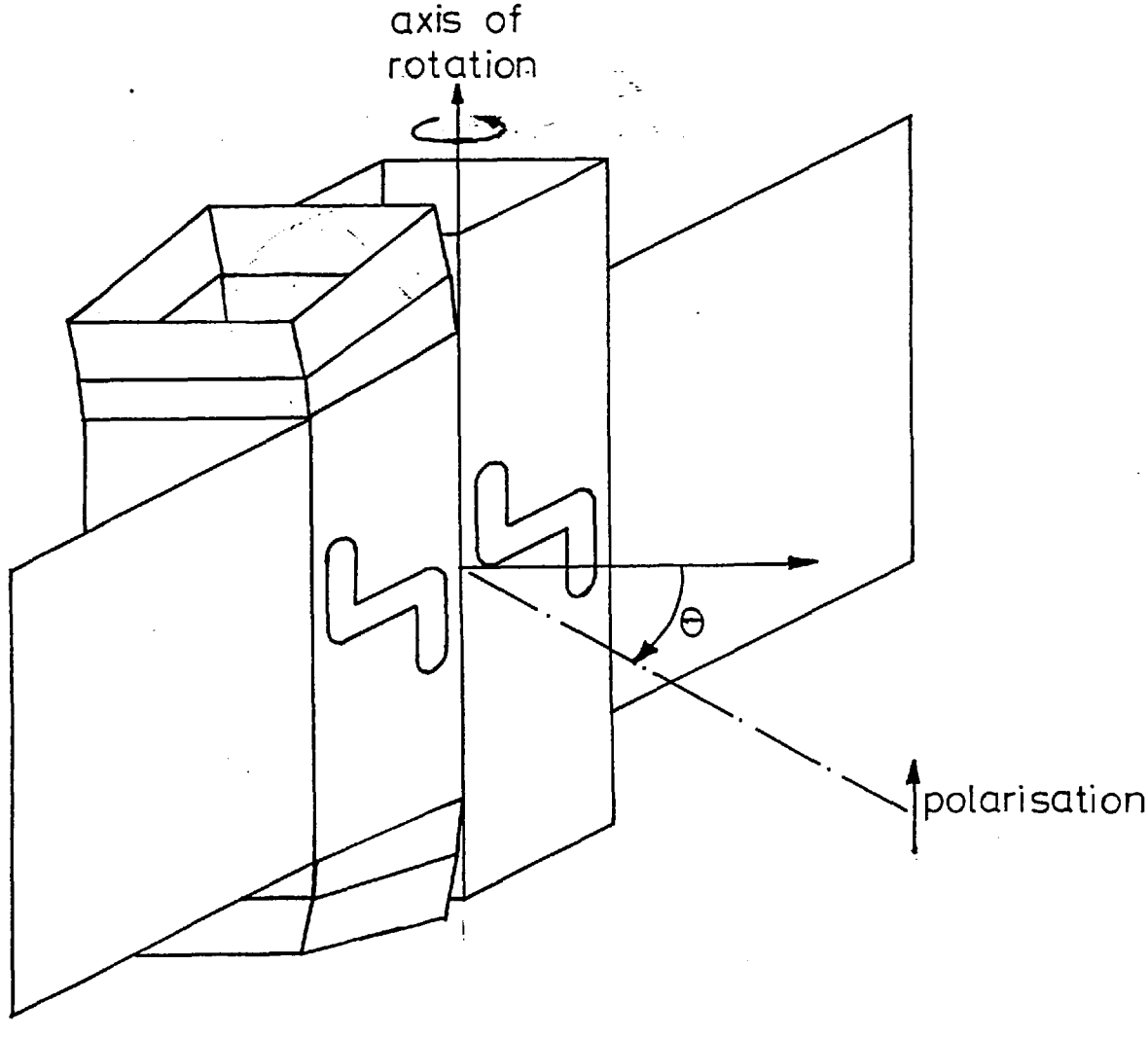

Fig. 5.29: Arrangement for radiation pattern measurement.

This has been evaluated by substituting in the previously measured values of the slot excitations and, with the theoretical radiation pattern of an isolated slot, used to calculate the array radiation patterns. If the isolated radiation patterns are not assumed to be equal for the two slots, the array pattern may be obtained by adding the actual contributions from the two slots at each angle. The excitation of the slots is again assumed to be that calculated from the mutual coupling measurements.

5.5.3. EXPERIMENTAL EVALUATION

The pattern measurements were carried out with the arrays consisting of the same slotted waveguides used in the mutual coupling experiments and at the same frequency, 5.60GHz. The radiation patterns were recorded in the anechoic chamber installed at ASWE, Hambrook. The waveguides were mounted vertically on the receiving turntable as shown in Figure 5.29. The receiving system consisted of a Scientific Atlanta remote waveguide mixer and superheterodyne receiver coupled to a chart recorder. The power radiation patterns may be plotted on a linear scale which provides greater detail of the main lobes than the usual logarithmic scale. Measurements were made with three different slot arrangements: slots of the same hand at spacings of $.332\lambda_o$ and $.732\lambda_o$ and slots of opposite hand at a spacing of $.332\lambda_o$. For each arrangement the isolated radiation pattern of both slots were plotted. Then the array patterns were recorded, first with one slot parasitic and then the other. Sample patterns for each arrangement are reproduced in Figures 5.30, 5.31 and 5.32, with the appropriate theoretical predictions.

SLOTS OF THE SAME HAND SPACING = 0.332λ

(a) Isolated patterns of the two slots.

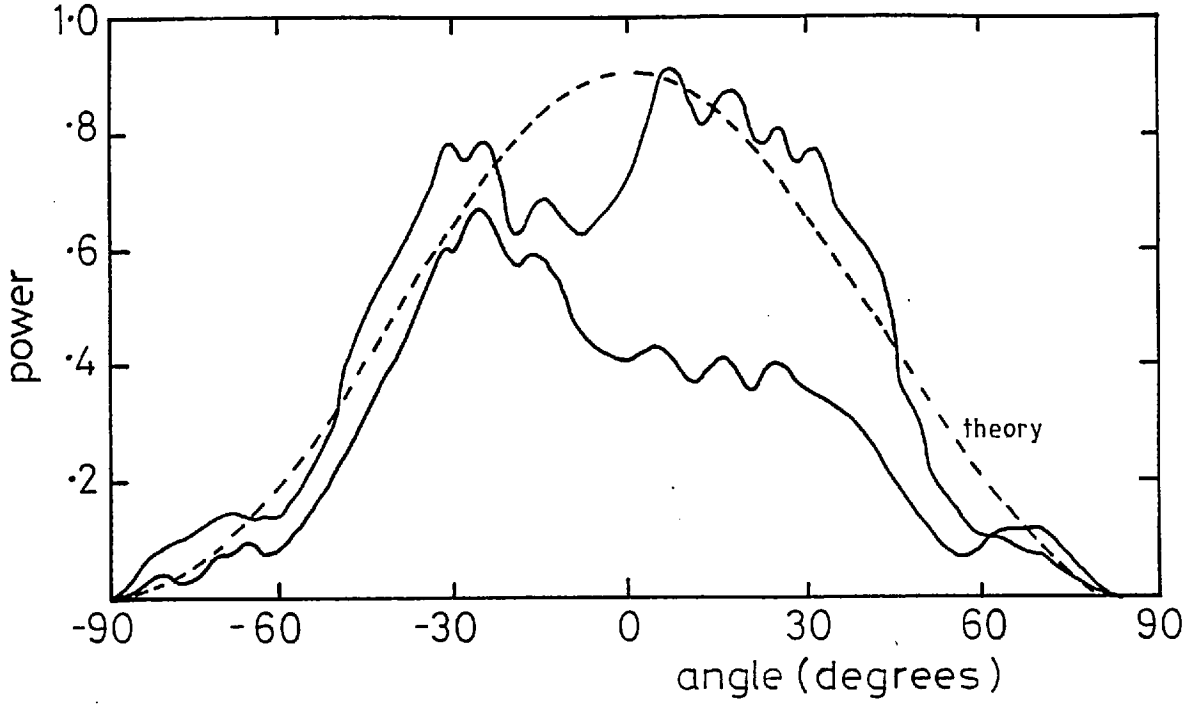

(b) Parasitic array patterns with mitred guide slot receiving.

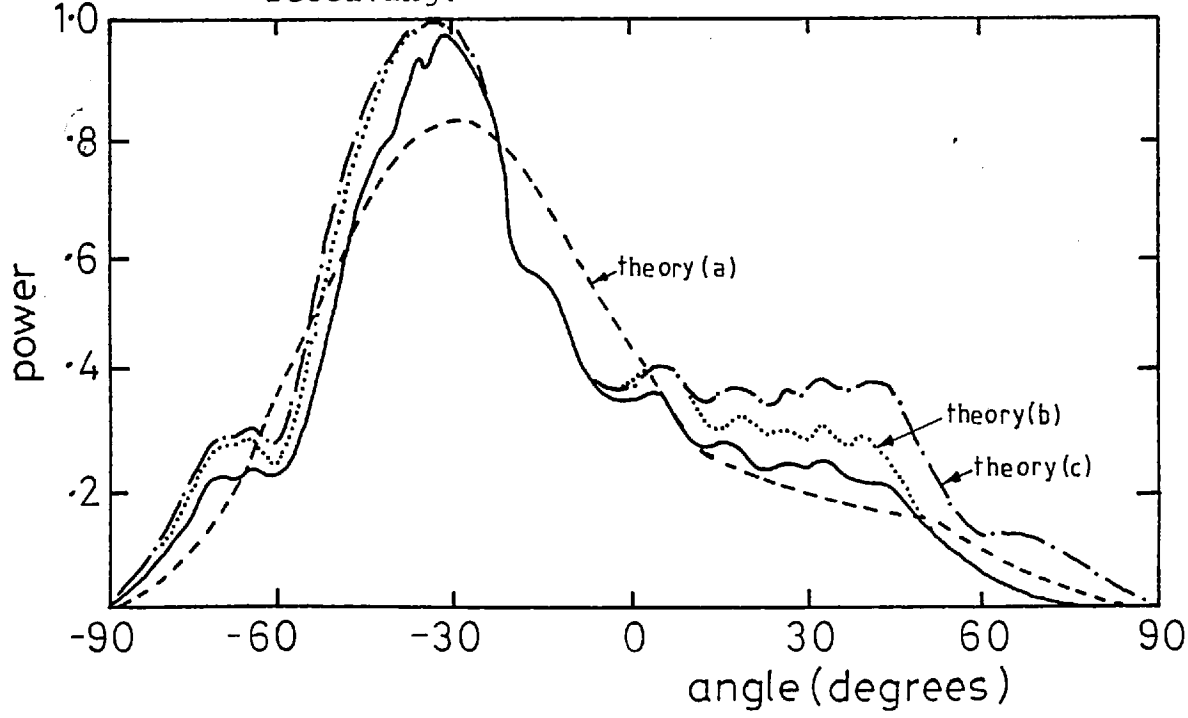

Fig. 5.30: Radiation patterns of two slots of the same hand, at adjacent waveguide spacing.

SLOTS OF THE SAME HAND SPACING = 0.732λ

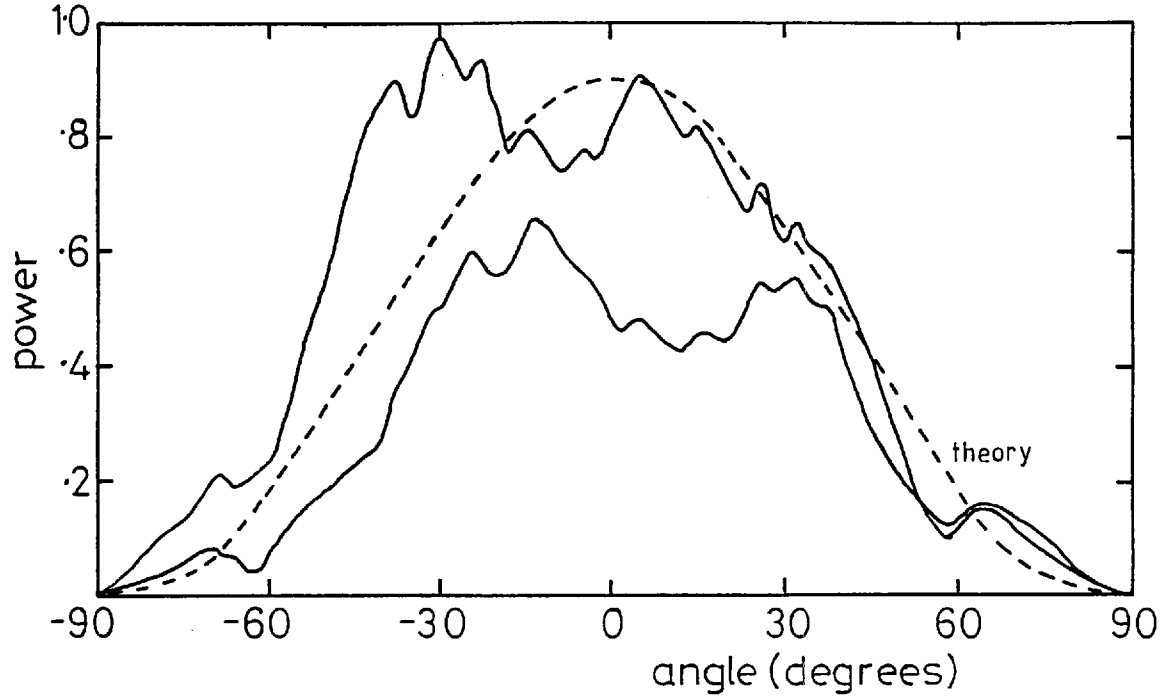

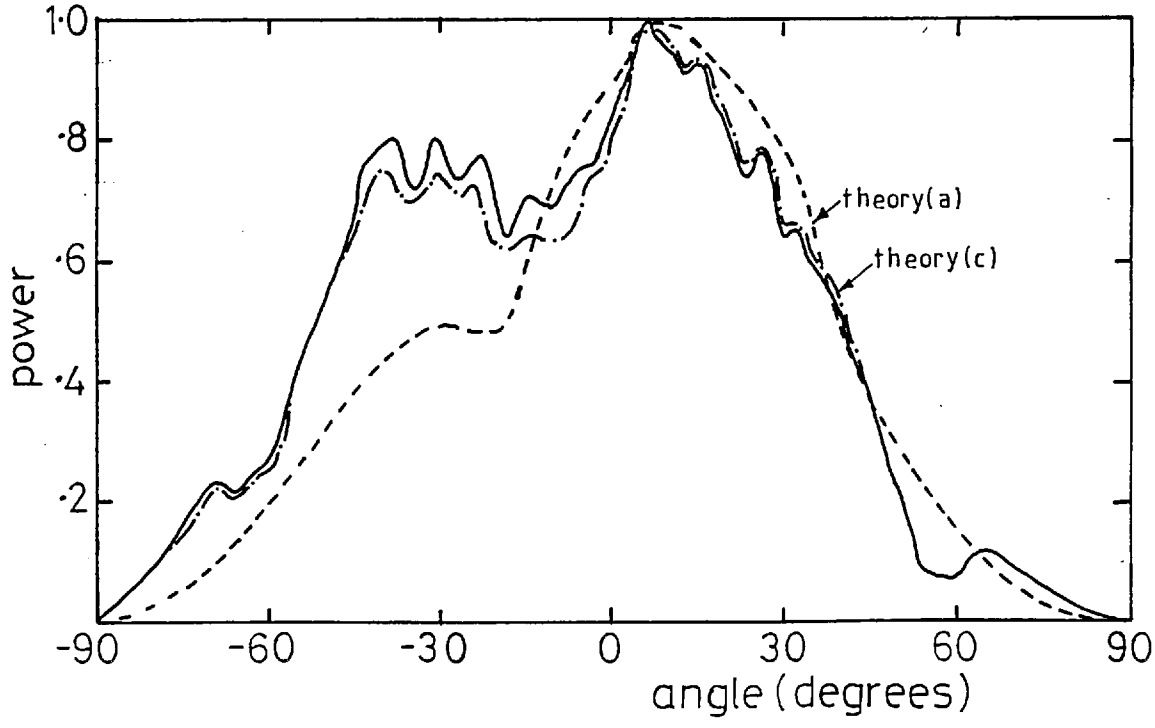

Fig. 5.31: Radiation pattern of two slots of the same hand at spacing $0.732\lambda_o$.

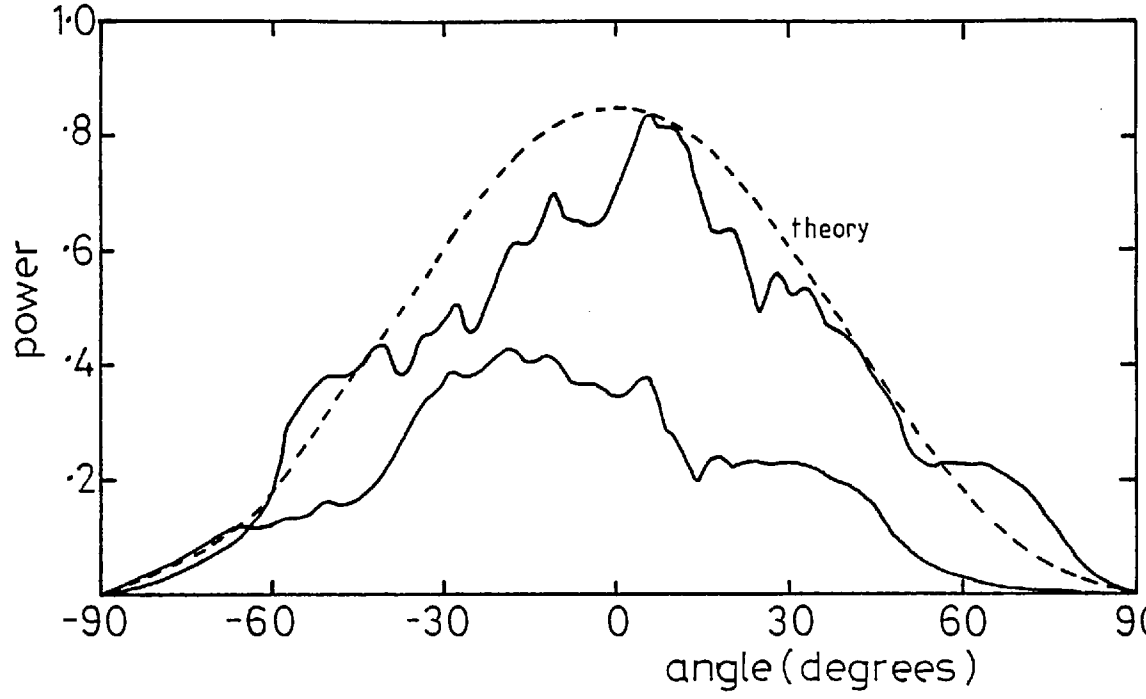

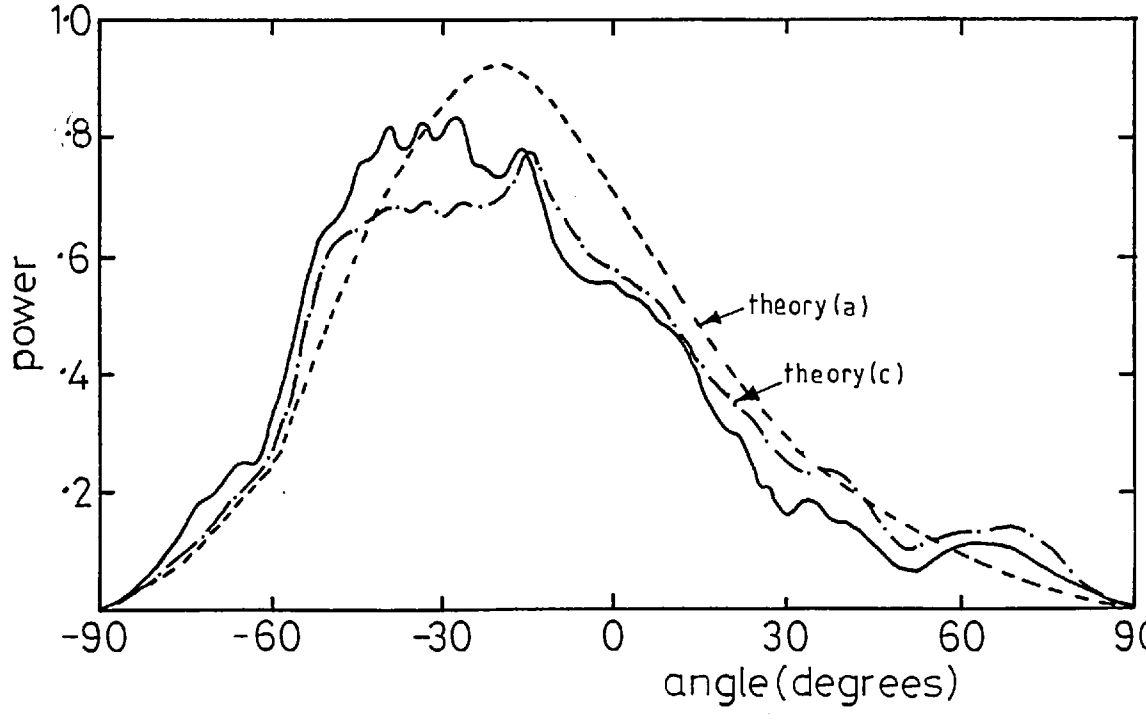

Fig. 5.32: Radiation pattern of two slots of opposite hand at adjacent waveguide spacing.

The array patterns were calculated as:

(a) the product of the array factor and the theoretical isolated pattern

(b) the product of the array factor and the measured radiation pattern of the driven slot

(c) the addition of the contributions from each slot using the two measured isolated slot radiation pattern and the relative slot excitations in Section 5.3.

5.5.4. DISCUSSION OF RESULTS

It may first be noted that the level of the experimental isolated radiation patterns are quite different. (The receiver gain was constant for the two measurements). This is due to the poor VSWR of the waveguide mixer which gives rise to large mismatch uncertainties when interacting with the heavily coupled slots. The mismatch losses will thus be different for the two slotted waveguides because of their different electrical lengths. The asymmetry in the isolated patterns is thought to be due to the conducting adhesive aluminium tape used to seal the joints between the waveguides and also short out the second slot. The fine ripple structure is associated with reflections off the chamber walls and is accentuated by the low gain of the slots.

The theoretical array patterns are all well correlated with the experimental plots particularly when measured isolated radiation patterns are used in the predictions, which indicates that the measured values of mutual coupling coefficients and

the procedures used to calculate the relative slot excitations are adequate. However, the array patterns are not sufficiently sensitive to phase variations to confirm the phase measurements to an accuracy better than $\pm 10^{\circ}$, particularly with the irregularities noted in the isolated radiation patterns.

6. MUTUAL COUPLING BETWEEN I SHAPED SLOTS AND ARRAY DESIGN

6.1. INTRODUCTION

In previous chapters the characteristics of the new class of low loss complex shaped slots have been examined experimentally using the Z shaped slot as example. It was chosen for the initial investigations because, in addition to being the simplest configuration, it is tightly coupled to the waveguide and eases the dynamic range requirements in the measurement of mutual coupling. It was found that the first order approximation of the fields in the slot provides reliable predictions of the coupling between the slot and the dominant waveguide mode. The calculation of mutual coupling employing the same approximation is not, however, sufficiently accurate to be used in an actual design, even though it provides a good indication of the basic mutual coupling behaviour. The aim of the work described in this chapter was to study the effects of changing the end arm dimensions of I shaped slots and obtain empirical data for the final array design.

The I shaped slot was developed from the Z shaped slot to provide a variation in the coupling to the dominant TE_{10} waveguide mode whilst maintaining the centre section dimensions constant. The slot is shown in Figure 3.11 and the theoretical expressions for the parameters of the admittance invertor are presented in Chapter 3. In order to simplify the treatment of mutual coupling in a large array design, certain assumptions were proposed in Chapter 4 which, for convenience, are summarised below:

1. The cross polarisation suppressors required in the final array were designed such that the mutual coupling over them was minimised and only the mutual coupling between slots in the trough formed by the suppressors need be considered.

2. It was shown that, for the range of slot conductances (referred to the equivalent TE_{10} mode transmission line) required in the array design, the effect of the waveguide loading on the slots could be ignored. The mutual coupling could then be expressed in quantities referred to terminals across the slot centres and the presence of the waveguide could be ignored, that is, the slots are effectively open circuited.

3. The self conductances of the I shaped slots (referred to the slot terminals) are virtually constant with variation of the end arm dimensions. This allows the mutual coupling to be expressed in terms of the voltage coupling coefficient defined in Chapter 4.

The information required for the final array design is therefore the value of the voltage coupling coefficient as a function of the end arm dimensions for slots situated in the trough formed by the cross polarisation baffles. It was thought that the mutual coupling at extended spacings would be due only to the fields in the centre sections as the modes excited by the end arms are evanescent in the parallel region. It was shown by Chignell that the mutual coupling is independent of the orientation of the slots at large spacings which provided confirmation of this assumption. Therefore, the investigations described here concentrated

on small slot spacings.

In the following section,the expressions used to derive the voltage coupling coefficient are modified to accommodate slots with different end arm dimensions.

6.2. NETWORK ANALYSIS OF THE MUTUAL COUPLING BETWEEN I SHAPED SLOTS WITH DIFFERENT END ARM DIMENSIONS

In Chapter 5 the mutual coupling coefficients were derived for pairs of identical slots. Similar relationships can be obtained for I shaped slots with different end arm dimensions (and hence different coupling to the waveguide) by modifying the equivalent circuit of Figure 4.5. At resonance, the I shaped slots have a near constant self conductance, g_{11}. Let K^2_1 and K^2_2 be the parameters of the admittance invertors of two mutually coupled resonant I shaped slots with different end arm dimensions. Then, the matrix equation relating the generator voltage, V_1, and current, I_1, and the detected voltage,V_2, and current, I_2 in the coupled waveguide is:

$$\begin{pmatrix} V_1 \\ I_1 \end{pmatrix} = \begin{bmatrix} 1 & 1 \\ 0 & 1 \end{bmatrix} \begin{bmatrix} 1 & 0 \\ 1 & 0 \end{bmatrix} \begin{bmatrix} 0 & 1/K_1 \\ K_1 & 0 \end{bmatrix} - \frac{1}{y_{12}} \begin{bmatrix} g_{11} & 1 \\ g_{11}^2 - y_{12}^2 & g_{11} \end{bmatrix}$$

$$\begin{bmatrix} 0 & 1/K_2 \\ K_2 & 0 \end{bmatrix} \begin{bmatrix} 1 & 0 \\ 2 & 1 \end{bmatrix} \begin{pmatrix} V_2 \\ 0 \end{pmatrix} \qquad (6.1)$$

After multiplying out the matrices and extracting the A element (see Chapter 4):

$$\frac{V_2}{V_1} = \frac{-K_1K_2y_{12}}{4(g_{11}^2-y_{12}^2) + 2g_{11}(K_1^2+K_2^2)+K_1^2K_2^2} \qquad (6.2)$$

The ratio is independent of which slot is excited and thus reciprocity is satisfied. If it is again assumed that low coupling slots are used, such that K_1^2 and K_2^2 are small, and if $|y_{12}|$ is very much less than g_{11}:

$$\frac{V_2}{V_1} \approx -\frac{K_1K_2y_{12}}{4g_{11}^2} \qquad (6.3)$$

In the measurement of the mutual coupling between identical 'Z' shaped slots, the signals at the output ports of the two waveguides were compared. When the slots are not identical it is convenient to compare the signal generated in the second waveguide with the incident signal on the first slot (which is measured by shorting out the slot). If the incident voltage is V_i, then:

$$\frac{V_2}{V_i} \equiv -\frac{K_1K_2y_{12}}{2g_{11}^2} \qquad (6.4)$$

It was established in Chapter 4 that the ratio of the voltages across the centres of the coupled slots is appoximately given by:

$$\frac{v_2^s}{v_1^s} = -\frac{y_{12}}{g_{11}} \qquad (6.5)$$

Therefore, the two ratios are related by:

$$\frac{v_2^s}{v_1^s} = \frac{2g_{11}}{K_1 K_2} \cdot \frac{V_2}{V_i} \qquad (6.6)$$

The equivalent power relationship is:

$$R_p = 4 \frac{g_{11}}{K_1^2} \cdot \frac{g_{11}}{K_2^2} \cdot \left|\frac{V_2}{V_i}\right|^2 \qquad (6.7)$$

Now, for a resonant slot with a conductance G (normalised to the characteristic admittance of the dominant TE_{10} mode), the ratio of the power radiated by the slot relative to the power incident on it, P_r is:

$$P_r = \frac{4G}{(2 + G)^2} \qquad (6.8)$$

In terms of quantities defined across the centre of the slot, this becomes:

$$P_r = \frac{4K^2 g_{11}}{(2g_{11} + K^2)^2} \qquad (6.9)$$

For a low coupling slot this approximates to:

$$P_r = \frac{K^2}{g_{11}} \qquad (6.10)$$

Thus, Eqn. 6.7 can be expressed as:

$$R_p = \frac{4 \left|V_2/V_i\right|^2}{P_{r1} P_{r2}} \qquad (6.11)$$

where P_{r1} and P_{r2} are the values of P_r for the excited slot and coupled slot respectively.

This provides a convenient procedure for estimating the external mutual coupling from the waveguide parameters and vice-versa.

In the measurement of mutual coupling between Z shaped slots, the slot dimensions are nominally identical and the resonant frequencies of the experimental models were well correlated. In the case of I shaped slots with different end arm dimensions, however, it is far more difficult to fabricate the slots such that their resonant frequencies are identical. The amplitude of the power coupled to the second waveguide was therefore measured on a swept frequency basis. The corresponding measurement of phase is far more difficult on a swept frequency basis and is subject to greater errors. It was decided to establish the phase of the mutual coupling coefficient from a fixed frequency measurement, as before, and include a correction for the phase variation caused by operating the excited slot off-resonance.

In Chapter 4, a network representation was obtained for the mutual coupling between two waveguide fed slots. It was shown that for low coupling slots:

$$\arg \frac{V_2^s}{V_1^s} = \arg \frac{V_2}{V_i} - \arg Y_{11} \qquad (6.12)$$

where Y_{11} is the complex admittance of the slot normalised to the characteristic admittance of the dominant waveguide mode.

At resonance, the phase relation bewteen the two slot voltages is approximately $\arg(-y_{12})$. When the slots are off-resonance, this quantity is given by:

$$\arg(-y_{12}) = \arg \frac{V_2}{V_i} - 2 \arg(Y_{11}) \qquad (6.13)$$

If the signal generated in the parasitic slotted waveguide is compared with the signal past the excited slot, as in Chapter 5, the derivation of the phase between the slot voltages is more difficult when the excited slot is off-resonance. The phasor diagram of the waveguide voltages corresponding to this situation is shown in Figure 6.1. There, ϕ is the phase angle between the signal at the output port of the excited waveguide and the signal generated in the parasitic guide, as measured in the experiments of Chapter 5. The other angles are given approximately by [3]:

$$\theta = \tan^{-1} - \frac{B}{2}$$
$$\alpha = \pi + \tan^{-1} \frac{B}{G} \qquad (6.14)$$

Thus for, slots of the same hand, from Figure 6.1

$$\arg \frac{V_2}{V_1} = - \{\phi + \tan^{-1} \frac{B}{2} + \pi + \tan^{-1} \frac{B}{G}\} \qquad (6.15)$$

$$\arg (-y_{12}) = - \{\phi + \tan^{-1} \frac{B}{2} + \pi + 2\tan^{-1} \frac{B}{G}\} \qquad (6.16)$$

Similarly, for slots of opposite hand:

$$\arg (-y_{12}) = - \{\phi + \tan^{-1} \frac{B}{2} + 2\tan^{-1} \frac{B}{G}\} \qquad (6.17)$$

These relationships have been used in Section 6.3.2. to correct for the phase variation introduced when one slot is operated off-resonance.

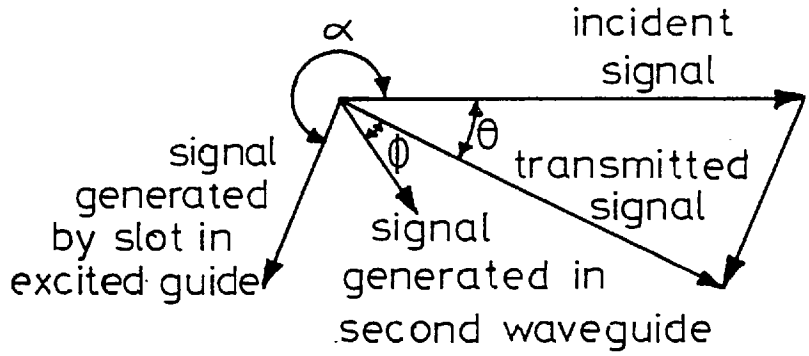

Fig. 6.1: Phasor diagram of voltages in mutually coupled slots.

6.3. EXPERIMENTAL EVALUATION OF MUTUAL COUPLING BETWEEN CLOSELY SPACED I SHAPED SLOTS

The mutual coupling has been measured between I shaped slots in the side wall of the reduced height waveguide. As explained in the introduction, a principal aim of the investigation was to examine the effects of changing the end arm dimensions. Four slot shapes were chosen to cover the range of normalised conductances required in an array design. The dimensions, of the slots are presented in Table 6.1 where, for convenience, they are numbered 1 to 4 , with slot 1 having the highest normalised conductance and slot 4 the lowest. The lengths ℓ_a, ℓ_b and ℓ_c are defined in Figure 3.11. Also included in Table 6.1 is the typical relative power coupled to a WG12 waveguide side arm. In this measurement, the peak attenuation past the slots occurred at a mean frequency of 5.87 GHz. With the slots radiating into .625" square baffles separated by 1.50" and covered with PTFE tape (for weather protection) the frequency of peak attenuation is lowered to around 5.6 GHz.

Three sets of slots were milled: one set in a waveguide with angled output arms, similar to that described in Chapter 5, and the other two in lengths of straight waveguide, one set of opposite hand to those in the first waveguide and one set of the same hand. One such waveguide is shown in Figure 6.2. The slot spacing is one inch and, in the first waveguide, the end slots are greater than one half wavelength from the double mitred corners. A measurement of mutual coupling included only one slot in any waveguide, the remaining slots were shorted out with conducting adhesive aluminium tape.

Table 6.1

	Slot dimensions (ins)			
Slot Number	ℓ_a	ℓ_b	ℓ_c	Power coupled to WG12 waveguide (-dB)
1	.100	.278	.405	4.78
2	.170	.238	.405	11.02
3	.190	.221	.405	17.52
4	.200	.212	.405	26.65

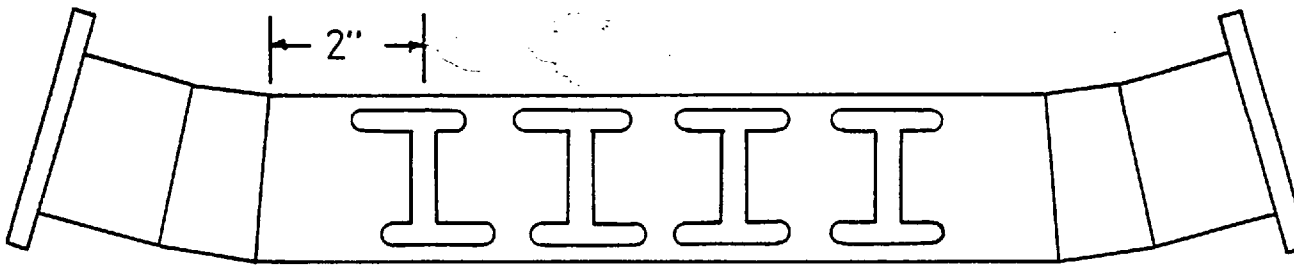

Fig. 6.2: Slotted waveguide used in mutual coupling experiment.

With the observation that the radiation over the baffles was insignificant, it was considered sufficient to confine the external structure to include only the baffles either side of the slots. (As explained previously, the measurement of mutual coupling is confined to slots within the same trough). The same clamping jig described in Chapter 5 was employed, with two .625" square baffles attached to the end plates of the jig. The waveguides could then be slid into position such that the appropriate slots were located centrally between the baffles and the remaining area between and either side of the baffles covered with aluminium sheet to form a ground-plane. A typical arrangement is shown in Figure 6.3. where details of the clamping jig have been omitted for clarity.

To reduce any possible reflection in the transverse direction, the groundplane was extended beyond the ends of baffles which were tapered and wedges of radio absorbent material were inserted into the ends of the channel. Varying the position of these wedges had no effect on the measurement and it was concluded that no transverse waves were present in the structure.

Several problems were encountered in evaluating the mutual coupling between the lightly coupled slots. First, the light coupling makes it very difficult to define the resonant conductance of the slot from measurements of the attenuation part of the slot. Other workers [39] have resorted to constructing one half wavelength spaced arrays of identical slots such that their reflection coefficients add in phase. The workshop effort required in such a measurement was not available for this study and, in addition, the tolerances on the dimensions of the low coupling slots make it difficult

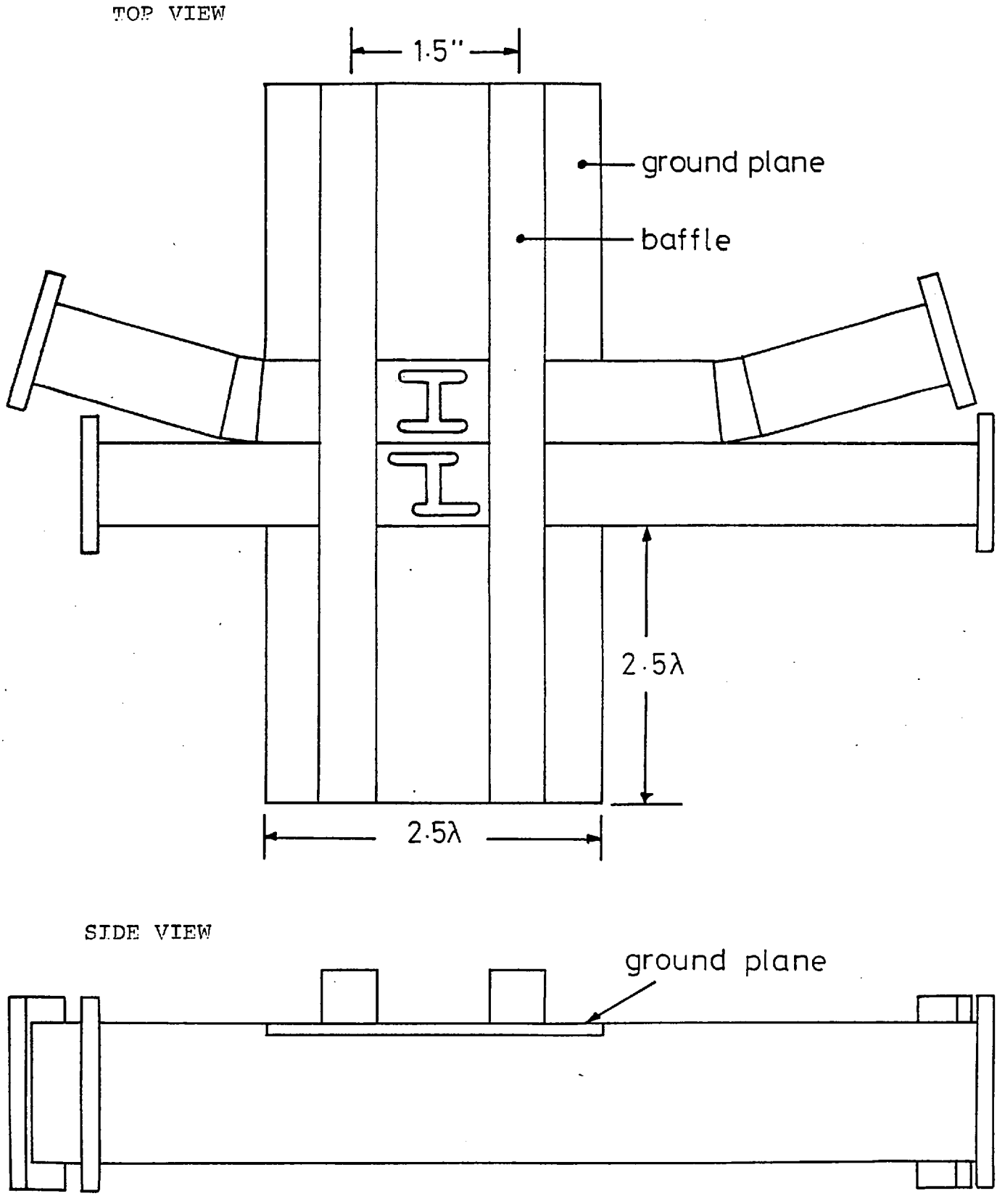

Fig. 6.3: Arrangement for the measurement of mutual coupling between I shaped slots.

to ensure that the slots have identical electrical performance. Here it was decided to use the design figures for the conductance in an estimate of the mutual coupling coefficients.

A second problem implied by the above observations is the difficulty in establishing the resonant frequency of the lower coupling slots. Also, the slots are narrowband devices and it is to be expected that the effective Q increases with a reduction in the coupling to the waveguide. This implies that mutually coupled power between waveguide fed slots becomes more frequency sensitive as the slot conductances decrease. The amplitude of the mutual coupling was therefore measured on a swept frequency basis.

6.3.1. MEASUREMENT OF THE AMPLITUDE OF THE MUTUAL COUPLING BETWEEN CLOSELY SPACED I SHAPED SLOTS

The slotted waveguides were clamped in position as shown in Figure 6.3. The insertion loss of each slot was measured with the second slot open and shorted out. The power coupled to the second waveguide was then recorded as a function of frequency, relative to the power incident on the first (excited slot). The calibration was obtained by shorting out the first slot with conducting-adhesive aluminium tape. A typical set of plots for the measurement of insertion loss and coupled power is shown in Figures 6.4 and 6.5. It was found that the no. 4 slots were too low in coupling to be measured and the results given here are for the three higher coupling slots only.

(a) Slot 1,

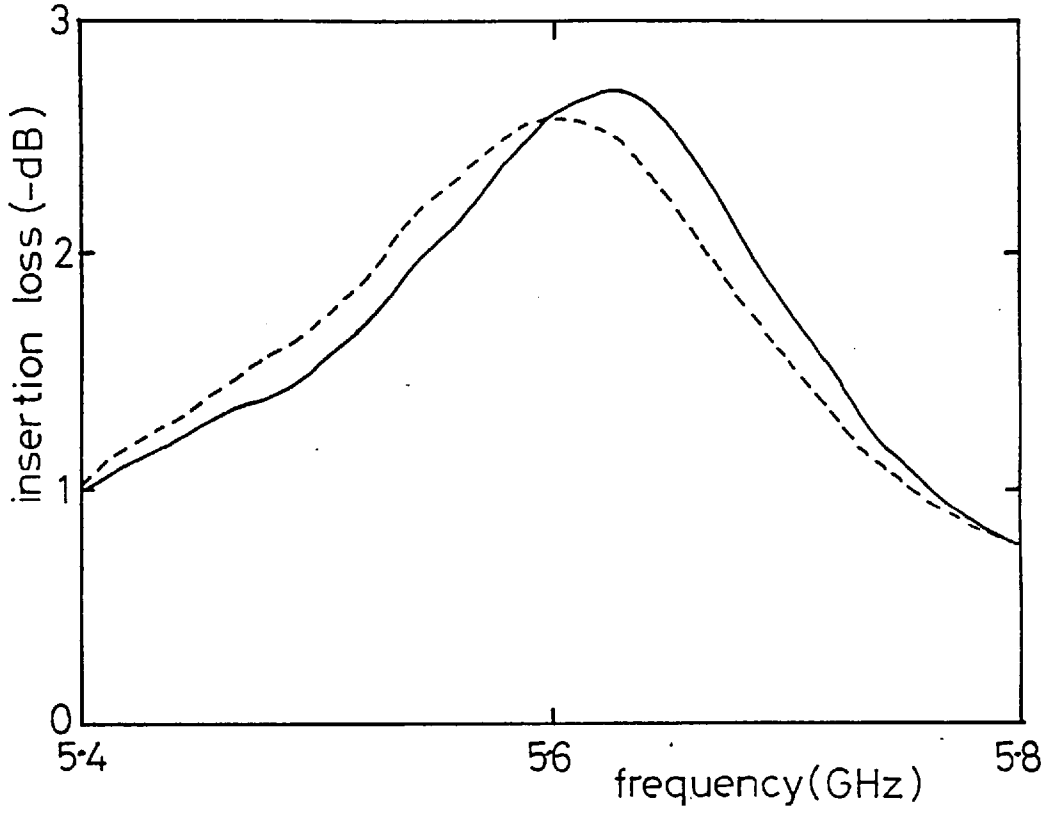

(b) Slot 1,

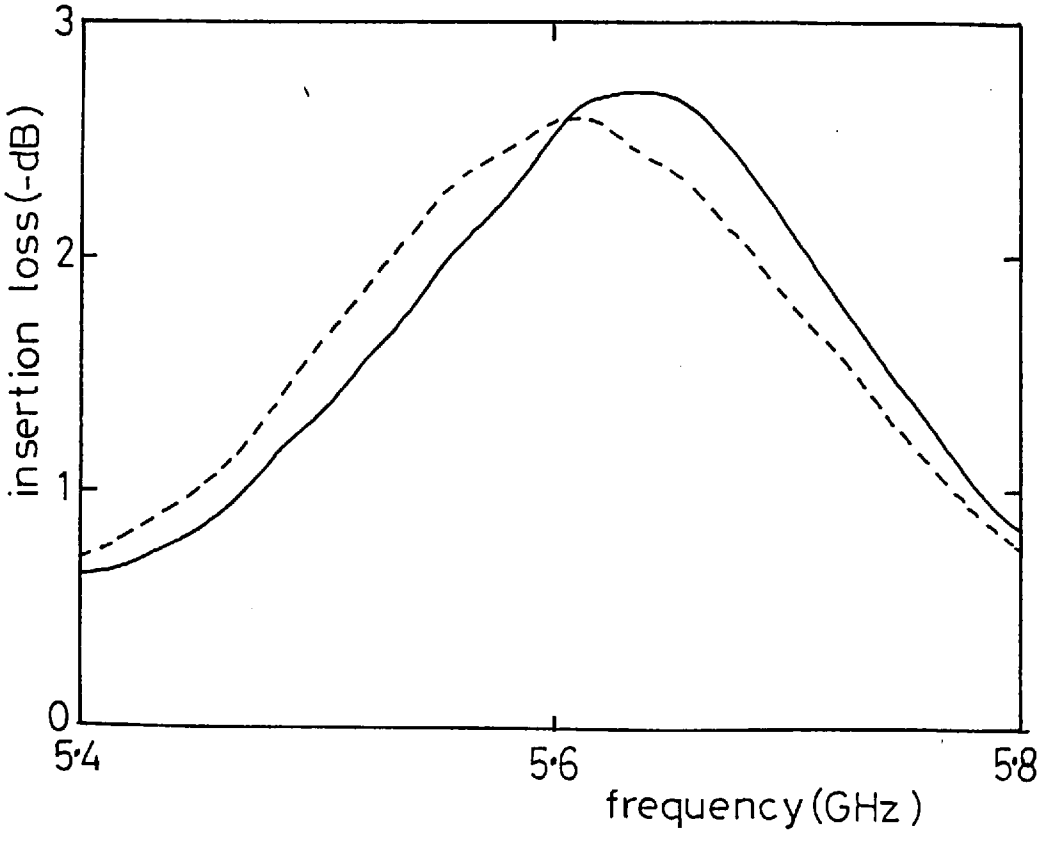

Fig. 6.4: Insertion loss of I shaped slots.

---- isolated

—— parasitic

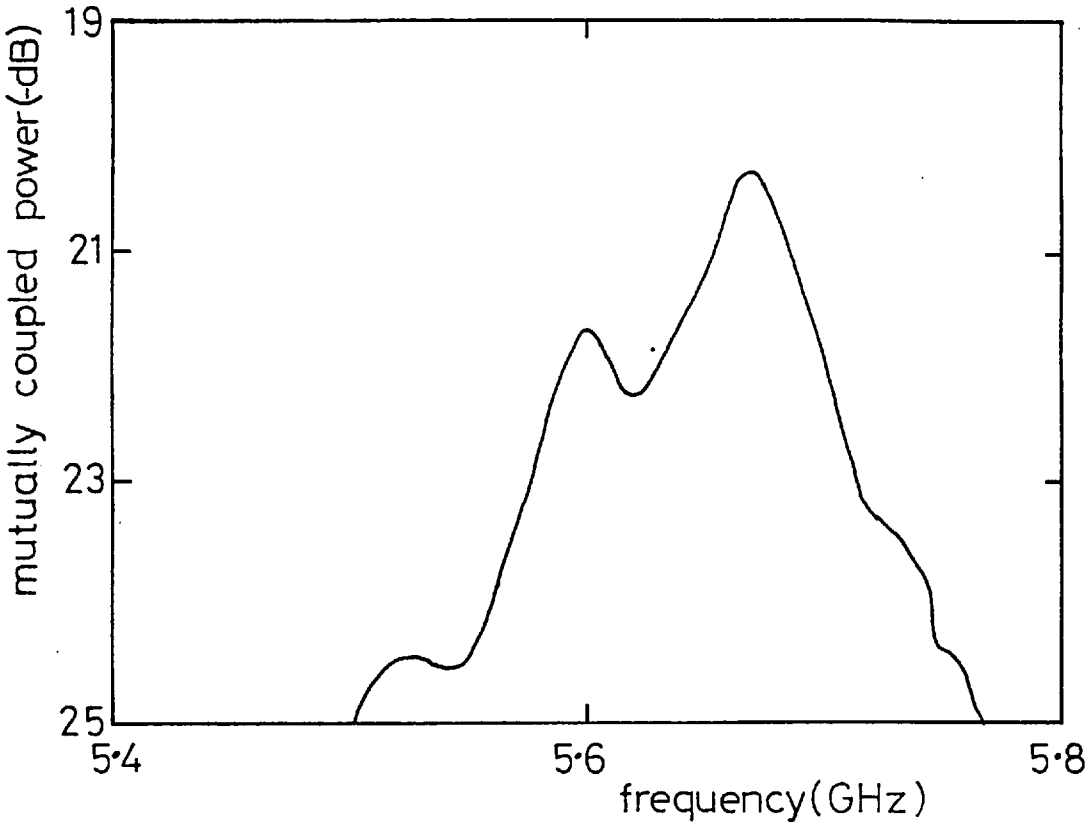

Fig. 6.5: Mutually coupled power between two waveguide fed I shaped slots.

A summary of the insertion loss characteristics of no. 1 and no. 2 slots is presented in Table 6.2. The slots are identified by the code: A - milled in the waveguide with angled output arms; BS - in the straight waveguide with slots of the same hand; BO - in the straight waveguide with slots of opposite hand. It can be seen that thereis a significant spread in the frequency of peak attenuation. This is expected both from the manufacturing tolerances and the influence of the parasitic slots. From the data in Table 6.2, the average frequency of peak attenuation with the second slot parasitic, is 5.630 GHz and the maximum deviationfrom this value is 30 MHz. For comparision, the insertion loss of the slots at the average frequency is included in Table 6.2.

The peak mutually coupled power in the second waveguide for the various combinations of the slots are presented in Table 6.3. Also included in Table 6.3. are the values of insertion loss of the slots at the frequency of the peak coupled power and the corresponding values of the relative slot excitations, the first column gives values obtained using Equation 6.12 and the second gives those derived using the relations of Section 5.4.

To examine the effects of the end arm dimensions the relative slot excitation has been plotted as a function of the product $P_{r1}\ P_{r2}$ (defined in Eqn. 6.11) in Figure 6.6. There is obviously quite a spread in the results, particularly for the lower coupling slots where theoretical values of the coupling to the waveguide were assumed. Errors are also introduced by the dimensional tolerances of the slots which result in a variation in the resonant frequency.

Table 6.2

Slot	Frequency of peak attenuation (GHz)			Attenuation past slot with coupled slot parasitic(-dB)	
	Isolated	Parasitic	Parasitic Slot	Peak	At f_{av}*
1BS	5.568	5.600	2A	2.44	2.20
1BS	5.564	5.614	3A	2.48	2.46
1A	5.600	5.620	1BS	2.78	2.74
2BS	5.620	5.636	2A	0.50	0.50
2A	5.600	5.626	1BS	0.394	0.39
1BO	5.610	5.636	1A	2.70	2.70
1BO	5.620	5.650	3A	2.68	2.56
1A	5.604	5.626	1BO	2.70	2.70
2BO	5.600	5.638	2A	0.42	0.42
2A	5.624	5.652	1BO	0.37	0.36
2A	5.620	5.634	2BO	0.43	0.43

* Average frequency of peak attenuation.

Table 6.3

Fed Slot	Coupled Slot	Peak Coupled Power (-dB)	Frequency of Peak Coupled Power (GHz)	Measured Insertion Loss of Fed Slot (-dB)	Measured Insertion Loss of Coupled Slot (-dB)	Relative Slot excitation (-dB)	
						Calculated using network approach	Calculated as in Chapter 5
1BO	1A	20.28	5.668	2.52	2.28	6.6	8.3
2A	1BO	27.13	5.652	.376	4.23	5.2	-
1A	3BO	34.7	5.528	1.74	-	6.3	-
2A	2BO	31.88	5.660	.393	.395	4.5	4.8
2A	3BO	38.4	5.588	.363	-	4.2	-
3A	3BO	46.1	5.652	-	-	5.9	6.2
1BS	1A	21.56	5.616	2.42	2.78	7.2	8.0
2BS	1A	25.92	5.648	.455	4.00	5.8	-
3A	1BS	32.92	5.646	-	2.44	5.6	-
2BS	2A	31.76	5.606	.455	.37	4.7	5.9
2BS	3A	39.56	5.642	.248	-	5.6	-
3BS	3A	44.92	5.634	-	-	4.7	5.0

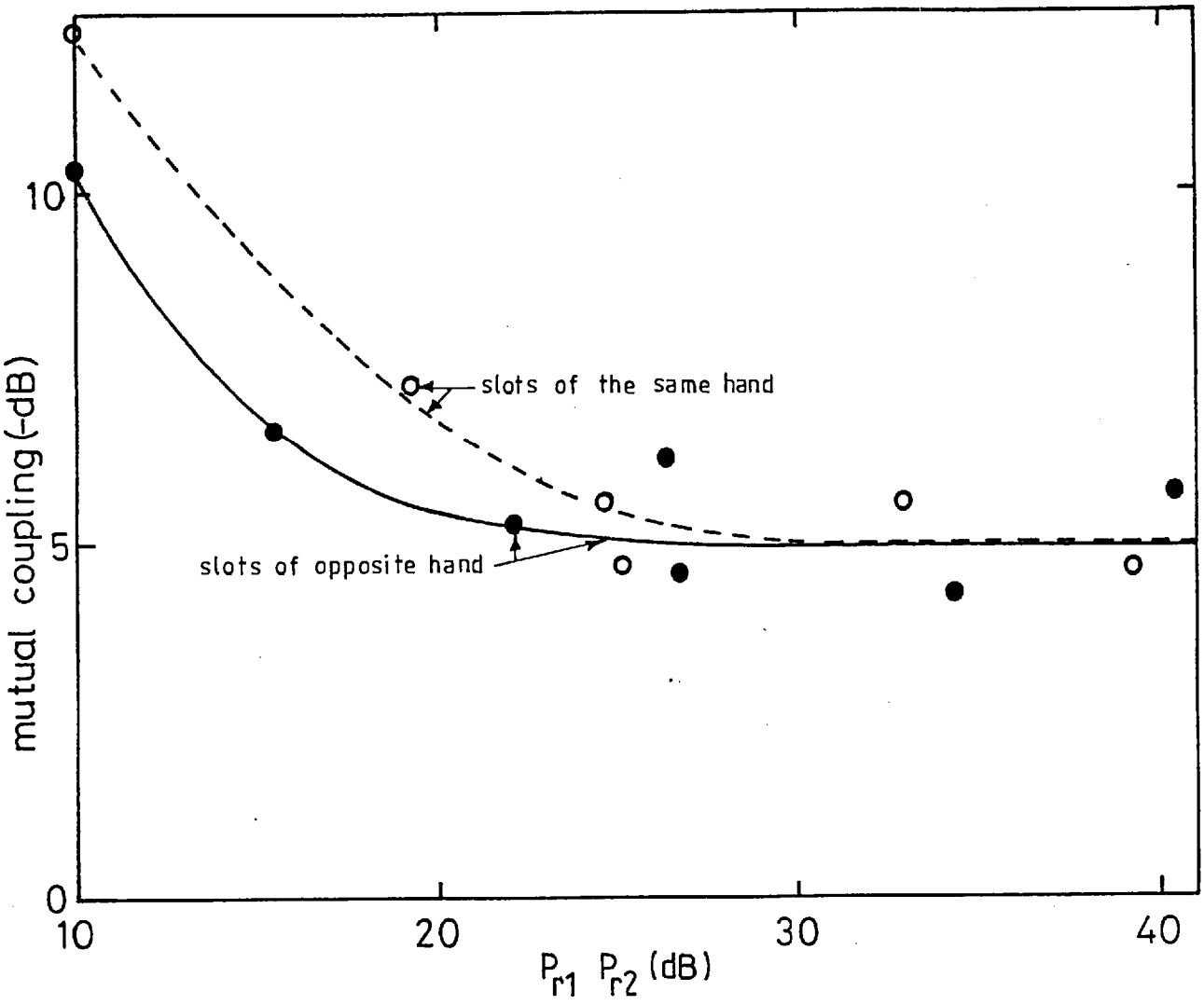

Fig. 6.6: Relative slot excitations as a function of the slot coupling to the waveguide.

It can be seen, however, that the mutual coupling is quite insensitive to variations in the end arm dimensions and there is little difference between the two configurations. This is expected from the theoretical calculations of the mutual coupling between 7 slots: at close spacings it was found that the principal components of the mutual coupling were between centre sections and between centre section and end arms. In the I shaped slots, with the two stubs of the end arms excited in opposition, the components involving the centre section and end arms will tend to cancel. Thus the component due to the centre section coupling will predominate. However, the relative slot excitation increases slightly with decrease in coupling to the waveguide, which suggests that the two components oppose each other.

6.3.2. MEASUREMENT OF THE PHASE OF THE MUTUAL COUPLING BETWEEN I SHAPED SLOTS

In determining the phase of the relative excitations of pairs of I shaped slots, one must take into account the effect of the slot susceptances which are introduced when the slots are not both resonant. The admittances of the experimental I shaped slots were measured about resonance using a slotted line bench. The measurement is quite inaccurate for the lower coupling slots and only the highest coupling slots were considered. For each pair of slots, the frequency at which one slot was resonant was chosen and the admittance of the other slot recorded at this frequency. The mutual coupling was then measured using the

technique described for Z shaped slots in Chapter 5 and the phase corrected for the effect of the slot self-susceptance using Eqns. 6.16 and 6.17. The results are presented in Table 6.4.

A quick verification of the relative phase of the coupling for the two configurations was afforded by the measurement of pairs of open circuited slots. This removed the need for the mitred corners to angle the output arms of one waveguide. The waveguides are terminated with a short circuit and the slots, which were individually resonant at 5.618 GHz (when covered with PTFE tape and with .625" square baffles in position), were milled a quarter of a guide wavelength away. The slotted waveguides were arranged in the clamping jig as shown in Figure 6.7.

The signals at the output port of the parasitically excited guide were compared for pairs of slots of the same and opposite hand. The phases of the coupled signals differed by less than 5^{o} for the two configurations, which confirms the above results.

6.3.3. SUMMARY OF THE RESULTS AND IMPLICATIONS ON THE FINAL ARRAY DESIGN

The amplitude and phase of the mutual coupling between pairs of I shaped slots have been established experimentally at a single waveguide spacing. The amplitude of the coupling is not strongly dependent on the dimensions of the end arms or their orientation and, to a reasonable approximation, may be assumed to be constant. At wider spacings it is argued that the mutual coupling is almost entirely due to the centre section coupling, as the trough

Table 6.4

Fed Slot	Coupled Slot	Signal Level at Port 4 Relative to Port 2 (-dB)	Phase of Signals (^{o})	Phase Difference Referred to Slot Terminals (^{o})	Relative Level of Generated Waves (-dB)	Phase of External Coupling(I^{o})
1BS	1A	20.2	+8	+4	7.9	-175
1BO	1A	19.65	-174	-172	9.3	-172

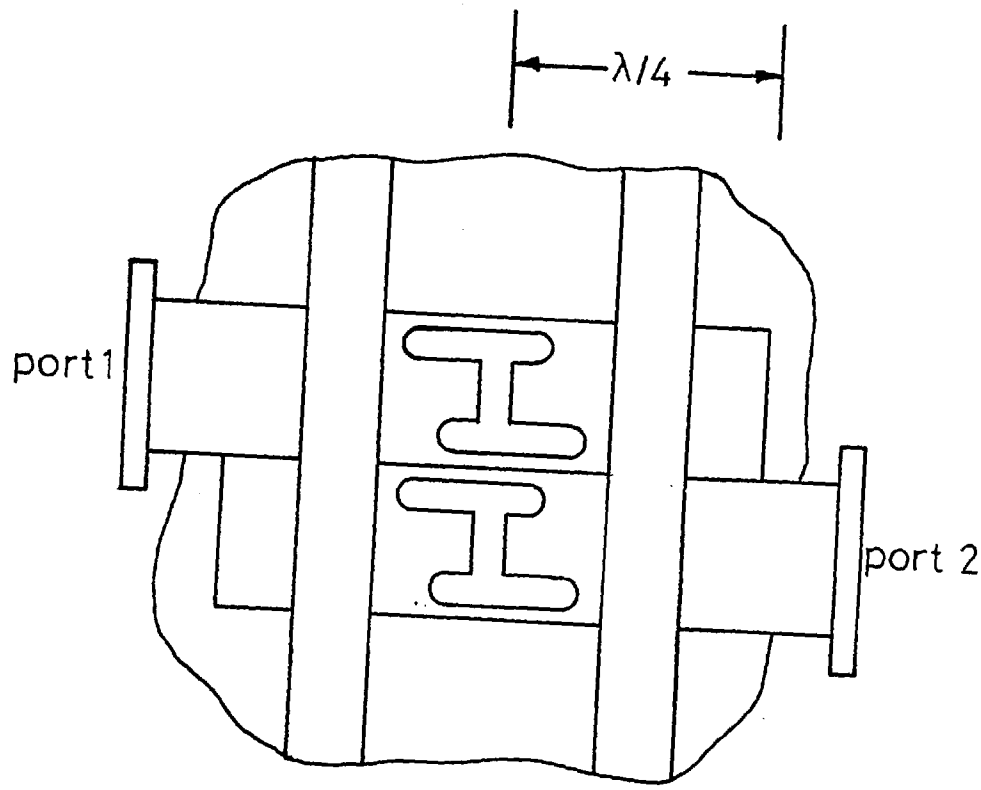

Fig. 6.7: Arrangement of open circuited I shaped slots.

waveguide formed between the baffles is cut-off to modes excited by the end arms. Some verification of this has been obtained by Chignell [1] who found that, at extended spacings, the mutual coupling was independent of the slot orientation. The phase was only measured for high coupling slots, but the values obtained were almost equal for the two configurations, which again suggest that the coupling is due principally to the components between the centre sections and the centre and end arms, which are independent of the slot orientation. The next section outlines the incorporation of these results in an actual array design.

6.4. MUTUAL COUPLING IN PRACTICAL ARRAY DESIGNS

6.4.1. DESIGN OF PROTOTYPE MONOPULSE ARRAY

A description of the monopulse antenna considered in this thesis was given in Chapter 1. The results obtained in the previous section have been incorporated in the design of a prototype array consisting of eight stacked waveguides, with slots in each waveguide, which was fabricated at Imperial College. As described in Chapter 1, the monopulse function is obtained by interlacing slotted waveguides forming sum and difference beams so that they form a common aperture.

Standard design procedures for slotted waveguide arrays were discussed in Chapter 1. These were incorporated in a computer programme by Chignell [1] which was used to design the first linear arrays using I shaped slots. It was then

modified to treat the final prototype monopulse array. The general procedure may be summarised as follows:

1. The aperture distribution was chosen to give the required radiation characteristics of each beam, and the relative power required to be radiated at each slot position deduced.

2. The normalised conductance of each slot was calculated with a specified percentage of power dissipated in the load, for each linear array in isolation, that is, neglecting mutual coupling. One possible formulation for this calculation is given in Chapter 1.

3. The active admittance of each slot was then computed with all the slots excited. Only the mutual coupling contributions from elements within the same trough were included. The reflection coefficient at each slot is obtained by considering the superimposition of the reflected wave from the isolated slot and the secondary waves generated by mutual coupling, using the concepts presented in Chapter 4. The amplitudes of the secondary waves were calculated using Eqn. 6.11 and experimental values of the relative slot excitations. For ease of computation, the relative slot excitation was assumed to be independent of the end arm dimensions and the orientation of the slots.

4. The aperture distributions corresponding to these complex admittances were then calculated and compared with the required distributions. This is, in effect reversing

the procedure described in steps 1 and 2 above. The difference arrays were fed in two halves so that their relative phase could be trimmed to optimise the difference null depth. It was found that, at certain positions along the linear array, this effected a large difference in power in adjacent sum and difference waveguides. Such differences could give rise to large perturbations in the effective power transmitted past slots in the waveguide with the smaller incident power and produce unacceptable errors in the aperture distribution. In the array design, these errors were reduced by increasing the power dissipated in the load, which reduced the slot loading and hence the effect which variations in that slot loading had on the power transmitted past the slots.

5. The beams were to be scanned over a sector ± 22.5° about the boresight direction, in the elevation plane by phase shifters placed at the input to each linear array. To calculate the effect of the change in the phase of the mutual coupling contributions, steps 3 and 4 were repeated at increments of 5° over the scan sector and the corresponding aperture distributions plotted. It was found that these modified distributions fell either side of the required distribution. It was decided that the initial slot dimensions represented the best approximation and no adjustments were made to compensate for the effects of mutual coupling. It may be noted that this greatly reduced the workshop effort required in fabricating the actual array as, for each channel, the four slotted waveguides were identical.

The array was constructed with the slot dimensions obtained from experimental data obtained in the isolated situation. The radiation patterns and near field aperture distributions were measured using facilities at A.S.W.E., Hambrook. A detailed presentation of the results have been given by Chignell [1]. The performance of the array was found to generally satisfactory and the beams scanned predictably over the required angular sector without any severe loss in gain. Only the results pertaining to the mutual coupling behaviour will be discussed here.

First, at specific frequencies, large secondary lobes occured in the radiation pattern of the fully excited array at angles close to broadside which were not present in the corresponding radiation pattern of one isolated linear array. The lobes were associated with large phase errors introduced by mutual coupling effects which were apparent in plots of the aperture phase distribution. Second, it was found that the lobes varied in magnitude as the beam was scanned, again indicating that the effect was due to mutual coupling.

6.4.2. ALTERNATIVE DESIGN PROCEDURES

In the last section it was noted that, in the monopulse array design, the aperture distributions calculated including the contributions of mutual coupling at angles over the specified scan sector fell either side of the desired distributions, calculated for the isolated linear arrays. Therefore, no compensation for the effects of mutual coupling could be made. If any compensation was necessary,

in the design format used there, it would involve an iterative procedure to vary the isolated admittances of the slots until the aperture distributions was optimised over the range of scan angles. With the same assumptions regarding the mutual coupling, alternative procedures may be more economical.

The aim of any design is to establish the aperture distribution required to obtain the desired radiation pattern. With identical elements, the aperture distribution can be expressed in terms of voltage, current or power radiated; in the present study it is convenient to consider the voltages appearing across the centre of the slots. As a general rule, the aperture distribution is determined from array theory neglecting the presence of mutual coupling. When the mutual coupling is significant, the slot excitations must be modified so that the required aperture distribution is regained. Consider one slot in the array. The final current, i_n, and voltage, v_n, at the slot terminals are related by the equation:

$$i_n = y_{nn} v_n + \sum_{m \neq n} y_{nm} v_m \qquad (6.18)$$

The active admittance is given by:

$$y_{an} = y_{nn} + \sum_{m \neq n} y_{nm} \frac{v_m}{v_n} \qquad (6.19)$$

The voltages are the final voltages occurring each slot terminal pair and should be directly related to the required aperture distribution.

In the study of I shaped slots, the following approximations have been employed with regard to the external mutual coupling problem:

1. The slots are lightly coupled to the waveguide in a realistic design. This implies that the effect of the waveguide loading on the slots is small and the external mutual coupling problem may be considered in isolation from the waveguide feed.

2. The self-conductances of the slots are insensitive to variations in the end arm dimensions.

3. The mutual admittance is insensitive to variations in the end arm dimensions and the slot orientations.

Thus, all the parameters appearing on the right hand side of Eqn. 6.19 are known and the active admittance of each slot may be calculated before specifying the end arm dimensions. These must now be determined, from a consideration of the waveguide feed problem.

The normalised admittance presented by the slot across the dominant mode TE_{10} equivalent transmission line is related to the slot admittance by:

$$Y_n = \frac{K_n^2}{y_{an}} \qquad (6.20)$$

In general, the active admittance is complex, and, since K_n^2 is real, the normalised waveguide admittance Y_n is also complex. The equivalent transmission line representation of a single linear array is that shown in Fig. 1.3. Consider the slot represented by Y_o , immediately preceding the load, Y_L. Y_o is chosen to be the largest conductance acceptable in a linear array design. From Eqn. 6.20 it is necessary to adjust the end arm dimensions of the slot, first to introduce a susceptance in the self-admittance to make the active admittance real and, second, provide the correct value of K^2 to satisfy Eqn. 6.20. By choosing Y_o, we have effectively set the ratio between v_o and V_o, the voltage across the equivalent waveguide transmission line. Moving to the next slot in the direction towards the input end, the ratio v_1/V_1 is established from v_o/V_o, the required aperture distribution and the recurrence relationships, in the waveguide feed, described in Chapter 1. From Chapter 4:

$$K_1 = \frac{V_1}{v_1} \, y_{a1} \qquad (6.21)$$

This is used to establish the end arm dimensions of slot 1. This procedure is then repeated for the remaining slots.

Thus the array can be designed directly, although no indication of its scanning performance is provided. It has the advantage, however, of automatically taking into account the effect of mismatches past the slot. A major disadvantage is that it requires detailed knowledge of

the susceptance of the slots about resonance, as a function of the end arm dimensions. Due to the complex nature of the slots, the susceptance is not a smooth function of the slot dimensions. It may be more appropriate to introduce the required susceptance with a discontinuity, such as an iris, inside the waveguide. The relation between K^2 and the slot dimensions may be established empirically or by the theory presented in Chapter 3. The mutual admittances can be deduced from the relative slot excitations.

7. CONCLUSIONS AND RECOMMENDATIONS FOR FURTHER WORK

7.1. CONCLUSIONS

The principal objective of this work was to establish models which account for the effects of mutual coupling in the monopulse antenna described in Chapter 1 and provide appropriate design data for the complex shaped slots used in the array. From a survey of possible approaches it was found in Chapter 2 that the usual "large array approximations" were not valid because of the required monopulse excitation and a mutual admittance network model was chosen as being most suitable.

In Chapter 3, the admittance properties of complex shaped slots were examined. A variational technique which had been used successfully with straight slots milled in the broad wall of rectangular waveguide was applied to obtain a first order equivalent circuit of these complex shaped slots. Equivalent circuits were also derived for the case where the slots were positioned in the end wall. The equivalent circuits were used with experimental data to derive values for the external admittances of Z shaped slots in the two positions. A comparison of these values demonstrated the validity of the approximation for the slot fields and confirmed the relative independence of the field to the position of the slots in the waveguide about resonance.

In Chapter 4 the equivalent circuits were used to derive network relationships describing the mutual coupling between waveguide excited slots. It was realised that,

even in the design of moderately sized arrays, an exact network description is not feasible and approximations are required. For the application discussed here, the following initial approximations were argued:

1. The mutual coupling between slots separated by the cross polarisation suppressors is negligible. This is a result of the suppressor design.

2. From the network relationships for the mutual coupling between pairs of slots, it was found that, when considering the external mutual coupling, the waveguide loading may be ignored.

3. The self conductance of the I shaped slot is independent of the end arm dimensions. This is implied by the model used to calculate the slot dimensions, in which the composite input impedance of the end arm equivalent transverse transmission lines is held constant to secure resonance.

Chapter 5 dealt exclusively with the mutual coupling between pairs of slots radiating into a half space. A first order expression for the mutual admittance of Z shaped slots was derived using the same field distribution employed in the waveguide coupling problem in Chapter 3. The formulation was found to be particularly convenient since the contributions from each section could be easily identified. The results were confirmed by comparison with experimental data. The experimental programme involved measuring the phase and amplitude of the signals coupled between slots milled in the walls of separate

waveguides and deriving the excitations across the centre of each slot. These quantities are required in the actual array design. Some confirmation of the slot excitations was obtained by measuring the radiation patterns of small parasitic arrays of the same slots.

The mutual coupling between the I shaped slots used in the final array was examined in Chapter 6. Emphasis was placed on securing practical design information and no theoretical predictions of the mutual coupling was attempted, although qualitative arguments based on the results obtained for Z shaped slots were presented.

Measurements were made to determine the effects of varying the end arm dimensions on the mutual coupling at adjacent waveguide spacing. Difficulties were encountered with lower coupling slots because of their frequency sensitivity and swept frequency techniques were used to measure the amplitude of the mutual coupling. A swept frequency measurement of the phase of the mutual coupling was not considered to be feasible. A single frequency measurement was made and the errors introduced by operating the slots off-resonance were corrected for using admittance data of the isolated slots.

The incorporation of this data into the final array design was then outlined. The design procedure was not optimised as it involved the modification of earlier computer programmes used in the design of slotted waveguide linear arrays. In order to simplify the calculations, the external mutual coupling was assumed to be independent of th end arm dimensions and the slot orientation. This was justified from the experimental results.

Finally, alternative design techniques were proposed. These involved calculating the effects of the mutual coupling at the slot terminals. This considerably simplifies the problem as, initially, the coupling to the waveguide is not considered. The slot dimensions are then obtained using standard series feed linear array calculations.

Summarising, the principal objective of this study was to establish models for evaluating the effects of mutual coupling in a specific array configuration. The usual large array techniques were found to be unsuitable as the approximations on which they are based are not valid for the application considered. This led to original investigations of the admittance characteristics of the complex shaped slots employed in the array, and their mutual coupling behaviour, to deduce a different set of approximations which made the array design calculations tractable. Although these approximations are not general, it is felt that their derivation provides a different viewpoint on the treatment of mutual coupling.

Finally, it is concluded that, with the array considered here, emphasis should be placed on modifying the array structure to reduce the high level of mutual coupling between closely spaced slots. This is expanded upon in the next section.

7.2. RECOMMENDATIONS FOR FURTHER WORK

The design proposed in section 6.4. requires detailed information on the slots in terms of the equivalent circuit

parameters, particularly away from resonance. As was seen in Chapter 3 the coupling factor K^2 is not strongly dependent on frequency. The mutual coupling and the self-conductances of the slots are also expected to be relatively insensitive to frequency changes. However, due to the complex shape of the slots and the presence of the cross polarisation baffles, the slot susceptance does not vary monotomically with frequency about resonance and is thus difficult to include in a design procedure. A better solution may be to secure the required susceptance with elements within the waveguide. Considering the resultsof Chapter 2, the characteristics of the low coupling slots may be investigated by positioning them in the end wall, where they will radiate a greater proportion of energy.

From the performance of the prototype monopulse array, it is apparent that the mutual coupling must be reduced in the transverse direction. More investigations are required into the design of the cross polarisation suppressors using, for example, techniques described by DuFort [40]. The beamwidth of the slot element radiation pattern in the plane parallel to the baffles was strongly dependent on their height, and in the array design, the cross polarisation specification was relaxed to reduce the scanning loss and reduce the mutual coupling between slots separated by the baffles. Recent work [41] has demonstrated the ability of parasitic monopoles to shape the element radiation pattern. Such techniques may be applicable to complex shaped slots to improve the mutual

coupling and cross-polarisation properties. It should be remembered, however, that a reduction in mutual coupling is often associated with a narrower element pattern and hence, greater scanning losses.

REFERENCES

1. CHIGNELL, R.J. (1975) Slot loss and coupling studies in stacked linear array applications. Ph.D. Thesis - University of London.

2. BRADY, M.M. (1971) Single slotted waveguide linear arrays. Advances in Microwaves 7, pp 131-176.

3. HANSEN, R.C. (Editor) (1966) Microwave scanning antennas, Volume III, Academic Press, New York.

4. KERNS, D.M. and BEATTY, R.W. (1967) Basic theory of waveguide junctions and introductory microwave networks. Pergamon Press.

5. BARTON, D.K. (1969) Handbook of radar measurement Englewood Cliffs.

6. LOPEZ, A.R. (1968) Monopulse networks for series feeding an array antenna I.E.E.E. Transactions AP-16, pp 436-440.

7. LEWIS, D.J. LEE, J.R. and McCARTHY, D.K. (1972) A single plane electronically scanned antenna for airborne radar applications. Phased Array Antennas (Editors : Oliner A.A. and Knittel, G.H). Artech House. pp 366-370.

8. KILLICK, E.A., PORTER, N.E. and SALT, H. (1969). The design of waveguide arrays providing sum and difference beams and suitable for scanning in one plane. European Microwave Conf. Digest. pp 160-163.

9. KAHN, W.H. and WASYLKIWISKYJ, W. (1966) Theory of coupling, radiation and scattering by antennas. Proc. Symp on Generalised Networks, 16, Brooklyn, New York. Polytechnic Press. pp 83-114.

10. CARTER, P.S. (1932) Circuit relations in radiating systems and applications to antenna problems. Proc. IRE 20(b), pp 1004-1041.

11. STARK, L.(1972) Comparison of array element types. Phased array antennas (Editors: Oliner, A.A. and Knittel, G.H.) Artech House.

12. WHEELER, H.A. (ref. 37.)

13. BLASS, J. and RABINOWITZ, S.J. (1957) Mutual coupling in two dimensional arrays. IRE Wescon 1(1) pp 134-139.

14. HANNAN, P.W. and BALFOUR, M.A. (1965) Simulation of a phased array antenna in waveguide. IEEE Transactions. AP-13, pp 342-353.

15. KURTZ, L.A. ELLIOT, R.S., WEHN, S. and FLOCK, W.L. Mutual coupling effects in scanning dipole arrays. IRE Trans. AP-5, p.433.

16. STEIN, S. (1962) On cross coupling in multiple-beam antennas IRE Trans. AP-10, pp 548-557.

17. STEVENSON, A.F. (1948) Theory of slots in rectangular waveguide. J. Appl. Phys. 19, pp 24-38.

18. SILVER, S. (1949) Microwave antenna theory and design, Vol. 12. MIT Radiation Laboratory Series, McGraw-Hill, New York.

19. FRADIN, A.Z. (1961) Microwave antennas. Pergamon Press.

20. LEWIN, L. (1951) Advanced theory of waveguides. Iliffe.

21. OLINER, A.A. (1957) Impedance properties of narrow radiating slots in the broad face of rectangular waveguide IRE. Trans. AP-5, pp 4-20.

22. DAS, B.N. and SENGAL, G.S. (1968) Investigations of a waveguide fed slot antenna : equivalent network representation. J. Inst. Telecomm. Engs. 14(b), pp. 247-264.

23. BAILEY, M.C. (1970) The impedance properties of dielectric covered narrow radiating slots in the broad face of a rectangular waveguide. IEEE Trans. AP-18, pp 596-603.

24. YEE, H.Y. (1974) Impedance of a narrow rectangular shunt slot in a slotted waveguide array. IEEE Trans. AP-22, pp 589-592.

25. HARRINGTON, R.F. (1961) Time harmonic electromagnetic fields. McGraw-Hill, New York.

26. BOOKER, H.G. (1946) Slot aerials and their relations to complementary wire aerials. J. IEE Pt. IIIA, 93, pp 620-626.

27. KING, R.W.P. (1956) The theory of linear antennas. Harvard University Press.

28. PUTNAM, J.L. (1948) Input impedance of centre fed slot aerials near half-wave resonance. J. IEE Pt. III 95, pp 290-294.

29. TAI, C.T. (1967) The induced MMF method. IEEE Trans. AP-15, pp 527-530.

30. MARCUVITZ, N. and SCHWINGER, J. (1951) On the representation of electric and magnetic fields produced by currents and discontinuities in waveguides. J. Appl. Phys. 22, pp. 806-819.

31. The Microwave Engineers' Handbook (published annually) Horizon-House - Microwave Inc.

32. EHLRICH, M.J. and SHORT, J.(1954) Mutual coupling considerations in linear slot array design. Proc. IRE 42, pp 956-961.

33. KAY, A.F. and SIMMONS, A.J. (1960) Mutual coupling of shunt slots. IRE Trans. AP-8, pp 389-400.

34. DAS, B.N. and SENGAL, G.S. Mutual impedance between two resonant slot radiators. Proc. IEE 118, pp. 1535-1538.

35. IISUKA, K. (1965) Technique for measuring mutual admittance of antennas. IRE Trans. AP-13, pp. 469-470.

36. MAILLOUX, R.J. and LARUSSA, F.J. (1968) A microwave bridge for measuring the mutual coupling of identical coupled antennas. IEEE Trans. MTT-16, pp. 129-130.

37. HANSEN, R.C. (Editor) (1966) Microwave scanning antennas Volume II, Academic Press.

38. KING, R.W.P. MACK, B.M. and SANDLER, S.S. (1968) Arrays of cylindrical dipoles. Cambridge University Press.

39. MILLAR, D. and RABURN, L.E. (1963) An accurate technique for measuring weakly coupled slots in rectangular waveguide. Microwave Journal, 6, pp 70-74.

40. DUFORT, E.C. (1968) A design procedure for matching volumetrically scanned waveguide arrays. Special issue on electronic scanning. Proc. IEEE 56, pp. 1851-1860.

41. CLAVIN, A., HUEBNER, D.A. and KILBURG, F.T. (1974) An improved element for use in array antennas. IEEE Trans. AP-22, pp 521-526.

42. SCHELKHNOFF, S.A. (1943) A mathematical theory of linear arrays. Bell. System. Tech. J. 22, pp. 80-107.

APPENDIX 1

CLASSICAL ARRAY THEORY APPLIED TO SLOT RADIATORS

Consider an array of slots in an infinite conducting ground plane. It is assumed that the slots may be represented by an equivalent system of sources consisting of magnetic currents $\underline{M}$ and magnetic charges ρ_m, only. Introducing vector and scalar potentials $\underline{F}$ and ψ where:

$$\begin{aligned} \underline{D} &= -\nabla \times \underline{F} \\ \underline{H} &= -\nabla\psi - \frac{\partial \underline{F}}{\partial t} \end{aligned} \qquad \text{A1.1}$$

and considering only the time periodic case which allows ψ to be directly specified by:

$$\nabla . \underline{F} = -j\omega\mu\psi \qquad \text{A1.2}$$

Maxwell's equations may be reduced to the vector wave equation form:

$$\nabla^2 \underline{F} + \mu\varepsilon\omega^2 \underline{F} = -\varepsilon\underline{M} \qquad \text{A1.3}$$

The solution is:

$$\underline{F}(r) = \varepsilon \int_V \frac{\underline{M}\, e^{-jkr}}{4\pi r}\, dv \qquad \text{A1.4}$$

where r is the distance from the source point to the field point and the integral is taken over all space.

Making the far field assumptions of Schelkunoff [42] and separating the above equation into two factors yields:

$$\underline{F} = \varepsilon \frac{e^{-jkr}}{4\pi r} \underline{L}(\underline{M}) \qquad \text{A1.5}$$

$$\text{where} \quad \underline{L}(\underline{M}) = \int_{v'} \underline{M}.e^{jkr'\cos\psi} \, dv' \qquad \text{A1.6}$$

where the integral is confined to a volume containing the sources and r' and ψ are defined in Figure A1.1.

In spherical co-ordinates, define:

$$\underline{F} = \varepsilon \frac{e^{-jkr}}{4\pi r} (\hat{\underline{a}}_r L_r + \hat{\underline{a}}_\phi L_\phi + \hat{\underline{a}}_\theta L_\theta) \qquad \text{A1.7}$$

where $\hat{\underline{a}}_r$, $\hat{\underline{a}}_\phi$ and $\hat{\underline{a}}_\theta$ are unit vectors in the r, ϕ and θ directions.

Therefore, the angular dependence and hence the radiation patterns are specified by $\underline{L}$. For identical radiators, assuming no mutual coupling:

$$\underline{L} = \underline{L}_o \left(C_1 e^{jkr_1'\cos\psi_1} + C_2 e^{jkr_2'\cos\psi_2} + \ldots.\right) \qquad \text{A1.8}$$

where $\underline{L}_o$ represents the radiation pattern of an isolated radiator and the bracketed term represents the array factor.

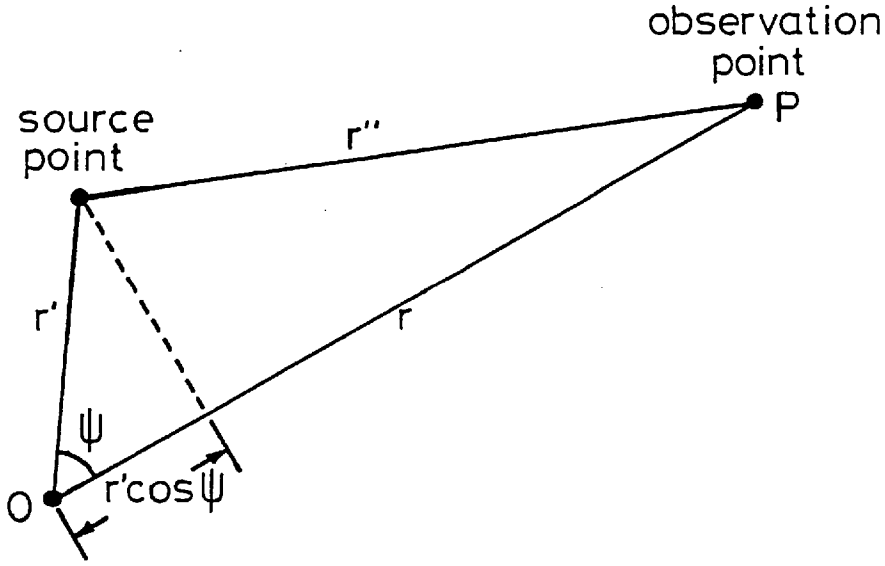

Fig. A1.1: Spatial parameters in array factor calculation.

APPENDIX 2

CROSS COUPLING IN MULTIPLE BEAM ANTENNAS

Consider an array of equally spaced radiators located along the y axis as shown in Figure A2.1, which radiates into the half-space $Z \geq 0$. With the centre of the array at O, let the complex field radiated by the array be described by an outgoing spherical wave, such that the filed at P is:

$$\underline{E} \quad C_1 \quad \underline{G}_1(\theta,\phi) \; \frac{e^{jkr}}{r} \qquad \text{A2.1}$$

where C_1 is a normalising constant

$\underline{G}_1$ is the radiation pattern of the array.

The power flow across a hemisphere of radius r is then [8]

$$P_R = C_2 \int_{-\pi/2}^{+\pi/2} \int_{-\pi/2}^{\pi/2} r^2 \; \underline{G}_1 \cdot \underline{G}_1^* \, d\theta d\phi \qquad \text{A2.2}$$

With a second linear array, parallel to the first and located at x = d, say, the cross coupled power in the far field may be expressed as:

$$P_C = C_2 r^2 \int_{-\pi/2}^{\pi/2} \int_{-\pi/2}^{\pi/2} \underline{G}_1 \cdot \underline{G}_2^* \, d\theta d\phi \qquad \text{A2.3}$$

where $\underline{G}_2^*$ is the complex conjugate of the radiation pattern of the second array, referred to O.

Assuming that $\underline{G}_1$ and $\underline{G}_2$ can be expressed as the product of the two field patterns in the θ and ϕ co-ordinate planes and letting:

$$\underline{G}_1(\theta,0) = \underline{G}_2(\theta,0) = \cos\theta \quad , \qquad \text{A2.4}$$

simple array theory yields:

$$P_C = C_r r^2 \int_{-\pi/2}^{\pi/2} \cos^2\theta \; e^{-jkd\sin\theta} \, d\theta \int_{\pi/2}^{\pi/2} \sum_n A_n e^{jkan\sin\phi} \sum_m B_m^* e^{-jkam\sin\phi} \, d\phi \qquad \text{A2.5}$$

where a is the spacing between radiators

A_n is the aperture distribution of the first array

B_m is the aperture distribution of the second array.

and the element pattern in the ϕ plane is ignored.

Changing the order of integration and summation in the ϕ co-ordinate integral produces:

$$P_C = C_2 r^2 \int_{-\pi/2}^{\pi/2} \cos^2\theta e^{-jkd\sin\theta} d\theta \sum_n A_n \sum_m B_m^* \int_{-\pi/2}^{\pi/2} e^{jka(n-m)\sin\phi} d\phi \qquad \text{A2.6}$$

The integrals may be identified as Bessel Functions, and the final expression for P_C is:

$$P_C = C_3 r^2 \frac{J_1(kd)}{kd} \sum_n A_n \sum_m B_m^* J_o[(n-m)ka] \qquad \text{A2.7}$$

This differs from the expression obtained in Reference 8. The most important modification occurs in the summations; as the ϕ integral is not a delta function, the cross coupled power flow is no longer due only to adjacent radiators and theoretically, the contributions from all the radiators should be considered.

The functions involving kd are also different. This is due to the fact that the pattern in the $\phi = 0$ plane was taken to be $\cos\theta$ and not $\sqrt{\cos\theta}$ (which was used in the calculations in Reference 8). This highlights the dependence of the cross coupled power flow on the element patterns in the $\phi = 0$ plane.

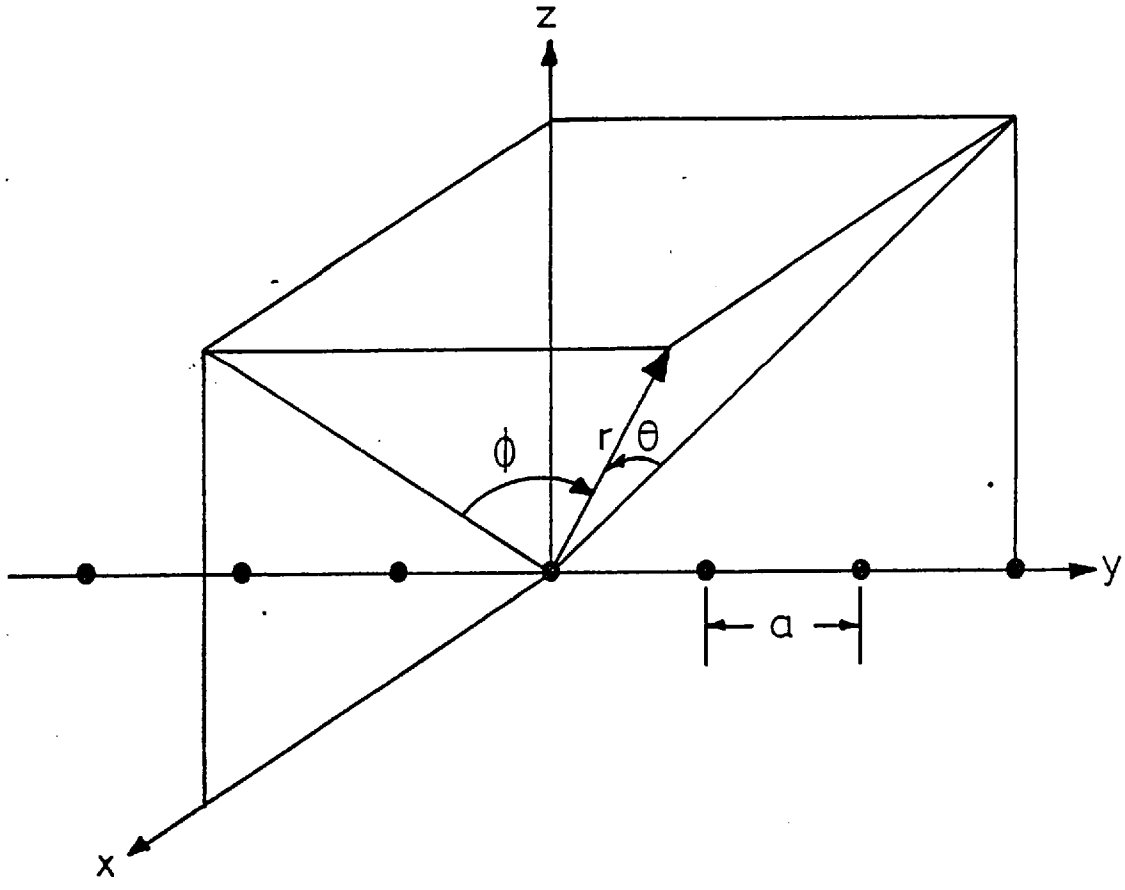

Fig. A2.1: Co-ordination system of linear array.

APPENDIX 3

THE RELATIONSHIP BETWEEN SIDE AND END WALL SLOT MUTUAL COUPLING RESULTS

For the case of slots in the side wall, the quantity r_1/r_2 was considered in section 5.3. which is the relative complex amplitudes of the wave generated by the slots in the respective guides. In the bridge measurements using end wall slots, the power coupling coefficient, C_p, is obtained, which is defined as:

$$C_p = \frac{\text{power received by the coupled slot}}{\text{power transmitted by the coupled slot}} \qquad \text{A3.1}$$

To compare these results , consider first the transmitting slot of the side wall case. From Eqn. 5.31,

$$\text{Power transmitted} = 2|r_1| \ (1-|r_1|) \qquad \text{A3.2}$$

The total power received by the second slot is just $2|r_2|^2$ and

$$C_p = \frac{2|r_2|^2}{2|r_1|(1-|r_1|)} \qquad \text{A3.3}$$

after making the assumptions described in Section 4.3. Then, C_p can be derived from the quantity r_1/r_2 and a knowledge of r_1.